

# ON LARGE-SCALE OCEANIC WIND-DRIFT CURRENTS

CHRISTIAN PUNTINI<sup>1,\*</sup>, LUIGI ROBERTI<sup>2</sup>, AND EDUARD STEFANESCU<sup>3</sup>

<sup>1</sup>Faculty of Mathematics, University of Vienna,  
Oskar–Morgenstern–Platz 1, 1090 Vienna, Austria

<sup>2</sup>Institut für Angewandte Mathematik, Leibniz Universität Hannover,  
Welfengarten 1, 30167 Hannover, Germany

<sup>3</sup>Institut für Analysis und Zahlentheorie, TU Graz,  
Steyrergasse 30, 8010 Graz, Austria

**ABSTRACT.** Starting from the Navier–Stokes equations in rotating spherical coordinates with constant density and eddy viscosity varying only with depth, and appropriate, physically motivated boundary conditions, we derive an asymptotic model for the description of non-equatorial wind-generated oceanic drift currents. We do not invoke any tangent-plane approximations, thus allowing for large-scale flows that would not be captured by the classical  $f$ -plane approach. The strategy is to identify two small intrinsic scales for the flow (namely, the ratio between the depth of the Ekman layer and the Earth’s radius, and the Rossby number) and, after a careful scaling, perform a double asymptotic expansion with respect to these small parameters. This leads to a system of linear ordinary differential equations with nonlinear boundary conditions for the leading-order dynamics, in addition to which we identify the governing equations for the first-order correction with respect to the Rossby number. First, we establish the existence and uniqueness of the solution to the leading-order equations and show that the solution behaves like a classical Ekman spiral for any eddy viscosity profile; moreover, we discuss the solution of the equations for the first-order correction, for which we also provide *a priori* bounds in terms of the leading-order solution. Finally, we discuss several cases of explicit eddy viscosity profiles (constant, linearly decreasing, linearly increasing, piecewise linear, and exponentially decaying) and compute the surface deflection angle of the wind-drift current. We obtain results that are remarkably consistent with observations.

## 1. INTRODUCTION

Physical oceanography is the fascinating field that studies the physical processes driving ocean motion. In its modern form, its roots trace back to the pioneering work of Ekman (1905), in which he determined the role of Earth’s rotation in explaining the observation—made by Nansen during his celebrated *Fram* Arctic expedition of 1893–1896 (see Nansen (1897) for his own accounts of the voyage)—that steady wind-driven ocean currents are deflected to the right of the prevailing wind direction in the northern hemisphere. This deflection is due to the momentum balance between the Coriolis acceleration acting on the upper ocean layers and the frictional forces generated by the turbulent stress exerted by the wind. Subsequently to Ekman’s contribution, the advent of more sophisticated measuring instruments and the development of the theoretical framework now known as geophysical fluid dynamics (for which we refer to the monographs by Gill (1982), Pedlosky (1987) and Vallis (2017)) have led to the establishment of physical oceanography as a lively and independent discipline that investigates a remarkably broad range of phenomena. However, the extensive knowledge and well-established techniques of classical fluid mechanics appear to have been overshadowed in recent years, with greater emphasis being placed on

2020 *Mathematics Subject Classification.* 35Q30; 35Q35; 76D05; 76U60; 86A05.

*Key words and phrases.* Air-sea interactions; Ocean processes; Rotating flows.

\*Corresponding author.

*E-mail addresses:* [christian.puntini@univie.ac.at](mailto:christian.puntini@univie.ac.at) (C. Puntini); [roberti@ifam.uni-hannover.de](mailto:roberti@ifam.uni-hannover.de) (L. Roberti); [eduard.stefanescu@tugraz.at](mailto:eduard.stefanescu@tugraz.at) (E. Stefanescu).

data analysis and numerical methods. Needless to say, data are invaluable to validate new ideas and theories, and sometimes the interpretation of available measurements reveals significant correlations, uncovers hidden patterns, or highlights unexpected phenomena—a notable example being the discovery of the Equatorial Undercurrent by Cromwell (1953) through the analysis of subsurface ocean flow data near the Pacific Equator. Nevertheless, we believe that the careful and systematic (asymptotic) analysis of the governing equations may provide meaningful insights that not only complement empirical findings, but also deepen our fundamental understanding of the underlying mechanisms driving such complex phenomena.

The purpose of this paper is to provide a framework for the most classical problem of physical oceanography, namely the effects of a wind blowing on the surface of the ocean (the very problem investigated by Ekman (1905)), which should be both mathematically rigorous and physically sound. As one may reasonably expect, the action of the wind is inconsequential at great depths, hence to obtain physically relevant qualitative results it suffices to focus on the upper ocean—the layer of sea water located between the surface of the ocean and the thermocline, with depths of the order of 50 m and rarely exceeding 100 m, where the most complex ocean dynamics takes place. Upper ocean currents typically consist of a superposition of surface waves, wind-driven (Ekman) flows, and tidal and pressure-driven (geostrophic) fluid motion. The sub-layer of the upper ocean where the Ekman flows take place is called the *Ekman layer*.

The standard theoretical framework for the dynamics of the Ekman layer is based on the *f*-plane approximation and involves the *ad hoc* removal of certain terms from the governing equations, resulting in a balance between Coriolis and viscous forces. The literature on Ekman flows is extensive; for some recent results, see, for instance, Grisogono (1995); Lewis and Belcher (2004); Constantin et al. (2020); Constantin (2021); Roberti (2021, 2022); Marynets (2022); Stefanescu (2024); Puntini (2026). However, the use of the *f*-plane approximation is a substantial limitation to the generality of the model, since it is a reasonable approximation only for flows of fairly limited extent. Therefore, it is desirable to have a model in full spherical coordinates, which may be able to capture large-scale flows as well. Unfortunately, the full Navier–Stokes equations in spherical coordinates are intractable analytically; thus, it is necessary to make some approximations while trying to minimise the assumptions required. The approach we will pursue relies on *asymptotic expansions* and has had a well-documented success in fluid mechanics; see, e.g., Chambon et al. (2020); Fernández-Nieto et al. (2010); Balmforth and Liu (2004) for applications to non-Newtonian fluids or Peregrine (1967); Johnson (1980); Constantin and Johnson (2008); Yuan et al. (2025) in the context of water waves. In geophysical fluid dynamics, this method was pioneered by Constantin and Johnson (2017) for the description of ocean gyres and has subsequently been successfully applied to a plethora of problems; see Constantin and Johnson (2018, 2019a,b, 2021, 2023, 2024a); Zhang and Zhang (2025). For a detailed review of similar asymptotic methods in oceanography, we refer to Johnson (2018, 2022).

In the present work, we proceed as follows. We begin with the Navier–Stokes equations, expressed in a rotating system of spherical coordinates, along with the equation of mass conservation and appropriate boundary conditions. Only two simplifications are made *a priori*: we assume the water’s density to be constant above the thermocline and the eddy viscosity to be only depth-dependent. Density stratification seems to have minimal influence on these flows, while the importance of depth-dependent eddy viscosity has been emphasised in the works of Cronin and Kessler (2009) and Cronin and Tozuka (2016). Then, we carefully rescale all the quantities appearing in the equations and identify two tiny parameters, which are independent of each other: the *thin shell parameter* and the *Rossby number*. The former represents the ratio of a depth scale—in our case, the so-called *Ekman depth*—and the radius of the Earth, and is guaranteed to be small regardless of the nature of the flow; the latter is a well-known parameter in physical oceanography

that is typically small for large-scale flows strongly affected by the Coriolis force (cf. the discussion by Kantha and Clayson (2000)). As noted by Constantin and Johnson (2019b), performing an asymptotic expansion first in the thin-shell parameter and then in the Rossby number effectively separates the dynamical effects of the geometry (via the thin-shell parameter) and the properties of the flow due to the dominant time and length scales (via the Rossby number). The novelty of our discussion lies in the choice of the scaling and of the boundary conditions describing the wind stress on the surface of the ocean; both aspects are, in our opinion, an important improvement to the existing literature on this problem in the thin-shell approximation, such as Constantin and Johnson (2019a,b) and Constantin and Johnson (2023). We believe that the strong combination of mathematical rigour and physical accuracy that characterises our derivation and analysis makes it a valuable contribution to the modelling of wind-drift currents.

**Plan of the paper.** The paper is organised as follows. In § 2, after some remarks on the frame of reference and the coordinate system, we first present the governing equations and discuss the boundary conditions in great detail, then proceed to rescaling all quantities and non-dimensionalising the equations and the boundary conditions, thereby identifying the thin-shell parameter and the Rossby number. Then, § 3 is devoted to the derivation of the model through asymptotics: first, we make an asymptotic expansion of all variables with respect to the thin-shell parameter; then, within the leading order equations thus derived, we perform a second asymptotic expansion—now with respect to the Rossby number. In § 3.1, we derive the leading-order problem for the Ekman flow away from the equator by splitting the solution into a geostrophic and an ageostrophic (Ekman) part; in § 3.2, we investigate the problem for the first-order correction with respect to the Rossby number. Some analytical results are presented in § 4: in particular, we prove the existence and the uniqueness of the solution to the problem for the leading-order Ekman flow and show that this solution describes a classical Ekman spiral, analyse the surface deflection angle (that is, the angle between the direction of the wind and the induce wind-drift current on the surface), and provide *a priori* bounds for the first-order correction in terms of the solution at leading order. Finally, in § 5, we discuss some concrete examples of explicit eddy viscosity profiles, namely: constant (§ 5.1), linearly decaying (§ 5.2), linearly increasing (§ 5.3), piecewise linear (§ 5.4), and exponentially decaying (§ 5.5). Here, we can solve the equation explicitly, draw numerical plots that help to visualise the flow, and calculate the surface deflection angle—using the theory developed in § 4—as well as the integrated mass transport due to the Ekman current.

## 2. GOVERNING EQUATIONS

In this section, we will first present the equations of motion and the boundary conditions, then we will introduce an appropriate scaling and non-dimensionalise the problem. In the following, we use primes to denote physical (dimensional) quantities; we will remove them when we rescale the variables.

First of all, let us discuss the frame of reference in which the problem is formulated. A suitable coordinate system is the system of (right-handed) spherical coordinates  $(\varphi, \theta, r')$ , where  $\theta \in [-\frac{\pi}{2}, \frac{\pi}{2}]$  is the angle of latitude,  $\varphi \in [0, 2\pi]$  is the angle of longitude, and  $r' \in [0, \infty)$  is the radial distance from the origin. The coordinate change from these spherical coordinates to the standard Cartesian coordinates  $(x', y', z')$  is given by

$$\begin{cases} x' = r' \cos \theta \cos \varphi, \\ y' = r' \cos \theta \sin \varphi, \\ z' = r' \sin \theta, \end{cases}$$

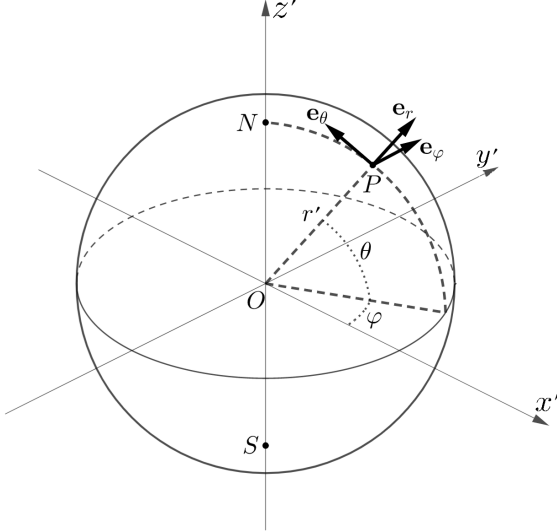


FIGURE 1. The classical spherical coordinate system.

with inverse

$$\begin{cases} \varphi = \tan^{-1} \left( \frac{y'}{x'} \right), \\ \theta = \sin^{-1} \left( \frac{z'}{\sqrt{x'^2 + y'^2 + z'^2}} \right), \\ r' = \sqrt{x'^2 + y'^2 + z'^2}. \end{cases}$$

To each point for which  $r > 0$  and  $\theta \notin \{\pm\frac{\pi}{2}\}$  we can associate the usual local orthonormal basis for  $\mathbb{R}^3$  of unit vectors  $(\mathbf{e}_\varphi, \mathbf{e}_\theta, \mathbf{e}_r)$ :  $\mathbf{e}_\varphi$  points eastward,  $\mathbf{e}_\theta$  northward, and  $\mathbf{e}_r$  radially. The velocity field is denoted by  $\mathbf{u}' = u' \mathbf{e}_\varphi + v' \mathbf{e}_\theta + w' \mathbf{e}_r$ . Note that we must take care to exclude the poles, where the tangent vectors  $\mathbf{e}_\varphi$  and  $\mathbf{e}_\theta$  are not defined, as a consequence of the Hairy Ball Theorem (Renteln, 2013); flows that extend to the poles may be treated, for instance, by rotating the coordinate system and moving the singularities to the equator, as done by Constantin and Johnson (2024b) and Puntini (2025), but we will not pursue this in the present paper. The vectors  $(\mathbf{e}_\varphi, \mathbf{e}_\theta, \mathbf{e}_r)$  are related to the Cartesian unit basis vectors  $(\mathbf{e}_1, \mathbf{e}_2, \mathbf{e}_3)$  through

$$\begin{cases} \mathbf{e}_\varphi = -\sin \varphi \mathbf{e}_1 + \cos \varphi \mathbf{e}_2, \\ \mathbf{e}_\theta = -\cos \varphi \sin \theta \mathbf{e}_1 - \sin \varphi \sin \theta \mathbf{e}_2 + \cos \theta \mathbf{e}_3, \\ \mathbf{e}_r = \cos \varphi \cos \theta \mathbf{e}_1 + \sin \varphi \cos \theta \mathbf{e}_2 + \sin \theta \mathbf{e}_3. \end{cases}$$

See figure 1 for a sketch of these spherical coordinates.

Moreover, it is crucial to point out that, denoting by  $\boldsymbol{\Omega}'$  the Earth's constant angular velocity, with magnitude  $\Omega' = |\boldsymbol{\Omega}'| \approx 7.29 \cdot 10^{-5} \text{ rad s}^{-1}$ , we choose the reference system so that it rotates about the  $z'$  axis, which is aligned with  $\boldsymbol{\Omega}'$ , at angular speed  $\Omega'$ ; as a result, the Earth appears stationary. Although this choice is advantageous in many ways, it has the drawback of not being inertial, which—as discussed, for example, by Pedlosky (1987), Phillips (1987), and Vallis (2017)—will give rise to additional terms (corresponding to apparent forces) in the momentum equations, namely, the Coriolis force  $2\boldsymbol{\Omega}' \times \mathbf{u}'$  and the centrifugal force  $\boldsymbol{\Omega}' \times (\boldsymbol{\Omega}' \times \mathbf{r}')$ , where  $\mathbf{r}'$  is the position vector.

Since, for most geophysical flows, the Earth's oblateness is not relevant (see the discussions by Constantin and Johnson (2021) and White (2002)), we would like to approximate the Earth's surface as a sphere of radius  $R' \approx 6371 \text{ km}$ . However, some care is needed in

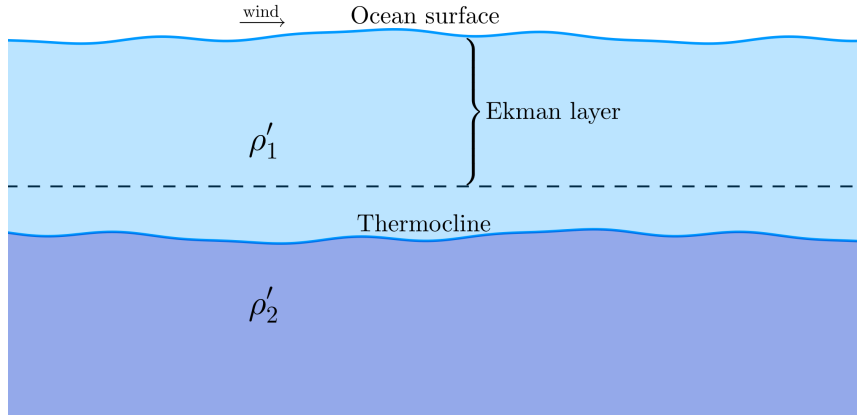


FIGURE 2. Schematic depiction of the flow configuration.

order to minimise the dynamical error due to this approximation. Let us first define the *geopotential*  $\Phi'$  as the sum of the gravitational potential and the term  $-\frac{1}{2}\Omega'^2\ell^2$ , where  $\ell$  is the distance of  $\mathbf{r}'$  from the axis of rotation. Over time, Earth has developed an equatorial bulge to counteract the centrifugal force, making the *geopotential force* (or *effective gravity*)  $\mathbf{g}' = -\nabla\Phi'$  act everywhere nearly perpendicularly to the Earth's surface; in other words, the Earth's surface is essentially a level set of the geopotential  $\Phi'$ . Therefore, we choose to treat the level sets of the geopotential  $\Phi$  (which, in reality, would be rotation ellipsoids of tiny eccentricity) as if they were perfect spheres. Thus, in this approximation, the horizontal component of effective gravity vanishes, and we replace a potentially significant dynamic error with a minor geometric error; the geopotential  $\Phi'$  then depends solely on the vertical coordinate, and, for many applications, we can approximate  $\Phi'(r') = g'r'$ . Given that the Earth's oblateness is minimal, the spherical approximation provides a highly accurate representation of the spheroid.

**2.1. The equations of motion.** Before we proceed to write down the equations of motion, we ought to make some comments about the density (henceforth denoted by  $\rho'$ ). In the ocean, density variations are very small in the upper ocean above the so-called *thermocline*, a very thin layer where, within a depth of a few metres, the temperature decreases and the density increases abruptly, only to once again vary very little at further depths; see the data provided by [Vallis \(2017\)](#). As a first approximation, the thermocline can be reasonably modelled as a sharp interface that, as such, behaves like an internal wave (see, for example, [Henry and Villari \(2022\)](#)). Therefore, we can model the ocean as a stably stratified fluid of two layers of respective density  $\rho'_1$  and  $\rho'_2$ , with  $\rho'_1 < \rho'_2$ ; the boundary of these two layers is the thermocline,  $\rho'_2$  is the water density in the deeper layer, and  $\rho'_1$  is the water density between the surface and the thermocline. Since the object of our analysis is the Ekman layer, which is the water layer below the surface where the frictional effects due to the wind are relevant and which is observed to lie, usually, above the thermocline, for our purposes we can simply assume the density  $\rho' = \rho'_1$  in the equations of motion to be constant, analogously to [Constantin and Johnson \(2024a\)](#) and [Constantin and Johnson \(2019b\)](#), disregarding the dynamics below the Ekman layer. See figure 2 for an illustration of this situation. Nevertheless, considering (continuous) density variations in the vertical direction might be an interesting object of further research.

Having settled this, we can present the equations of motion within the upper layer above the thermocline. The Navier–Stokes equations in spherical rotating coordinates for

constant density are (Puntini, 2025):

$$\begin{aligned}
& \left( \frac{\partial}{\partial t'} + \frac{u'}{r' \cos \theta} \frac{\partial}{\partial \varphi} + \frac{v'}{r'} \frac{\partial}{\partial \theta} + w' \frac{\partial}{\partial r'} \right) \begin{pmatrix} u' \\ v' \\ w' \end{pmatrix} \\
& + \frac{1}{r'} \begin{pmatrix} -u'v' \tan \theta + u'w' \\ u'^2 \tan \theta + v'w' \\ -u'^2 - v'^2 \end{pmatrix} + 2\Omega' \begin{pmatrix} -v' \sin \theta + w' \cos \theta \\ u' \sin \theta \\ -u' \cos \theta \end{pmatrix} \\
& = -\frac{1}{\rho'} \nabla' P' + A'_v \left( \frac{\partial^2}{\partial r'^2} + \frac{2}{r'} \frac{\partial}{\partial r'} \right) \begin{pmatrix} u' \\ v' \\ w' \end{pmatrix} + \frac{A'_h}{r'^2} \left( \frac{1}{\cos^2 \theta} \frac{\partial^2}{\partial \varphi^2} + \frac{\partial^2}{\partial \theta^2} - \tan \theta \frac{\partial}{\partial \theta} \right) \begin{pmatrix} u' \\ v' \\ w' \end{pmatrix} \\
& - \frac{1}{r'^2 \cos^2 \theta} \begin{pmatrix} A'_h u \\ A'_h v \\ 2A'_v (w' \cos^2 \theta - v' \sin \theta \cos \theta) \end{pmatrix} + \frac{2A'_h}{r'^2} \frac{\partial}{\partial \theta} \begin{pmatrix} 0 \\ w' \\ -v' \end{pmatrix} \\
& + \frac{2A'_h}{r'^2 \cos \theta} \frac{\partial}{\partial \phi} \begin{pmatrix} w' - v' \tan \theta \\ u' \tan \theta \\ -u' \end{pmatrix} + \frac{dA'_v}{dr'} \begin{pmatrix} r' \frac{\partial}{\partial r'} \left( \frac{u'}{r'} \right) \\ r' \frac{\partial}{\partial r'} \left( \frac{v'}{r'} \right) \\ 2 \frac{\partial w'}{\partial r'} \end{pmatrix} + \frac{dA'_h}{dr'} \begin{pmatrix} \frac{1}{r' \cos \theta} \frac{\partial w'}{\partial \phi} \\ \frac{1}{r'} \frac{\partial w'}{\partial \theta} \\ 0 \end{pmatrix}, \tag{2.1}
\end{aligned}$$

where

$$\nabla' = \left( \frac{1}{r' \cos \theta} \frac{\partial}{\partial \varphi}, \frac{1}{r'} \frac{\partial}{\partial \theta}, \frac{\partial}{\partial r'} \right)^T,$$

$P'$  is a modified pressure defined through

$$P'(\varphi, \theta, r', t') = \rho' g'(r' - R') - p'(\varphi, \theta, r', t'), \tag{2.2}$$

for the usual pressure  $p'$ , the Earth's average radius  $R' \approx 6371$  km and the average gravitational acceleration  $g' \approx 9.81 \text{ m s}^{-2}$  at ground level, and

$$A'_h = \frac{\mu'_h}{\rho'} \quad \text{and} \quad A'_v = \frac{\mu'_v}{\rho'} \tag{2.3}$$

are the horizontal and vertical kinematic eddy viscosities, corresponding to the dynamic (effective) horizontal and vertical viscosities  $\mu'_h$  and  $\mu'_v$ , which are assumed to vary only with respect to depth. We note that the concept of eddy viscosity represents a simple model for the closure of the turbulence problem, based on the hypothesis that Reynolds stresses are proportional to the mean velocity gradient (and thus depend on flow conditions) but do not represent a physical characteristic of the fluid (Pedlosky, 1987; Pope, 2000).

In addition to the Navier–Stokes equation, which expresses Newton's second law, we have the continuity equation in spherical coordinates, describing conservation of mass within the fluid bulk. For constant density, this reduces to the incompressibility condition

$$\frac{1}{r' \cos \theta} \frac{\partial u'}{\partial \varphi} + \frac{1}{r' \cos \theta} \frac{\partial}{\partial \theta} (v' \cos \theta) + \frac{1}{r'^2} \frac{\partial}{\partial r'} (r'^2 w') = 0. \tag{2.4}$$

**2.2. Boundary conditions.** Let us now discuss the boundary conditions that characterise the dynamics of the Ekman layer. At the free surface of the ocean, which we assume to be described by the equation

$$r' = R' + h'(\varphi, \theta, t'),$$

for an unknown function  $h'$ , we impose the dynamic boundary condition

$$p' = P_s \quad \text{on } \{r' = R' + h'(\varphi, \theta, t')\}, \tag{2.5}$$

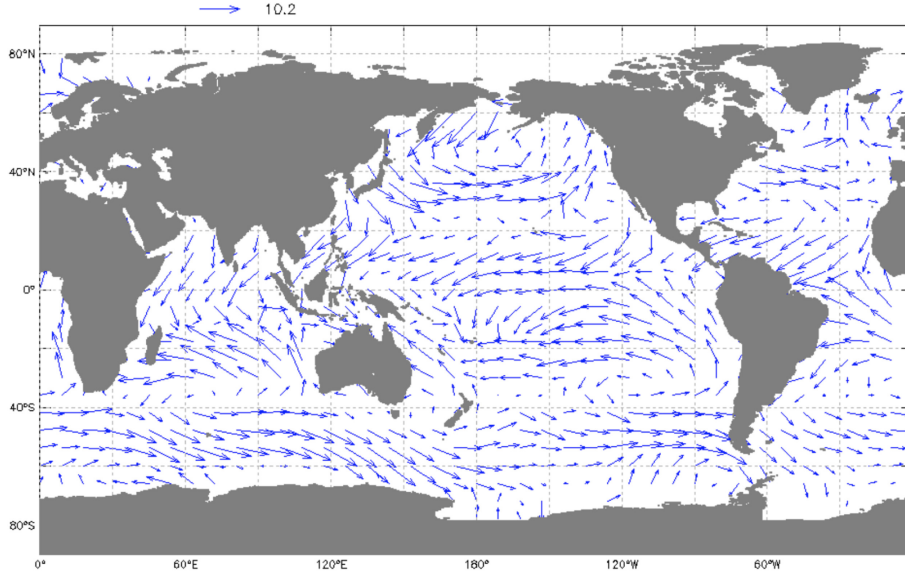


FIGURE 3. Monthly-averaged ocean wind speed and direction vectors, with vector lengths proportional to the reference scale (in  $\text{m s}^{-1}$ ), based on observations from NASA's QuikSCAT satellite. Image credit: NOAA.

where  $P_s$  is the given (and, in general, non-constant) surface (atmospheric) pressure, and the kinematic boundary condition

$$w' = \frac{\partial h'}{\partial t'} + \frac{u'}{r' \cos \theta} \frac{\partial h'}{\partial \varphi} + \frac{v'}{r'} \frac{\partial h'}{\partial \theta} \quad \text{on } \{r' = R' + h'(\varphi, \theta, t')\}, \quad (2.6)$$

which ensures that no fluid particles escape the fluid via the free surface.

Furthermore, since our goal is to describe wind-driven currents, we need an expression for the stress generated by the wind blowing over the water. This is given by the bulk formula

$$\tau'_a = \rho'_a C_{aw} |\mathbf{u}'_a - \mathbf{u}'| (\mathbf{u}'_a - \mathbf{u}') \quad \text{on } \{r' = R' + h'(\varphi, \theta, t')\} \quad (2.7)$$

(Soloviev and Lucas, 2014), where  $\rho'_a$  is the density of the air,  $C_{aw}$  is the non-dimensional drag coefficient of air over water and  $\mathbf{u}'_a = u'_a \mathbf{e}_\varphi + v'_a \mathbf{e}_\theta$  is the horizontal wind velocity, conventionally measured at 10 m above the sea surface. For estimates of the order of magnitude, we follow Soloviev and Lucas (2014) and set

$$C_{aw} \approx \begin{cases} 1.1 \cdot 10^{-3} & \text{for } |\mathbf{u}'_a| \lesssim 5 \text{ m s}^{-1}, \\ (0.61 + 0.063|\mathbf{u}'_a|) \cdot 10^{-3} & \text{for } 5 \text{ m s}^{-1} \lesssim |\mathbf{u}'_a| \lesssim 22 \text{ m s}^{-1}, \end{cases}$$

where the second expression corresponds to the linear parameterisation proposed by Smith (1988). This relation is consistent with a mean wind stress of magnitude 0.01–0.1  $\text{N m}^{-2}$  on the ocean surface (see the data by Paldor (2024) and Talley et al. (2011)). More detailed formulations for  $C_{aw}$  are available (e.g., Yelland and Taylor (1996)), but such precision is unnecessary here, as only the order of magnitude is required. Moreover, for wind speeds exceeding 22  $\text{m s}^{-1}$ , reliable formulations for the drag coefficient are difficult to obtain, as pointed out by Soloviev and Lucas (2014), although such extreme wind conditions are rare and typically occur only as short-lived gusts and thus are not relevant for our present analysis. See figure 3 and Trenberth et al. (1990) for data on the mean wind velocity over the ocean.

The bulk formula (2.7) provides us with an additional boundary condition for our problem. In fact, on the surface of the ocean, the shear stress is given by

$$\tau'_w(\varphi, \theta, t') = \rho' A'_v \left( \frac{\partial u'}{\partial r'} \mathbf{e}_\varphi + \frac{\partial v'}{\partial r'} \mathbf{e}_\theta \right) \quad \text{on } \{r' = R' + h'(\varphi, \theta, t')\},$$

where  $A'_v$  is the vertical kinematic viscosity introduced in (2.3), and consequently, in view of (2.7), the continuity of the stress across the water surface yields

$$\rho' A'_v \begin{pmatrix} \frac{\partial u'}{\partial r'} \\ \frac{\partial v'}{\partial r'} \end{pmatrix} = \rho'_a C_{aw} \sqrt{(u'_a - u')^2 + (v'_a - v')^2} \begin{pmatrix} u'_a - u' \\ v'_a - v' \end{pmatrix} \quad \text{on } \{r' = R' + h'(\varphi, \theta, t')\}. \quad (2.8)$$

Finally, recall that the flow we are considering is located in the layer between the free surface and the thermocline, which we assume to be described by the equation

$$r' = R' + d'(\varphi, \theta, t'),$$

for an unknown function satisfying  $d'(\varphi, \theta, t') < h'(\varphi, \theta, t')$  for all  $(\varphi, \theta, t')$ . Then, analogously as on the free surface, on the thermocline we have a kinematic boundary condition that reads

$$w' = \frac{\partial h'}{\partial t'} + \frac{u'}{r' \cos \theta} \frac{\partial h'}{\partial \varphi} + \frac{v'}{r'} \frac{\partial h'}{\partial \theta} \quad \text{on } \{r' = R' + d'(\varphi, \theta, t')\} \quad (2.9)$$

and a dynamic boundary condition stating that the pressure must be continuous across the thermocline. However, since the Ekman layer will be located above the thermocline and we are not interested in the dynamics below the thermocline, these conditions will be of little importance for us.

**2.3. Scaling and non-dimensionalisation.** Clearly, the Navier–Stokes equations (2.1) are intractable by analytical means in their full generality. In order to simplify them, we will be guided by the scaling of the variables appearing in the equations; through this, we will be able to identify the terms in the equations that contribute the most and those that, on the contrary, may be neglected with little error. To this end, we non-dimensionalise the equations (2.1) and (2.4) according to the scaling

$$\begin{aligned} r' &= R' + D' z, & (u', v', w') &= U'(u, v, kw), & P' &= \rho' U' \Omega' R' P, \\ t' &= \frac{R'}{U'} t, & A'_h(r') &= \frac{\bar{\mu}'_h}{\rho'} n(z) = \bar{A}'_h n(z), & A'_v(r') &= \frac{\bar{\mu}'_v}{\rho'} m(z) = \bar{A}'_v m(z), \end{aligned} \quad (2.10)$$

where

$$D' = \sqrt{\frac{\bar{A}'_v}{\Omega'}} \approx 12 \text{ m}$$

is the classical *Ekman depth*,  $U'$  an appropriate speed scale (typically,  $U' \approx 0.1 \text{ m s}^{-1}$  in the ocean),  $k$  a scaling factor that will be determined below, and  $\bar{\mu}'_h$ ,  $\bar{\mu}'_v$  [ $\bar{A}'_h$ ,  $\bar{A}'_v$ ] are the typical (mean) values for the horizontal and vertical dynamic [kinematic] eddy viscosity on the surface, respectively. A typical value for the vertical eddy viscosity, in the context of oceanic surface-flows, is  $\bar{A}'_v \approx 0.01 \text{ m}^2 \text{ s}^{-1}$  (Kamenkovich, 1977; Wenegrat et al., 2014), while a value for the horizontal kinematic viscosity is difficult to obtain. In fact, the vertical eddy viscosity is usually computed from *in situ* observations via the formula

$$A'_v = \frac{\tau'}{\rho' \frac{\partial u'}{\partial r'}} \quad \text{on } \{r' = R' + h'(\varphi, \theta, t')\}$$

(see, e.g., Wenegrat et al. (2014)), where  $\tau'$  is the wind stress; all quantities in this formula can be computed from the observational data. This equation for the vertical eddy viscosity is closely connected to the formula for the Reynolds stresses in a simple shear flow (Pope,

2000). An analogous expression to compute  $A_h$  from easily obtainable oceanographic observations is, to the best of our knowledge, not available in the literature; hence, the difficulty in obtaining estimates for  $A_h$ . Nevertheless, it is possible to say that  $\bar{A}'_h \gg \bar{A}'_v$ , with  $\bar{A}'_h/\bar{A}'_v$  typically of order  $10^3$  (Pedlosky, 1987; Constantin and Johnson, 2018; Constantin, 2022; Talley et al., 2011). It is convenient to denote the ratio between the kinematic eddy viscosities by

$$\nu = \frac{\bar{A}'_h}{\bar{A}'_v}.$$

Let us now define the non-dimensional parameters

$$\varepsilon = \frac{D'}{R'} \approx 2 \cdot 10^{-6} \quad \text{and} \quad \mathcal{R} = \frac{U'}{\Omega' R'} \approx 2 \cdot 10^{-4};$$

the former is the *thin-shell parameter* (the ratio of the Ekman length and the Earth's average radius), and the latter is the inverse Rossby number (a well-known parameter in oceanography, defined as the ratio between the scales of the advective terms and the Coriolis terms in the Navier–Stokes equations). Intuitively, a small Rossby number indicates that the advective terms are dominated by the Coriolis terms; this is usually the case for large-scale oceanic flows (cf. the discussion by Kantha and Clayson (2000) and Vallis (2017)).

We can now argue that the only consistent choice for the scaling parameter  $k$  in (2.10) is  $k = \varepsilon$ . Indeed, given the particle trajectories  $t' \mapsto \Phi(t') = (\varphi(t'), \theta(t'), r'(t'))$  in spherical coordinates, the velocity components are

$$\begin{aligned} u'(\Phi(t'), t') &= r'(t') \cos \theta(t') \frac{d\varphi(t')}{dt'}, \\ v'(\Phi(t'), t') &= r'(t') \frac{d\theta(t')}{dt'}, \\ w'(\Phi(t'), t') &= \frac{dr'(t')}{dt'}, \end{aligned}$$

hence, with the choices  $r' = R' + D'z = R'(1 + \varepsilon z)$ ,  $t' = T't$ , and  $U' = \frac{R'}{T'}$  as in (2.10), we see that

$$\begin{aligned} u' &= U'(1 + \varepsilon z) \cos \theta \frac{d\varphi}{dt}, \\ v' &= U'(1 + \varepsilon z) \frac{d\theta}{dt}, \\ w' &= \varepsilon U' \frac{dz}{dt}. \end{aligned}$$

Comparing with (2.10), we see that the only consistent choice for the scaling factor  $k$  in (2.10) is  $k = \varepsilon$ . This conclusion corroborates the argument of Constantin and Johnson (2019b) that having  $k = o(\varepsilon)$  as  $\varepsilon \searrow 0$  implies that the solution is valid only in a small region.

In view of these considerations, we can write down the non-dimensionalisation of (2.1). Its first two components are

$$\begin{aligned}
& \mathcal{R} \left( \frac{\partial}{\partial t} + \frac{u}{(1+\varepsilon z) \cos \theta} \frac{\partial}{\partial \varphi} + \frac{v}{1+\varepsilon z} \frac{\partial}{\partial \theta} + w \frac{\partial}{\partial z} \right) \begin{pmatrix} u \\ v \end{pmatrix} \\
& + \frac{\mathcal{R}}{1+\varepsilon z} \begin{pmatrix} -uv \tan \theta + \varepsilon uw \\ u^2 \tan \theta + \varepsilon vw \end{pmatrix} + 2 \begin{pmatrix} -v \sin \theta + \varepsilon w \cos \theta \\ u \sin \theta \end{pmatrix} \\
& = -\frac{1}{1+\varepsilon z} \begin{pmatrix} \frac{1}{\cos \theta} \frac{\partial P}{\partial \varphi} \\ \frac{\partial P}{\partial \theta} \end{pmatrix} + m \left( \frac{\partial^2}{\partial z^2} + \frac{2\varepsilon}{(1+\varepsilon z)} \frac{\partial}{\partial z} \right) \begin{pmatrix} u \\ v \end{pmatrix} \\
& + \frac{\varepsilon^2 \nu n}{(1+\varepsilon z)^2} \left( \frac{1}{\cos^2 \theta} \frac{\partial^2}{\partial \varphi^2} + \frac{\partial^2}{\partial \theta^2} - \tan \theta \frac{\partial}{\partial \theta} \right) \begin{pmatrix} u \\ v \end{pmatrix} \\
& - \frac{\varepsilon^2 \nu n}{(1+\varepsilon z)^2 \cos^2 \theta} \begin{pmatrix} u \\ v \end{pmatrix} + \frac{2\varepsilon^2 \nu n}{(1+\varepsilon z)^2} \left( \frac{\partial}{\partial \theta} \begin{pmatrix} 0 \\ \varepsilon w \end{pmatrix} + \frac{1}{\cos \theta} \frac{\partial}{\partial \varphi} \begin{pmatrix} \varepsilon w - v \tan \theta \\ u \tan \theta \end{pmatrix} \right) \\
& + \frac{dm}{dz} \begin{pmatrix} \frac{\partial u}{\partial z} - \frac{u\varepsilon}{(1+\varepsilon z)^2} \\ \frac{\partial v}{\partial z} - \frac{v\varepsilon}{(1+\varepsilon z)^2} \end{pmatrix} + \varepsilon^2 \nu \frac{dn}{dz} \begin{pmatrix} \frac{1}{(1+\varepsilon z) \cos \theta} \frac{\partial w}{\partial \varphi} \\ \frac{1}{(1+\varepsilon z)} \frac{\partial w}{\partial \theta} \end{pmatrix}, \tag{2.11}
\end{aligned}$$

while the third component is

$$\begin{aligned}
& \varepsilon^2 \mathcal{R} \left( \frac{\partial w}{\partial t} + \frac{u}{(1+\varepsilon z) \cos \theta} \frac{\partial w}{\partial \varphi} + \frac{v}{(1+\varepsilon z)} \frac{\partial w}{\partial \theta} + w \frac{\partial w}{\partial z} \right) \\
& - \frac{\varepsilon \mathcal{R}}{1+\varepsilon z} (u^2 + v^2) - 2u\varepsilon \cos \theta \\
& = -\frac{\partial P}{\partial z} + \varepsilon^2 m \left( \frac{\partial^2 w}{\partial z^2} + \frac{2\varepsilon}{(1+\varepsilon z)} \frac{\partial w}{\partial z} \right) \\
& + \frac{\varepsilon^4 \nu n}{(1+\varepsilon z)^2} \left( \frac{1}{\cos^2 \theta} \frac{\partial^2 w}{\partial \varphi^2} + \frac{\partial^2 w}{\partial \theta^2} - \tan \theta \frac{\partial w}{\partial \theta} \right) \\
& - \frac{2\varepsilon^3 m}{(1+\varepsilon z)^2 \cos^2 \theta} (\varepsilon w \cos^2 \theta - v \sin \theta \cos \theta) \\
& - \frac{2\varepsilon^3 \nu n}{(1+\varepsilon z)^2} \left( \frac{\partial v}{\partial \theta} + \frac{1}{\cos \theta} \frac{\partial u}{\partial \varphi} \right) + 2\varepsilon^2 \frac{dm}{dz} \frac{\partial w}{\partial z}. \tag{2.12}
\end{aligned}$$

Similarly, from the continuity equation (2.4) we end up with the non-dimensional equation

$$(1+\varepsilon z) \left[ \frac{\partial u}{\partial \varphi} + \frac{\partial}{\partial \theta} (v \cos \theta) \right] + \cos \theta \frac{\partial}{\partial z} ((1+\varepsilon z)^2 w) = 0. \tag{2.13}$$

Analogously to the equations of motion, we have to non-dimensionalise the boundary conditions as well. In order to do so, we start from the upper and lower kinematic boundary condition. Setting  $h' = D'h$  and  $d' = D'd$ , the equations (2.6) and (2.9) become

$$\varepsilon w = \frac{\partial h}{\partial t} + \frac{u}{(1+\varepsilon z) \cos \theta} \frac{\partial h}{\partial \varphi} + \frac{v}{(1+\varepsilon z)} \frac{\partial h}{\partial \theta} \quad \text{on } \{z = h\} \tag{2.14}$$

and

$$\varepsilon w = \frac{\partial d}{\partial t} + \frac{u}{(1+\varepsilon z) \cos \theta} \frac{\partial d}{\partial \varphi} + \frac{v}{(1+\varepsilon z)} \frac{\partial d}{\partial \theta} \quad \text{on } \{z = d\}, \tag{2.15}$$

respectively. For the dynamic boundary condition, in view of (2.2) and (2.10), we have

$$P = \frac{p' + \rho' g' (r' - R')}{\rho' U' \Omega' R'},$$

hence, because of (2.5), on the free surface we have

$$P = P_s + \wp h \quad \text{on } \{z = h\}, \tag{2.16}$$

where

$$P_s = \frac{P'_s}{\rho' U' \Omega' R'} \quad \text{and} \quad \varphi = \frac{g' D'}{U' \Omega' R'}.$$

Finally, writing  $(u'_a, v'_a) = U'(u_a, v_a)$ , the non-dimensional form of (2.8) is

$$\begin{pmatrix} \frac{\partial u}{\partial z} \\ \frac{\partial v}{\partial z} \end{pmatrix} = \mathcal{C}_{aw} \sqrt{(u_a - u)^2 + (v_a - v)^2} \begin{pmatrix} u_a - u \\ v_a - v \end{pmatrix} \quad \text{on } \{z = h\}, \quad (2.17)$$

where we have introduced the non-dimensional parameter

$$\mathcal{C}_{aw} = \frac{\rho'_a U' D'}{\rho' A'_v} C_{aw}.$$

With  $U' \approx 0.1 \text{ m s}^{-1}$ ,  $A'_v \approx 0.01 \text{ m}^2 \text{ s}^{-1}$ ,  $D' \approx 12 \text{ m}$ ,  $\rho'_a/\rho' \approx 10^{-3}$  and  $C_{aw} \approx 10^{-3}$ , we can estimate the order of magnitude of  $\mathcal{C}_{aw}$  as

$$\mathcal{C}_{aw} \approx 10^{-4}.$$

### 3. ASYMPTOTICS

Now that the equations have been non-dimensionalised, we would like to exploit the smallness of the parameters  $\varepsilon$  and  $\mathcal{R}$  to simplify the problem. In order to do so rigorously and consistently, we first recall some basic notions from the theory of asymptotic expansions.

**Definition 3.1.** *We say that a sequence  $\{\phi_0, \phi_1, \dots\}$  of functions defined in a neighbourhood of  $\epsilon_0$  is an asymptotic sequence (or well ordered) as  $\epsilon \searrow \epsilon_0$ , if  $\phi_{m+1}(\epsilon) = o(\phi_m(\epsilon))$  as  $\epsilon \searrow \epsilon_0$  for all  $m$ . Moreover, if  $\{\phi_0, \phi_1, \dots\}$  is an asymptotic sequence, then we say that the function  $f$  has an asymptotic expansion to  $n$  terms, with respect to this sequence, if*

$$f(\epsilon) = \sum_{k=0}^m a_k \phi_k(\epsilon) \quad \text{as } \epsilon \searrow \epsilon_0 \text{ for } m = 0, \dots, n,$$

where the coefficients  $a_k$  are independent of  $\epsilon$ . In this case, we write

$$f \sim a_1 \phi_0(\epsilon) + \dots + a_n \phi_n(\epsilon) \quad \text{as } \epsilon \searrow \epsilon_0. \quad (3.1)$$

It is crucial to note that, unlike, for example, a Taylor series, an asymptotic expansion is a statement about the limit  $\epsilon \searrow \epsilon_0$ , not about the limit  $n \rightarrow \infty$ ; adding more terms to the expansion does not necessarily increase its accuracy. In fact, an asymptotic expansion such as (3.1) may not converge for  $n \rightarrow \infty$  in the first place, and even if it does, it does not necessarily converge to the function that was expanded; the standard example of a divergent asymptotic expansion is that of the Bessel function  $J_0$ . However, this is not a shortcoming: the asymptotic approach is designed to uncover the mathematical structure of the problem, which it achieves effectively, and its usefulness lies in the simple approximation of a function in the neighbourhood of a point through a few terms. We refer to Van Dyke (1975), Johnson (2005), and Holmes (2015) for more details on the theory of asymptotic expansions, as well as to Hardy (1949) for techniques needed when dealing with and interpreting divergent series.

Asymptotic expansions can be a valuable tool when looking for approximate solutions to differential equations that, in their full generality, are intractable—as is the case for us with the full Navier–Stokes equations (2.11)–(2.12). The idea is to exploit the smallness of the parameters  $\varepsilon$  and  $\mathcal{R}$  to seek asymptotic expansions of the unknowns, which should provide us at least with viable approximations of the full solution. Note that  $\phi_k(\epsilon) = \epsilon^k$ ,

$k = 0, 1, \dots$ , is an asymptotic sequence. First, let us forget about  $\mathcal{R}$  for the moment and make the ansatz

$$q(\varphi, \theta, z, t; \varepsilon) = q_0(\varphi, \theta, z, t) + o(\varepsilon) \quad \text{as } \varepsilon \searrow 0, \quad (3.2)$$

where  $q$  (and, correspondingly,  $q_0$ ) represents each of the variables  $u, v, w, P, h$ . This ansatz is motivated by the structure of (2.11) and (2.12), where  $\varepsilon$  appears only in integer powers, as well as through  $(1 + \varepsilon z)^{-1} = 1 - \varepsilon z + o(\varepsilon)$ . Plugging (3.2) into (2.11) and equating the coefficients of the various powers of  $\varepsilon$ , we obtain, at the leading order with respect to  $\varepsilon$ ,

$$\begin{aligned} \mathcal{R} \left\{ \left( \frac{\partial}{\partial t} + \frac{u_0}{\cos \theta} \frac{\partial}{\partial \varphi} + v_0 \frac{\partial}{\partial \theta} + w_0 \frac{\partial}{\partial z} \right) \begin{pmatrix} u_0 \\ v_0 \end{pmatrix} + \begin{pmatrix} -u_0 v_0 \tan \theta \\ u_0^2 \tan \theta \end{pmatrix} \right\} \\ + 2 \begin{pmatrix} -v_0 \sin \theta \\ u_0 \sin \theta \end{pmatrix} + \begin{pmatrix} \frac{1}{\cos \theta} \frac{\partial P_0}{\partial \varphi} \\ \frac{\partial P_0}{\partial \theta} \end{pmatrix} - \frac{\partial}{\partial z} \left( m \frac{\partial}{\partial z} \begin{pmatrix} u_0 \\ v_0 \end{pmatrix} \right) = 0, \end{aligned} \quad (3.3)$$

while from (2.12) we get

$$\frac{\partial P_0}{\partial z} = 0,$$

and the continuity equation (2.13) yields

$$\frac{\partial u_0}{\partial \varphi} + \frac{\partial}{\partial \theta} (v_0 \cos \theta) + \cos \theta \frac{\partial w_0}{\partial z} = 0. \quad (3.4)$$

From the kinematic boundary conditions (2.14) and (2.15), we obtain

$$\frac{\partial h_0}{\partial t} + \frac{u_0}{\cos \theta} \frac{\partial h_0}{\partial \varphi} + v_0 \frac{\partial h_0}{\partial \theta} = 0 \quad \text{on } \{z = h_0\} \quad (3.5)$$

and

$$\frac{\partial d_0}{\partial t} + \frac{u_0}{\cos \theta} \frac{\partial d_0}{\partial \varphi} + v_0 \frac{\partial d_0}{\partial \theta} = 0 \quad \text{on } \{z = d_0\}. \quad (3.6)$$

Equations (3.5) and (3.6) tell us that  $h_0$  and  $d_0$  are invariants of the fluid flow. For the remainder of this paper, we will assume  $h_0$  and  $d_0$  to be simple flat surfaces, that is,

$$h_0(\varphi, \theta, t) = 0 \quad \text{and} \quad d_0(\varphi, \theta, t) \equiv d_0 = \text{const.}$$

Note that the presence of a flat free surface—meaning the absence of surface waves—is compatible with the asymptotic behaviour of the governing equations under the scaling given in (2.10) with  $k = \varepsilon$ , which is specific to the problem at hand. Surface waves typically arise when the vertical and horizontal velocity components,  $w'$  and  $u', v'$ , are of the same order of magnitude (Soloviev and Lucas, 2014). However, a key feature of our flow model is that the vertical velocity  $w'$  is smaller than the horizontal components  $u'$  and  $v'$  by a factor of  $\varepsilon$ , which prevents the formation of such waves. With this assumption on the free surface, the dynamic boundary condition (2.16) is simply

$$P_0(\varphi, \theta) = P_s(\varphi, \theta) \quad \text{on } \{z = 0\},$$

and the upper boundary condition (2.17) for the wind stress gives

$$\begin{pmatrix} \frac{\partial u_0}{\partial z} \\ \frac{\partial v_0}{\partial z} \end{pmatrix} = \mathcal{C}_{aw} \sqrt{(u_a - u_0)^2 + (v_a - v_0)^2} \begin{pmatrix} u_a - u_0 \\ v_a - v_0 \end{pmatrix} \quad \text{on } \{z = 0\}. \quad (3.7)$$

The next step is to perform a second asymptotic expansion, this time with respect to  $\mathcal{R}$ , within the leading-order equations with respect to  $\varepsilon$  that we have derived. To this end, let us make the ansatz

$$q_0(\varphi, \theta, z, t; \mathcal{R}) \sim \tilde{q}(\varphi, \theta, y, t) + \mathcal{R} \hat{q}(\varphi, \theta, y, t) + o(\mathcal{R}), \quad (3.8)$$

where, as in (3.2),  $q$  denotes each of the variables  $u$ ,  $v$ ,  $w$ , and  $P$ . Plugging (3.8) into (3.3) and collecting terms of the same order in  $\mathcal{R}$ , we see that

$$\begin{aligned} & \left\{ 2 \begin{pmatrix} -\tilde{v} \sin \theta \\ \tilde{u} \sin \theta \end{pmatrix} + \begin{pmatrix} \frac{1}{\cos \theta} \frac{\partial \tilde{P}}{\partial \varphi} \\ \frac{\partial \tilde{P}}{\partial \theta} \end{pmatrix} - \frac{\partial}{\partial z} \left( m \frac{\partial}{\partial z} \begin{pmatrix} \tilde{u} \\ \tilde{v} \end{pmatrix} \right) \right\} \\ & + \mathcal{R} \left\{ \left( \frac{\partial}{\partial t} + \frac{\tilde{u}}{\cos \theta} \frac{\partial}{\partial \varphi} + \tilde{v} \frac{\partial}{\partial \theta} + \tilde{w} \frac{\partial}{\partial z} \right) \begin{pmatrix} \tilde{u} \\ \tilde{v} \end{pmatrix} + \begin{pmatrix} -\tilde{u} \tilde{v} \tan \theta \\ \tilde{u}^2 \tan \theta \end{pmatrix} \right. \\ & \left. + 2 \begin{pmatrix} -\hat{v} \sin \theta \\ \hat{u} \sin \theta \end{pmatrix} + \begin{pmatrix} \frac{1}{\cos \theta} \frac{\partial \hat{P}}{\partial \varphi} \\ \frac{\partial \hat{P}}{\partial \theta} \end{pmatrix} - \frac{\partial}{\partial z} \left( m \frac{\partial}{\partial z} \begin{pmatrix} \hat{u} \\ \hat{v} \end{pmatrix} \right) \right\} + o(\mathcal{R}) = 0, \end{aligned} \quad (3.9)$$

while doing the same in (2.12) yields

$$\frac{\partial \tilde{P}}{\partial z} + \mathcal{R} \frac{\partial \hat{P}}{\partial z} + o(\mathcal{R}) = 0. \quad (3.10)$$

Performing the same procedure in the continuity equation (3.4) leads us to

$$\frac{\partial \tilde{u}}{\partial \varphi} + \frac{\partial}{\partial \theta} (\tilde{v} \cos \theta) + \cos \theta \frac{\partial \tilde{w}}{\partial z} + \mathcal{R} \left\{ \frac{\partial \hat{u}}{\partial \varphi} + \frac{\partial}{\partial \theta} (\hat{v} \cos \theta) + \cos \theta \frac{\partial \hat{w}}{\partial z} \right\} + o(\mathcal{R}) = 0. \quad (3.11)$$

Clearly, for the dynamic boundary condition, we have

$$\tilde{P} + \mathcal{R} \hat{P} + o(\mathcal{R}) = 0 \quad \text{on } \{z = 0\}. \quad (3.12)$$

For the wind stress, plugging (3.8) into (3.7), and using the Taylor expansion  $\sqrt{1+x} = 1 + \frac{1}{2}x + o(x)$  as  $x \rightarrow 0$ , we see that

$$\begin{aligned} \sqrt{(u_a - u)^2 + (v_a - v)^2} &= \sqrt{(u_a - \tilde{u})^2 + (v_a - \tilde{v})^2} \\ &- \mathcal{R} \frac{\hat{u}(u_a - \tilde{u}) + \hat{v}(v_a - \tilde{v})}{\sqrt{(u_a - \tilde{u})^2 + (v_a - \tilde{v})^2}} + o(\mathcal{R}) \quad \text{on } \{z = 0\}. \end{aligned} \quad (3.13)$$

By setting the coefficients of the various powers of  $\mathcal{R}$  to zero in the previous asymptotic expansions, we can write down the problems for the leading-order and first-order dynamics with respect to  $\mathcal{R}$ , as we discuss next.

**3.1. The leading-order problem.** Setting coefficients to zero in (3.9), (3.10), and (3.11), we obtain the leading-order set of equations

$$\left. \begin{aligned} \frac{\partial}{\partial z} \left( m \frac{\partial \tilde{u}}{\partial z} \right) + 2\tilde{v} \sin \theta &= \frac{1}{\cos \theta} \frac{\partial \tilde{P}}{\partial \varphi} \\ \frac{\partial}{\partial z} \left( m \frac{\partial \tilde{v}}{\partial z} \right) - 2\tilde{u} \sin \theta &= \frac{\partial \tilde{P}}{\partial \theta} \\ \frac{\partial \tilde{P}}{\partial z} &= 0 \\ \frac{\partial \tilde{u}}{\partial \varphi} + \frac{\partial}{\partial \theta} (\tilde{v} \cos \theta) + \cos \theta \frac{\partial \tilde{w}}{\partial z} &= 0 \end{aligned} \right\} \quad \text{in } \{d_0 < z < 0\}. \quad (3.14)$$

The dynamic boundary condition (3.12) with (2.16) yields

$$\tilde{P} = P_s \quad \text{on } \{z = 0\}$$

and, from (3.13), we obtain at leading order:

$$\begin{pmatrix} \frac{\partial \tilde{u}}{\partial z} \\ \frac{\partial \tilde{v}}{\partial z} \end{pmatrix} = \mathcal{C}_{aw} \sqrt{(u_a - \tilde{u})^2 + (v_a - \tilde{v})^2} \begin{pmatrix} u_a - \tilde{u} \\ v_a - \tilde{v} \end{pmatrix} \quad \text{on } \{z = 0\}. \quad (3.15)$$

The first two equations in (3.14) are essentially a second-order system of ordinary differential equations with respect to the variable  $z$ , in which the other variables  $\varphi$  and  $\theta$  appear only parametrically. Physically, they describe a three-way balance between the Coriolis force, the horizontal pressure gradient force, and the viscous stress caused by the wind. They are to be solved in the interval  $z \in [z_0, 0]$ , where  $z_0 < 0$  is the fixed depth of the Ekman layer; see figure 2.

Note that there is no longer a time derivative appearing in (3.14); this is due to the fact that, according to the scaling (2.10), the time scales advectively, so the time derivative of the velocity field is multiplied by the Rossby number  $\mathcal{R}$  in the non-dimensional Navier–Stokes equations (2.11) and thus disappears from the leading-order equations. A (parametrical) time dependence at leading order could only be forced via a time varying wind  $(u_a, v_a)$ . Therefore, with this scaling, the model is necessarily essentially steady. In order to have an unsteady model, we would have to choose a much smaller time scale for the time, of the same order as the Rossby number. However, we will not pursue this direction in the present paper, instead possibly deferring it to future research. For some results on unsteady Ekman flows in the  $f$ -plane with linear boundary conditions, we refer the reader, for instance, to Lewis and Belcher (2004); Shrira and Almelah (2020); Roberti (2022); Puntini (2025, 2026).

From now on, we will restrict our attention to flows away from the equator. The reason is that, for  $\theta \neq 0$  it is convenient to perform the usual splitting of the horizontal velocity in a *geostrophic* and an *ageostrophic (Ekman)* component:

$$\begin{pmatrix} \tilde{u} \\ \tilde{v} \end{pmatrix} = \begin{pmatrix} \tilde{u}_g \\ \tilde{v}_g \end{pmatrix} + \begin{pmatrix} \tilde{u}_e \\ \tilde{v}_e \end{pmatrix},$$

where the geostrophic flow  $(\tilde{u}_g, \tilde{v}_g)$  is defined as the solution to the system

$$\left. \begin{aligned} 2\tilde{v}_g \sin \theta &= \frac{1}{\cos \theta} \frac{\partial \tilde{P}}{\partial \varphi} \\ 2\tilde{u}_g \sin \theta &= -\frac{\partial \tilde{P}}{\partial \theta} \end{aligned} \right\} \quad \text{in } \{d_0 < z < 0\}. \quad (3.16)$$

From the third equation in (3.14) (the hydrostatic relation), and assuming sufficient regularity for the pressure, we note that

$$\begin{aligned} \frac{\partial \tilde{v}_g}{\partial z} &= \frac{\partial}{\partial z} \left( \frac{1}{2 \sin \theta \cos \theta} \frac{\partial \tilde{P}}{\partial \varphi} \right) = \frac{1}{2 \sin \theta \cos \theta} \frac{\partial}{\partial \varphi} \left( \frac{\partial \tilde{P}}{\partial z} \right) = 0, \\ \frac{\partial \tilde{u}_g}{\partial z} &= -\frac{\partial}{\partial z} \left( \frac{1}{2 \sin \theta} \frac{\partial \tilde{P}}{\partial \theta} \right) = -\frac{1}{2 \sin \theta} \frac{\partial}{\partial \theta} \left( \frac{\partial \tilde{P}}{\partial z} \right) = 0, \end{aligned} \quad (3.17)$$

namely, the geostrophic component of the velocity does not depend on  $z$  and is thus uniquely determined by the surface pressure:

$$2\tilde{v}_g \sin \theta = \frac{1}{\cos \theta} \frac{\partial P_s}{\partial \varphi} \quad \text{and} \quad 2\tilde{u}_g \sin \theta = -\frac{\partial P_s}{\partial \theta} \quad \text{in } \{d_0 < z < 0\}.$$

Furthermore, note that

$$\frac{\partial \tilde{u}_g}{\partial \varphi} + \frac{\partial}{\partial \theta} (\tilde{v}_g \cos \theta) = 0. \quad (3.18)$$

Introducing the complex notation

$$W = \tilde{u}_e + i\tilde{v}_e \quad \text{and} \quad W_w = u_a - \tilde{u}_g + i(v_a - \tilde{v}_g), \quad (3.19)$$

dropping the (now parametric) dependence on  $\varphi$  and  $\theta$ , and denoting a derivative with respect to  $z$  by a prime for simplicity, we then obtain from (3.14), (3.16) and (3.15):

$$\begin{cases} (m(z)W'(z))' = 2iW(z) \sin \theta, & z_0 < z < 0, \\ W'(0) = \mathcal{C}_{aw} |W_w - W(0)| (W_w - W(0)), \\ W(z_0) = 0 \end{cases} \quad (3.20)$$

for the boundary value that describes the Ekman component of the flow. The third equation in (3.20) guarantees that the Ekman boundary layer correction vanishes below the fixed depth

$$d_0 \leq z_0 < 0,$$

which corresponds to the depth of the Ekman layer; cf. figure 2.

Once an expression for  $\tilde{u}$  and  $\tilde{v}$  is obtained, it is possible to recover  $\tilde{w}$  from the continuity equation (the fourth equation in (3.14)) and (3.18):

$$\tilde{w}(\varphi, \theta, z) = \begin{cases} 0, & d_0 \leq z < z_0, \\ -\frac{1}{\cos \theta} \int_{z_0}^z \left( \frac{\partial \tilde{u}_e}{\partial \varphi}(\varphi, \theta, s) + \frac{\partial}{\partial \theta}(\tilde{v}_e(\varphi, \theta, s) \cos \theta) \right) ds, & z_0 \leq z \leq 0. \end{cases}$$

**3.2. The problem at first order.** Now, let us derive the equations for the first-order correction of the leading-order dynamics. One more setting the coefficients to zero in the asymptotic expansions (3.9), (3.10), (3.11), (3.12), and (3.13), we obtain the problem

$$\left. \begin{array}{l} \frac{\partial}{\partial z} \left( m \frac{\partial \hat{u}}{\partial z} \right) + 2\hat{v} \sin \theta \\ = \frac{1}{\cos \theta} \frac{\partial \hat{P}}{\partial \varphi} - \left( \frac{\tilde{u}}{\cos \theta} \frac{\partial \tilde{u}}{\partial \varphi} + \tilde{v} \frac{\partial \tilde{u}}{\partial \theta} + \tilde{w} \frac{\partial \tilde{u}}{\partial z} \right) + \tilde{u} \tilde{v} \tan \theta \\ \frac{\partial}{\partial z} \left( m \frac{\partial \hat{v}}{\partial z} \right) - 2\hat{u} \sin \theta \\ = \frac{\partial \hat{P}}{\partial \theta} - \left( \frac{\tilde{u}}{\cos \theta} \frac{\partial \tilde{v}}{\partial \varphi} + \tilde{v} \frac{\partial \tilde{v}}{\partial \theta} + \tilde{w} \frac{\partial \tilde{v}}{\partial z} \right) - \tilde{u}^2 \tan \theta \\ \frac{\partial \hat{P}}{\partial z} = 0 \\ \frac{\partial \hat{u}}{\partial \varphi} + \frac{\partial}{\partial \theta}(\hat{v} \cos \theta) + \cos \theta \frac{\partial \hat{w}}{\partial z} = 0 \end{array} \right\} \quad \text{in } \{d_0 < z < 0\}, \quad (3.21)$$

with dynamic boundary condition

$$\hat{P} = 0 \quad \text{on } \{z = 0\}$$

and upper boundary condition due to the wind stress given by

$$\begin{pmatrix} \frac{\partial \hat{u}}{\partial z} \\ \frac{\partial \hat{v}}{\partial z} \end{pmatrix} = -\mathcal{C}_{aw} \left( \sqrt{(u_a - \tilde{u})^2 + (v_a - \tilde{v})^2} \begin{pmatrix} \hat{u} \\ \hat{v} \end{pmatrix} + \frac{\hat{u}(u_a - \tilde{u}) + \hat{v}(v_a - \tilde{v})}{\sqrt{(u_a - \tilde{u})^2 + (v_a - \tilde{v})^2}} \begin{pmatrix} u_a - \tilde{u} \\ v_a - \tilde{v} \end{pmatrix} \right) \quad (3.22)$$

on  $\{z = 0\}$ .

Similarly to what we did for the leading-order equations, for  $\theta \neq 0$  we may split  $\hat{u}$  and  $\hat{v}$  into the sum of a geostrophic and an ageostrophic component:

$$\begin{pmatrix} \hat{u} \\ \hat{v} \end{pmatrix} = \begin{pmatrix} \hat{u}_g \\ \hat{v}_g \end{pmatrix} + \begin{pmatrix} \hat{u}_e \\ \hat{v}_e \end{pmatrix},$$

where  $(\hat{u}_g, \hat{v}_g)$  is defined as the solution to the equations

$$\left. \begin{aligned} 2\hat{v}_g \sin \theta &= \frac{1}{\cos \theta} \frac{\partial \hat{P}}{\partial \varphi} \\ 2\hat{u}_g \sin \theta &= -\frac{\partial \hat{P}}{\partial \theta} \end{aligned} \right\} \quad \text{in } \{d_0 < z < 0\}.$$

From the hydrostatic relation (the third equation in (3.21)) it follows, analogously to (3.17), that

$$\frac{\partial \hat{v}_g}{\partial z} = \frac{\partial \hat{u}_g}{\partial z} = 0,$$

namely, the geostrophic component of the velocity does not depend on  $z$ ; thus, since  $\hat{P} = 0$  on  $z = 0$ , it turns out that, in fact,

$$\hat{u}_g = \hat{v}_g = 0.$$

Therefore, we are left with the problem

$$\left. \begin{aligned} \frac{\partial}{\partial z} \left( m \frac{\partial \hat{u}_e}{\partial z} \right) + 2\hat{v}_e \sin \theta &= \mathcal{F}(\tilde{u}, \tilde{v}) \\ \frac{\partial}{\partial z} \left( m \frac{\partial \hat{v}_e}{\partial z} \right) + 2\hat{u}_e \sin \theta &= \mathcal{G}(\tilde{u}, \tilde{v}) \end{aligned} \right\} \quad \text{in } \{d_0 < z < 0\}, \quad (3.23)$$

where

$$\mathcal{F}(\tilde{u}, \tilde{v}) = - \left( \frac{\tilde{u}}{\cos \theta} \frac{\partial \tilde{u}}{\partial \varphi} + \tilde{v} \frac{\partial \tilde{u}}{\partial \theta} + \tilde{w} \frac{\partial \tilde{u}}{\partial z} \right) + \tilde{u} \tilde{v} \tan \theta$$

and

$$\mathcal{G}(\tilde{u}, \tilde{v}) = - \left( \frac{\tilde{u}}{\cos \theta} \frac{\partial \tilde{v}}{\partial \varphi} + \tilde{v} \frac{\partial \tilde{v}}{\partial \theta} + \tilde{w} \frac{\partial \tilde{v}}{\partial z} \right) - \tilde{u}^2 \tan \theta.$$

The leading-order velocity  $(\tilde{u}, \tilde{v})$  enters the equations only through the inhomogeneity given by  $\mathcal{F}$  and  $\mathcal{G}$  and the upper boundary condition. Once the solution for  $(\hat{u}, \hat{v})$  has been obtained from these equations, from the continuity equation we can recover  $\hat{w}$  via

$$\frac{\partial \hat{w}}{\partial z} = -\frac{1}{\cos \theta} \frac{\partial \hat{u}}{\partial \varphi} - \frac{\partial \hat{v}}{\partial \theta} + \tan \theta \hat{v}.$$

As with the leading-order problem, it is convenient to introduce the complex notation

$$\hat{W} = \hat{u}_e + i\hat{v}_e \quad \text{and} \quad \mathcal{I} = \mathcal{F} + i\mathcal{G};$$

then, once again denoting a derivative with respect to  $z$  by a prime for simplicity, equation (3.23) becomes

$$(m\hat{W}')' - 2i\hat{W} \sin \theta = \mathcal{I}. \quad (3.24)$$

Moreover, with this notation, and using the identity  $\text{Re}(\alpha) = \frac{1}{2}(\alpha + \bar{\alpha})$  for  $\alpha \in \mathbb{C}$ , we can rewrite the boundary condition (3.22) as

$$\begin{aligned} \hat{W}'(0) &= -\mathcal{C}_{aw} \left( |W_w - W(0)|\hat{W}(0) + \frac{W_w - W(0)}{|W_w - W(0)|} \text{Re} \left\{ (W_w - W(0))\overline{\hat{W}(0)} \right\} \right) \\ &= -\frac{\mathcal{C}_{aw}}{2} \left( 3|W_w - W(0)|\hat{W}(0) + \frac{(W_w - W(0))^2}{|W_w - W(0)|} \overline{\hat{W}(0)} \right), \end{aligned}$$

where  $W_w$  and  $W$  are as in (3.19), and the bar denotes complex conjugation. Thus, taking the Ekman solution  $\hat{W}$  to vanish below the lower boundary  $\{z = z_0\}$  of the Ekman layer

(note that  $\mathcal{I}(z) = 0$  for  $d_0 \leq z \leq z_0$ ), we are left with the problem

$$\begin{cases} (m(z)\hat{W}'(z))' - 2i\hat{W}(z)\sin\theta = \mathcal{I}(z), & z_0 < z < 0, \\ \hat{W}'(0) = -\frac{\mathcal{C}_{\text{aw}}}{2} \left( 3|W_w - W(0)|\hat{W}(0) + \frac{(W_w - W(0))^2}{|W_w - W(0)|}\overline{\hat{W}(0)} \right), \\ \hat{W}(z_0) = 0. \end{cases} \quad (3.25)$$

#### 4. SOME ANALYTICAL RESULTS

In this section, we investigate the problems (3.20) and (3.25) by analytical means. First, we establish the existence and uniqueness of the solution to the problem (3.20) for arbitrary  $W_w \in \mathbb{C}$ , show that the solution exhibits the properties of a classical Ekman spiral, and discuss some properties of its surface deflection angle. Then we turn to solving (3.25) and provide *a priori* bounds on its solution using logarithmic matrix norms.

##### 4.1. The leading-order problem.

4.1.1. *Existence and uniqueness of the solution, and the Ekman spiral.* Interestingly, the problem (3.20) is nonlinear, because even though the equation itself is linear, the upper boundary condition is nonlinear. Therefore, it is not clear *a priori* whether this problem is solvable and, if so, whether the solution is unique. This is the subject of the next theorem, which not only establishes the existence of a unique solution to (3.20) for given  $\tilde{w}$ , but also provides some information on the qualitative behaviour of the solution.

**Theorem 4.1.** *Let  $W_w \in \mathbb{C} \setminus \{0\}$  be arbitrary,  $\theta \in (-\frac{\pi}{2}, \frac{\pi}{2}) \setminus \{0\}$ , and suppose that  $m \in C^1((z_0, 0)) \cap C([z_0, 0])$  with  $m(z) > 0$  for each  $z \in [z_0, 0]$ . Then, there exists a unique function  $W \in C^2((z_0, 0)) \cap C([z_0, 0])$  that solves (3.20). Moreover, writing*

$$W(z) = M(z) e^{i\vartheta(z)},$$

where  $M(z) = |W(z)|$ , we have that, for all  $z \in (z_0, 0)$ ,

$$M'(z) \geq 0 \quad \text{and} \quad \text{sign}(\theta)\vartheta'(z) > 0, \quad (4.1)$$

that is, the solution behaves as a classical Ekman spiral.

*Proof.* Let  $Y \in C^2((z_0, 0)) \cap C([z_0, 0])$  be the solution to the linear initial value problem

$$\begin{cases} (m(z)Y'(z))' - 2i\sin\theta Y(z) = 0, & z_0 < z < 0, \\ Y(z_0) = 0, \\ Y'(z_0) = 1; \end{cases} \quad (4.2)$$

the existence of a unique global solution to this problem follows from standard theory for second-order linear systems of ordinary differential equations (see, e.g., Teschl (2012)). Multiplying the first equation of (4.2) with the complex conjugate  $\overline{Y}$  of  $Y$ , integrating from  $z_0$  to  $z$ , performing an integration by parts, and taking the second equation in (4.2) into account, we obtain

$$m(z)Y'(z)\overline{Y(z)} = \int_{z_0}^z m(s)|Y'(s)|^2 ds + 2i\sin\theta \int_{z_0}^z |Y(s)|^2 ds. \quad (4.3)$$

Writing

$$Y(z) = r(z) e^{i\phi(z)},$$

plugging into (4.3), and taking the real and imaginary part, we see that, on the one hand,

$$m(z)r'(z)r(z) = \int_{z_0}^z m(s)|Y'(s)|^2 ds > 0,$$

hence, since  $m(z) > 0$  and  $r(z) \geq 0$ , we have

$$r(z) > 0 \quad \text{and} \quad r'(z) > 0 \quad \text{for all } z > z_0, \quad (4.4)$$

and, on the other hand,

$$m(z)\phi'(z)r(z)^2 = 2\sin\theta \int_{z_0}^z |Y(s)|^2 ds \begin{cases} > 0 & \text{if } \theta \in \left(0, \frac{\pi}{2}\right), \\ < 0 & \text{if } \theta \in \left(-\frac{\pi}{2}, 0\right), \end{cases}$$

thus

$$\text{sign}(\theta)\phi'(z) > 0 \quad \text{for all } z > z_0. \quad (4.5)$$

In particular, we have

$$Y(z) \neq 0 \quad \text{for all } z > z_0.$$

Now, note that a solution  $W$  to (3.20) must necessarily be of the form

$$W = cY$$

for some  $c \in \mathbb{C}$ ; therefore, we only have to show that we can find a unique  $c$  such that the nonlinear upper boundary condition is met. To this end, let us simplify the notation by setting

$$a := W(0) \quad \text{and} \quad d := W_w - a,$$

hence  $c = \frac{a}{Y(0)}$  (as we saw,  $Y(0) \neq 0$ ) and

$$W'(0) = \lambda a,$$

where

$$\lambda := \frac{Y'(0)}{Y(0)} = \frac{r'(0)}{r(0)} + i\phi'(0). \quad (4.6)$$

Note that  $\text{Re}(\lambda) > 0$  and  $\text{sign}(\theta)\text{Im}(\lambda) > 0$ , in view of (4.4) and (4.5).

In order for the second equation in (3.20) to be satisfied, we must have

$$\lambda(W_w - d) = \mathcal{C}_{aw}|d|d,$$

which, writing

$$d = \varrho e^{i\delta}$$

for  $\varrho = |d|$ , becomes

$$\lambda W_w = \varrho e^{i\delta}(\lambda + \mathcal{C}_{aw}\varrho). \quad (4.7)$$

Multiplying both sides of this equation by the respective complex conjugate and rearranging terms, we see that  $\varrho$  is determined through the positive solutions of the equation

$$p(\varrho) = 0, \quad (4.8)$$

where  $p$  is the real fourth-order polynomial

$$p(x) = \mathcal{C}_{aw}^2 x^4 + 2\mathcal{C}_{aw} \text{Re}(\lambda) x^3 + |\lambda|^2 x^2 - |\lambda W_w|^2. \quad (4.9)$$

Note that  $p(0) < 0$ ,  $p(x) \rightarrow \infty$  as  $x \rightarrow \infty$ , and  $p$  is strictly increasing on  $(0, \infty)$ , because

$$p'(x) = 2x(2\mathcal{C}_{aw}^2 x^2 + 3\mathcal{C}_{aw} \text{Re}(\lambda)x + |\lambda|^2) > 0 \quad \text{for } x > 0;$$

therefore, there is a unique positive solution  $\varrho$  of (4.8), from which, in view of (4.7), we recover the constant  $c$  through

$$c = \frac{a}{Y(0)} = \frac{W_w - d}{Y(0)} = \frac{\mathcal{C}_{aw}\varrho}{\mathcal{C}_{aw}\varrho + \lambda} \cdot \frac{W_w}{Y(0)} \quad (4.10)$$

(note that  $\mathcal{C}_{aw}\varrho + \lambda \neq 0$ , since  $\varrho > 0$  and  $\lambda \in \mathbb{C} \setminus \mathbb{R}$ ).

Finally, since  $W$  is a multiple of  $Y$ , the claimed properties (4.1) of the Ekman spiral follow immediately from (4.4) and (4.5).  $\square$

Theorem 4.1 remains valid if the eddy viscosity  $m$  is only piecewise continuously differentiable (but continuous everywhere), as one can see upon inspection of the proof. For later reference, note that (4.10) implies that

$$W(0) = \frac{\mathcal{C}_{\text{aw}}\varrho}{\mathcal{C}_{\text{aw}}\varrho + \lambda} W_w, \quad (4.11)$$

with  $\lambda$  and  $\varrho$  as in (4.6) and (4.8); in particular, the ratio between the intensity of the surface current and that of the wind is given by the formula

$$\left| \frac{W(0)}{W_w} \right| = \frac{W_w - d}{Y(0)} = \frac{\mathcal{C}_{\text{aw}}\varrho}{|\mathcal{C}_{\text{aw}}\varrho + \lambda|}. \quad (4.12)$$

These formulae will prove very useful later, when we compute explicit solutions.

**4.1.2. The surface deflection angle.** Observing the proof of Theorem 4.1, we see that we can also infer a formula for the *surface deflection angle*, which is defined as the angle between the surface Ekman current  $W(0)$  and the difference  $W_w = W_a - W_g$  between the wind and the geostrophic current. This is the object of the next theorem.

**Theorem 4.2.** *Let  $Y$  be the solution of (4.2) and  $\varrho > 0$  be the unique solution of (4.8), and write*

$$\lambda = \frac{Y'(0)}{Y(0)} = \frac{W'(0)}{W(0)}, \quad (4.13)$$

*as in the proof of Theorem 4.1, where  $W$  is the solution of (3.20). Denote*

$$W(0) = |W(0)| e^{i\Theta} \quad \text{and} \quad W_w = |W_w| e^{i\Gamma}.$$

*Then the surface deflection angle  $\Gamma - \Theta$  is determined by the formula*

$$\tan(\Gamma - \Theta) = \frac{\text{Im}(\lambda)}{\mathcal{C}_{\text{aw}}\varrho + \text{Re}(\lambda)}, \quad (4.14)$$

*hence, since  $\text{sign}(\theta)\text{Im}(\lambda) > 0$  and  $\text{Re}(\lambda) > 0$ , the deflection is to the right in the northern hemisphere and to the left in the southern hemisphere. In particular, we have the bounds*

$$\frac{|\text{Im}(\lambda)|}{\alpha + \text{Re}(\lambda)} \leq |\tan(\Gamma - \Theta)| \leq \frac{|\text{Im}(\lambda)|}{\beta + \text{Re}(\lambda)}, \quad (4.15)$$

*where*

$$\alpha = \frac{-\text{Re}(\lambda) + \sqrt{\text{Re}(\lambda)^2 + 4\mathcal{C}_{\text{aw}}|\lambda W_w|}}{2} \quad \text{and} \quad \beta = \frac{-|\lambda| + \sqrt{|\lambda|^2 + 4\mathcal{C}_{\text{aw}}|\lambda W_w|}}{2}.$$

*Proof.* By (4.10), we have

$$|W(0)| e^{i\Theta} = W(0) = \frac{\mathcal{C}_{\text{aw}}\varrho}{\mathcal{C}_{\text{aw}}\varrho + \lambda} W_w = \left( 1 + \frac{\lambda}{\mathcal{C}_{\text{aw}}\varrho} \right)^{-1} |W_w| e^{i\Gamma},$$

thus

$$\left| \frac{W_w}{W(0)} \right| e^{i(\Gamma - \Theta)} = 1 + \frac{\lambda}{\mathcal{C}_{\text{aw}}\varrho},$$

whence (4.14) follows immediately. To prove the bounds (4.15), note that, with  $p$  as in (4.9), since  $\text{Re}(\lambda) \leq |\lambda|$  we have

$$q(x) \leq p(x) \leq r(x), \quad x > 0,$$

where

$$r(x) = |\lambda|^2 x^2 \left( \frac{\mathcal{C}_{\text{aw}}}{|\lambda|} x + 1 \right)^2 - |\lambda W_w|^2, \quad q(x) = \text{Re}(\lambda)^2 x^2 \left( \frac{\mathcal{C}_{\text{aw}}}{\text{Re}(\lambda)} x + 1 \right)^2 - |\lambda W_w|^2.$$

Therefore, the unique positive root  $\varrho$  of  $p$  must be smaller than the unique positive root of  $q$  and larger than the unique positive root of  $r$ , which are given by  $\alpha/\mathcal{C}_{\text{aw}}$  and  $\beta/\mathcal{C}_{\text{aw}}$ , respectively, and the bounds (4.15) follow.  $\square$

Moreover, although our solution is not defined for  $\theta = 0$ , where the definition of the geostrophic flow breaks down, we recover the classical observation that the deflection angle vanishes as one approaches the equator. Before proving this fact, we recall the notion of the *logarithmic matrix norm*.

**Definition 4.3.** For  $n \in \mathbb{N}$ , let  $\|\cdot\|_*$  denote a matrix norm on  $\mathbb{C}^{n \times n}$  induced by a vector norm  $\|\cdot\|$  on  $\mathbb{C}^n$ . For a matrix  $A \in \mathbb{C}^{n \times n}$ , we define its logarithmic matrix norm  $\mu_*[A]$  associated to  $\|\cdot\|_*$  as

$$\mu_*[A] = \lim_{h \searrow 0} \frac{\|\mathbb{I} + hA\|_* - 1}{h},$$

where  $\mathbb{I}$  denotes the identity matrix in  $\mathbb{C}^{n \times n}$ .

It is easy to show that  $\mu_*[A]$  is well-defined for all  $A \in \mathbb{C}^{n \times n}$ . For more properties of the logarithmic matrix norm, we refer to Söderlind (2024). These logarithmic matrix norms were first applied to the classical Ekman problem by Marynets (2022). In fact, they can be especially useful, among other things, in determining bounds on solutions to ordinary differential equations. The following result, which will be useful to us, can be found in section 6.6 of Söderlind (2024).

**Lemma 4.4.** For  $T > 0$ , let  $A : [0, T) \rightarrow \mathbb{C}^{n \times n}$  and  $f : [0, T) \rightarrow \mathbb{C}^n$  be continuous. Suppose that  $u \in C^1((0, T), \mathbb{C}^n) \cap C([0, T), \mathbb{C}^n)$  solves the inhomogeneous linear initial value problem

$$u'(t) = A(t)u(t) + f(t), \quad u(0) = u_0.$$

Denote

$$L(t) = \int_0^t \mu_*[A(\tau)] \, d\tau.$$

Then

$$\|u(t)\| \leq e^{L(t)} \|u_0\| + e^{L(t)} \int_0^t e^{-L(s)} \|f(s)\| \, ds.$$

In order to apply Lemma 4.4 to our problem, we transform the second-order equation (3.23) into a first-order linear system of two equations by introducing the change of variables

$$x_1 = \hat{W}, \quad x_2 = \hat{W}',$$

which allows us to rewrite (3.24) as

$$x'(z) = A(z)x(z) + B(z), \quad z \in (z_0, 0),$$

where

$$A = \begin{pmatrix} 0 & 1 \\ \frac{2i \sin \theta}{m} & -\frac{m'}{m} \end{pmatrix}, \quad B = \begin{pmatrix} 0 \\ \frac{\mathcal{I}}{m} \end{pmatrix}, \quad x = \begin{pmatrix} x_1 \\ x_2 \end{pmatrix}.$$

As we pointed out previously, the logarithmic matrix norm depends on the choice of the vector norm; in particular cases, it can be computed explicitly. For instance, denoting  $A = (a_{jk})_{1 \leq j, k \leq 2}$ , for

$$\|x\|_1 = |x_1| + |x_2| \quad \text{or} \quad \|x\|_\infty = \max\{|x_1|, |x_2|\},$$

the corresponding logarithmic matrix norms can be computed explicitly as

$$\mu_1[A(z)] = \max_k \left\{ \operatorname{Re}(a_{kk}(z)) + \sum_{j \neq k} |a_{jk}(z)| \right\} = \max \left\{ 2|\sin \theta|, 1 - \frac{m'(z)}{m(z)} \right\} \quad (4.16)$$

or

$$\mu_\infty[A(z)] = \max_j \left\{ \operatorname{Re}(a_{jj}(z)) + \sum_{k \neq j} |a_{jk}(z)| \right\} = \max \left\{ 1, \frac{2|\sin \theta| - m'(z)}{m(z)} \right\}, \quad (4.17)$$

respectively (Söderlind, 2024). Moreover, for

$$\|x\|_2 = \sqrt{|x_1|^2 + |x_2|^2},$$

denoting by  $\lambda_{\max}(M)$  the maximal eigenvalue of a symmetric matrix  $M \in \mathbb{C}^{2 \times 2}$ , we have

$$\mu_2[A(z)] = \lambda_{\max}\left(\frac{A(z) + A(z)^T}{2}\right) = \frac{1}{2} \left( -\frac{m'(z)}{m(z)} + \sqrt{1 + \frac{m'(z)^2 + 4 \sin^2 \theta}{m(z)^2}} \right). \quad (4.18)$$

With this preparation, we can prove the following result:

**Theorem 4.5.** *Denote by  $\omega(\theta)$  the surface deflection angle determined using the formula (4.14). Then*

$$\lim_{\theta \rightarrow 0} \omega(\theta) = 0.$$

*Proof.* Let  $Y_\theta(z)$  (denoting the  $\theta$ -dependence explicitly via the lower index, since we are considering the limit  $\theta \rightarrow 0$ ) and  $Y_0(z)$  be the solution of (4.2) and

$$\begin{cases} (m(z)Y'_0(z))' = 0, & z_0 < z < 0, \\ Y_0(z_0) = 0, \\ Y'_0(z_0) = 1, \end{cases}$$

respectively. The solution  $Y_0$  is straightforwardly determined explicitly as

$$Y_0(z) = \int_{z_0}^z \frac{m(s)}{m(s)} ds.$$

Define

$$\lambda(\theta) = \frac{Y'_\theta(0)}{Y_\theta(0)} \in \mathbb{C} \setminus \mathbb{R} \quad \text{and} \quad \lambda_0 = \frac{Y'_0(0)}{Y_0(0)} > 0,$$

analogously to (4.13). Defining  $\hat{Y}_\theta(z) = Y_\theta(z) - Y_0(z)$ , we see that  $\hat{Y}$  solves the inhomogeneous initial value problem

$$\begin{cases} (m(z)\hat{Y}'_\theta(z))' - 2i \sin \theta \hat{Y}_\theta(z) = 2i \sin \theta Y_0(z), & z_0 < z < 0, \\ \hat{Y}_\theta(z_0) = 0, \\ \hat{Y}'_\theta(z_0) = 0. \end{cases}$$

Using Lemma 4.4 and, for example, (4.16), it follows that

$$|\hat{Y}_\theta(z)| + |\hat{Y}'_\theta(z)| \leq C |\sin \theta|, \quad z \in [z_0, 0],$$

where the constant  $C > 0$  can be chosen to be independent of  $\theta$  and  $z$ . In particular,  $Y_\theta(0) \rightarrow Y_0(0)$  and  $Y'_\theta(0) \rightarrow Y'_0(0)$  as  $\theta \rightarrow 0$ , hence  $\lambda(\theta) \rightarrow \lambda_0$  as  $\theta \rightarrow 0$ , and, arguing by continuity in the formula (4.14), it follows that the surface deflection angle of the solution  $W$  to the leading-order problem (3.20) converges to zero (since  $\lambda_0 > 0$  is real) as  $\theta \rightarrow 0$ .  $\square$

**4.2. The problem at first order.** In order to solve (3.25), the standard solution method is the variation of constants: first, we look for a basis  $\{\hat{W}_1, \hat{W}_2\}$  of the solution space of the homogeneous equation

$$(m(z)\hat{W}'(z))' - 2i \hat{W}(z) \sin \theta = 0.$$

Then, a particular solution  $\hat{W}_p$  of the inhomogeneous equation (3.24) is given by

$$\hat{W}_p = w_1 \hat{W}_1 + w_2 \hat{W}_2;$$

here, the coefficients  $w_1$  and  $w_2$  are functions that are determined by integrating

$$\frac{\partial w_1}{\partial z} = \frac{\hat{W}_2 \mathcal{J}}{\mathcal{W}(\hat{W}_1, \hat{W}_2)} \quad \text{and} \quad \frac{\partial w_2}{\partial z} = -\frac{\hat{W}_1 \mathcal{J}}{\mathcal{W}(\hat{W}_1, \hat{W}_2)},$$

where

$$\mathcal{W}(\hat{W}_1, \hat{W}_2) = \hat{W}_1 \hat{W}'_2 - \hat{W}_2 \hat{W}'_1$$

denotes the *Wronskian* of  $\hat{W}_1$  and  $\hat{W}_2$  (which is always non-zero, because  $\hat{W}_1$  and  $\hat{W}_2$  are linearly independent). Without loss of generality, we can choose  $w_1(z_0) = w_2(z_0) = 0$ . The general solution of (3.24) is then given by

$$\hat{W} = C_1 \hat{W}_1 + C_2 \hat{W}_2 + \hat{W}_p,$$

where  $C_1, C_2 \in \mathbb{C}$  are arbitrary constants, to be determined through the boundary conditions. In fact, assuming without loss of generality that  $\hat{W}_2(z_0) \neq 0$ , the third equation in (3.25), together with  $\hat{W}_p(z_0) = 0$ , implies

$$C_2 = -\frac{\hat{W}_1(z_0)}{\hat{W}_2(z_0)} C_1,$$

hence

$$\hat{W}(z) = C_1 \left( \hat{W}_1(z) - \frac{\hat{W}_1(z_0)}{\hat{W}_2(z_0)} \hat{W}_2(z) \right) + \hat{W}_p(z).$$

Then, plugging into the second equation of (3.25), we obtain the following equation for  $C_1$ :

$$\alpha C_1 + \beta \bar{C}_1 = \gamma, \quad (4.19)$$

where, as before, the bar denotes complex conjugation, and

$$\begin{aligned} \alpha &= \left( \hat{W}'_1(0) - \frac{\hat{W}_1(z_0)}{\hat{W}_2(z_0)} \hat{W}'_2(0) \right) + \frac{3}{2} \mathcal{C}_{aw} |W_w - W(0)| \left( \hat{W}_1(0) - \frac{\hat{W}_1(z_0)}{\hat{W}_2(z_0)} \hat{W}_2(0) \right), \\ \beta &= \frac{1}{2} \mathcal{C}_{aw} \frac{(W_w - W(0))^2}{|W_w - W(0)|} \left( \overline{\hat{W}_1(0)} - \frac{\overline{\hat{W}_1(z_0)}}{\overline{\hat{W}_2(z_0)}} \overline{\hat{W}_2(0)} \right), \\ \gamma &= -\frac{3}{2} \mathcal{C}_{aw} \left[ |W_w - W(0)| (w_1(0) \hat{W}_1(0) + w_2(0) \hat{W}_2(0)) \right. \\ &\quad \left. + \frac{(W_w - W(0))^2}{|W_w - W(0)|} \left( \overline{w_1(0) \hat{W}_1(0)} + \overline{w_2(0) \hat{W}_2(0)} \right) \right] \\ &\quad - w_1(0) \hat{W}'_1(0) - w_2(0) \hat{W}'_2(0). \end{aligned}$$

The equation (4.19) has the unique solution

$$C_1 = \frac{\bar{\alpha}\gamma - \beta\bar{\gamma}}{|\alpha| - |\beta|},$$

as long as  $|\alpha| \neq |\beta|$ . This condition can be reformulated as follows. Denote

$$Y(z) = \hat{W}_1(z) - \frac{\hat{W}_1(z_0)}{\hat{W}_2(z_0)} \hat{W}_2(z);$$

then, assuming without loss of generality that  $Y'(z_0) = 1$ , the function  $Y$  is the solution of (4.2). Thus, writing

$$\lambda = \frac{Y'(0)}{Y(0)}$$

and letting  $\varrho$  be the unique positive solution of (4.8), as in the proof of Theorem 4.1, we see that  $|\alpha| \neq |\beta|$  is equivalent to

$$\left| \lambda + \frac{3}{2} \mathcal{C}_{aw} \varrho \right| \neq \frac{1}{2} \mathcal{C}_{aw} \varrho. \quad (4.20)$$

Since

$$\left| \lambda + \frac{3}{2} \mathcal{C}_{\text{aw}} \varrho \right| \geq |\lambda| - \frac{3}{2} \mathcal{C}_{\text{aw}} \varrho \quad (4.21)$$

and, as we argued in the proof of Theorem 4.2,

$$\mathcal{C}_{\text{aw}} \varrho \leq \frac{-\text{Re}(\lambda) + \sqrt{\text{Re}(\lambda)^2 + 4\mathcal{C}_{\text{aw}} |\lambda W_{\text{w}}|}}{2} \leq \mathcal{C}_{\text{aw}} |W_{\text{w}}| \frac{|\lambda|}{\text{Re}(\lambda)}, \quad (4.22)$$

where we used the inequality  $\sqrt{1+x} \leq 1 + \frac{1}{2}x$ ,  $x \geq -1$ , combining (4.21) and (4.22) we have

$$\left| \lambda + \frac{3}{2} \mathcal{C}_{\text{aw}} \varrho \right| \geq \left( \frac{\text{Re}(\lambda)}{|W_{\text{w}}|} - \frac{3}{2} \mathcal{C}_{\text{aw}} \right) \varrho.$$

Therefore, the validity of (4.20) is guaranteed if

$$\text{Re}(\lambda) > 2\mathcal{C}_{\text{aw}} |W_{\text{w}}|. \quad (4.23)$$

Of course, this in fact boils down to a condition on the eddy viscosity and the wind's intensity, since  $\lambda$  depends only on the former. However, finding explicit bounds on  $\text{Re}(\lambda)$  in terms of a general  $m$  is difficult, so in practice, this condition would have to be checked case by case. In this place, let us only note that the right-hand side of (4.23) is very small, of order of magnitude typically not larger than  $10^{-2}$ , and in the explicit cases that we consider later, the condition is satisfied by a large margin.

In addition, using Lemma 4.4 we can provide estimates for the first-order correction of the horizontal velocity field provided by (3.25). Writing  $\mu_a[A(z)]$ ,  $a \in \{1, 2, \infty\}$ , by Lemma 4.4 and (4.16), (4.17) and (4.18) we have

$$\|x(z)\|_a \leq |\hat{W}'(z_0)| \exp \left( \int_{z_0}^z \mu_a[A(s)] \, ds \right) + \int_{z_0}^z \exp \left( \int_t^z \mu_a[A(s)] \, ds \right) \frac{|\mathcal{J}(t)|}{m(t)} \, dt,$$

with

$$\|x(z)\|_1 = |\hat{W}(z)| + |\hat{W}'(z)|, \quad \|x(z)\|_\infty = \max \left\{ |\hat{W}(z)|, |\hat{W}'(z)| \right\},$$

and

$$\|x(z)\|_2 = \sqrt{|\hat{W}(z)|^2 + |\hat{W}'(z)|^2}.$$

Note that this bound depends only on the eddy viscosity  $m$  and, through  $\mathcal{J}$  and  $\hat{W}'(z_0)$ , the leading-order solution  $W$  found in § 4.1.

## 5. EXPLICIT SOLUTIONS TO THE LEADING-ORDER PROBLEM

This section is devoted to gaining additional insight into the qualitative behaviour of the leading-order Ekman flow by investigating five concrete examples of explicit eddy viscosity profiles, along the lines of Constantin and Johnson (2019b) and Zikanov et al. (2003). These choices allow us to write down the solution explicitly, calculate the surface deflection angle and the Ekman transport (the integrated mass transport induced by the Ekman flow), compare our results with available measurements, and visualise the flow by means of numerical plots.

First, in § 5.1, we consider the easiest case possible, namely that of constant eddy viscosity. In § 5.2, we investigate the cases of linearly decaying eddy viscosity, similarly to Wenegrat and McPhaden (2016), while in § 5.3 we discuss the model, proposed by Madsen (1977), of an eddy viscosity that increases linearly with depth, before moving on, in § 5.4, to a piecewise linear eddy viscosity, as proposed by Zikanov et al. (2003). In all of these three cases, the solution is determined through Bessel functions. As a last example, in § 5.5 we turn our attention to exponentially decaying eddy viscosity (Wenegrat and McPhaden, 2016), where the solution can be written in terms of modified Bessel functions. For non-constant eddy viscosity, the computations become substantially more involved, but we are

still able to fully determine the solutions and compute the surface deflection angle and the Ekman transport.

For clarity and to facilitate reference of the equations later on, let us recall the leading-order problem (3.20) here. This problem consists of the complex-valued linear ordinary differential equation

$$(m(z)W'(z))' = 2iW(z)\sin\theta, \quad z_0 < z < 0, \quad (5.1)$$

with boundary conditions

$$W'(0) = \mathcal{C}_{aw}|W_w - W(0)|(W_w - W(0)) \quad (5.2)$$

and

$$W(z_0) = 0, \quad (5.3)$$

where  $W_w \in \mathbb{C}$  corresponds to the difference between the wind velocity and the geostrophic velocity (see (3.19)) and can be assumed to be known. One should keep in mind that, in fact,  $W(z) = W(\varphi, \theta, z)$ , but the dependence on  $\varphi$  and  $\theta$  is purely parametric (these variables are now introduced into the problem only through  $W_w = W_w(\varphi, \theta)$ ); therefore, we will suppress it to keep the notation as agile as possible.

**5.1. Constant eddy viscosity.** The first case we consider is that of a constant eddy viscosity in the upper layer, which, under the scaling (2.10), corresponds to  $m(z) = 1$  for  $z \in [z_0, 0]$ . Below this layer, the eddy viscosity is supposed to drop rapidly to the (much smaller) molecular viscosity, although this is irrelevant for our analysis. Although the assumption of constant eddy viscosity may seem unrealistic, it has been observed that it may provide a good fit to certain wind-driven drift currents (Polton et al., 2013). In this case, the solution of (5.1), for  $\theta \neq 0$ , is

$$W(z) = c_1 e^{(1+i\operatorname{sign}(\theta))z\sqrt{|\sin\theta|}} + c_2 e^{-(1+i\operatorname{sign}(\theta))z\sqrt{|\sin\theta|}},$$

where  $c_1, c_2 \in \mathbb{C}$  are determined from the boundary conditions. In fact, in view of (5.3), we see that

$$c_2 = -c_1 e^{2(1+i\operatorname{sign}(\theta))z_0\sqrt{|\sin\theta|}},$$

giving

$$W(z) = 2c_1 e^{2(1+i\operatorname{sign}(\theta))z_0\sqrt{|\sin\theta|}} \sinh((1+i\operatorname{sign}(\theta))\sqrt{|\sin\theta|}(z - z_0)). \quad (5.4)$$

Differentiating (5.4), we note

$$W'(0) = (1+i\operatorname{sign}(\theta))\sqrt{|\sin\theta|} \coth((1+i\operatorname{sign}(\theta))\sqrt{|\sin\theta|}|z_0|)W(0),$$

with the notation of Theorem 4.2 we find that

$$\lambda = (1+i\operatorname{sign}(\theta))\sqrt{|\sin\theta|} \coth((1+i\operatorname{sign}(\theta))\sqrt{|\sin\theta|}|z_0|).$$

This allows us to determine the coefficient  $c_1$ : in fact, evaluating (5.4) at  $z = 0$  and substituting into (4.11), we obtain

$$c_1 = \frac{\mathcal{C}_{aw}\varrho}{\mathcal{C}_{aw}\varrho + \lambda} \cdot \frac{e^{-2(1+i\operatorname{sign}(\theta))z_0\sqrt{|\sin\theta|}} W_w}{2 \sinh((1+i\operatorname{sign}(\theta))\sqrt{|\sin\theta|}|z_0|)},$$

where  $\varrho$  is the unique positive solution of (4.8). Therefore, substituting in (5.4), we see that the solution is given by

$$W(z) = \frac{\mathcal{C}_{aw}\varrho W_w}{\mathcal{C}_{aw}\varrho + \lambda} \cdot \frac{\sinh((1+i\operatorname{sign}(\theta))\sqrt{|\sin\theta|}(z - z_0))}{\sinh((1+i\operatorname{sign}(\theta))\sqrt{|\sin\theta|}|z_0|)}. \quad (5.5)$$

An illustration of the solution provided by (5.5) is given in figure 4. The ratio between  $|W(0)|$  and  $|W_w|$ , computed according to (4.12), is plotted in figure 5.

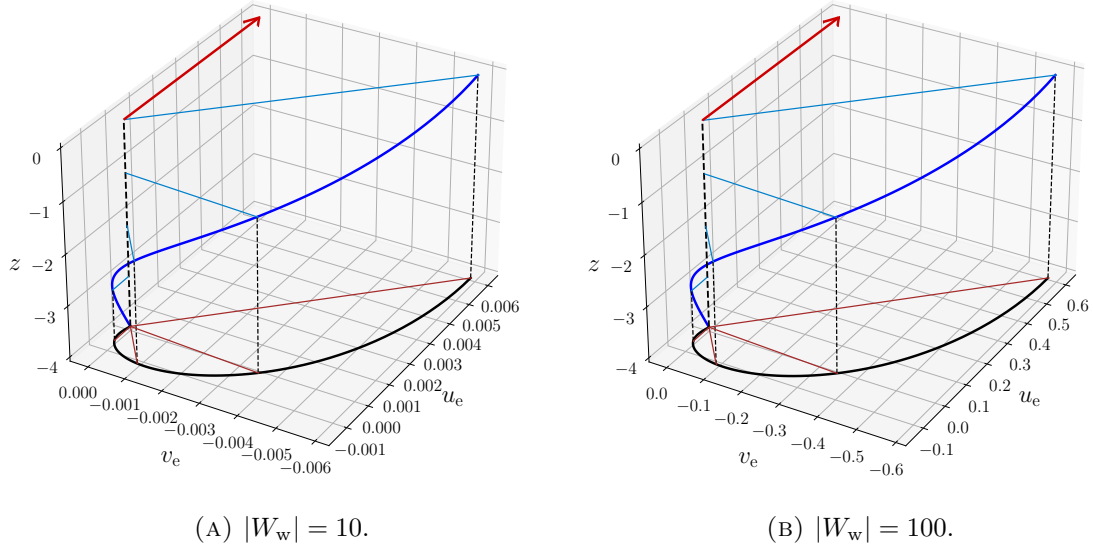


FIGURE 4. Depiction of the solution (5.4) (the blue curve) for  $\theta = 45^\circ$  and  $z_0 = -4$ . The latitude-dependent turning rate  $\sqrt{|\sin \theta|}$  is equal to its decay rate—one the features of the classical Ekman spiral. The surface deflection angle of approximately  $45^\circ$  between direction of the wind (in red, not in scale) and the surface current is clearly visible. The spiral traced out by the velocity field is also projected (in black) onto the bottom plane for clarity.

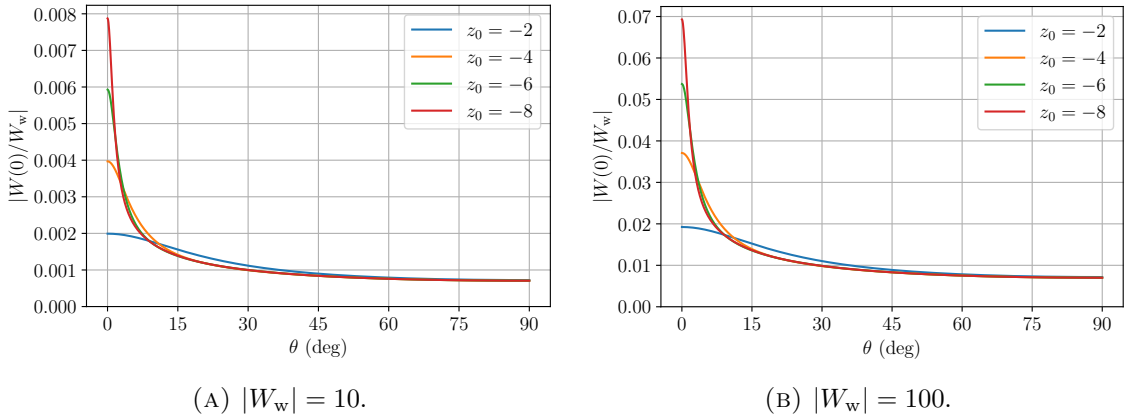


FIGURE 5. The ratio  $|W(0)/W_w|$  between the intensity of the surface current and that of the wind for the case of constant eddy viscosity.

Now, let us discuss the surface deflection angle, that is, the angle between the surface wind and the wind drift Ekman current that it generates, relative to the underlying geostrophic current. Writing

$$W(0) = |W(0)| e^{i\Theta} \quad \text{and} \quad W_w = |W_w| e^{i\Gamma}$$

as in Theorem 4.2, using the identity

$$\coth(x + iy) = \frac{1 + i \tanh(x) \tan(y)}{\tanh(x) + i \tan(y)} = \frac{\sinh(x) \cosh(x) - i \sin(y) \cos(y)}{\sinh^2(x) \cos^2(y) + \cosh^2(x) \sin^2(y)},$$

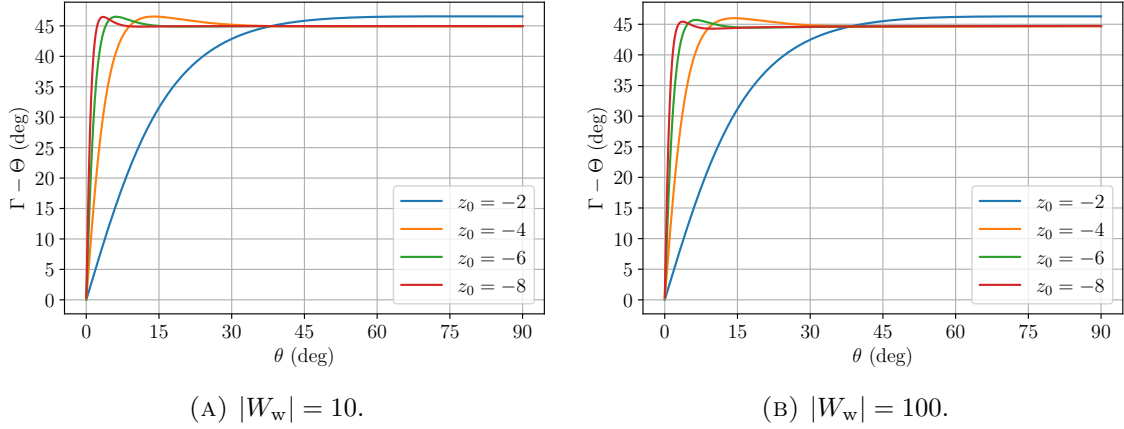


FIGURE 6. The surface deflection angle  $\Gamma - \Theta$  given by (5.6) for the case of constant eddy viscosity.

and introducing the abbreviations

$$\mathfrak{R} = \frac{\sinh(\zeta) \cosh(\zeta)}{\sinh^2(\zeta) \cos^2(\zeta) + \cosh^2(\zeta) \sin^2(\zeta)}$$

and

$$\mathfrak{I} = \frac{\sin(\zeta) \cos(\zeta)}{\sinh^2(\zeta) \cos^2(\zeta) + \cosh^2(\zeta) \sin^2(\zeta)},$$

with  $\zeta = \sqrt{|\sin \theta|} |z_0|$ , Theorem 4.2 yields

$$\tan(\Gamma - \Theta) = \text{sign}(\theta) \frac{(\mathfrak{R} - \mathfrak{I}) \sqrt{|\sin \theta|}}{\mathcal{C}_{aw} \varrho + (\mathfrak{R} + \mathfrak{I}) \sqrt{|\sin \theta|}} \quad (5.6)$$

for the surface deflection angle  $\Gamma - \Theta$ . Some curves for  $\Gamma - \Theta$  calculated through (5.6) depending on  $\theta$  and for different values of  $z_0$  and  $|W_w|$  are shown in figure 6.

Finally, we turn to the Ekman transport, which is defined as

$$\text{Ek} = \int_{z_0}^0 W(z) \, dz.$$

Physically, it describes the integrated mass transport due to the Ekman current. In view of (5.1), it can also be computed as

$$\text{Ek} = -\frac{i}{2 \sin \theta} (m(0)W'(0) - m(z_0)W'(z_0)).$$

In the present case, we obtain

$$\begin{aligned} \text{Ek} &= \frac{2c_1 e^{2(1+i \text{sign}(\theta))z_0 \sqrt{|\sin \theta|}}}{(1+i \text{sign}(\theta)) \sqrt{|\sin \theta|}} [\cosh((1+i \text{sign}(\theta)) \sqrt{|\sin \theta|} |z_0|) - 1] \\ &= \mathcal{X} \frac{e^{-i \text{sign}(\theta) \frac{\pi}{4}}}{\sqrt{2|\sin \theta|}} W(0), \end{aligned} \quad (5.7)$$

where the complex coefficient

$$\mathcal{X} = \coth((1+i \text{sign}(\theta)) \sqrt{|\sin \theta|} |z_0|) - \frac{1}{\sinh((1+i \text{sign}(\theta)) \sqrt{|\sin \theta|} |z_0|)}$$

will affect the angle between the Ekman transport and the surface wind-drift current, depending on  $\theta$  and  $z_0$ , and cause it to deviate from its classical value of  $45^\circ$ . Due to its complicated nature, it is not feasible to provide an explicit expression for its phase.

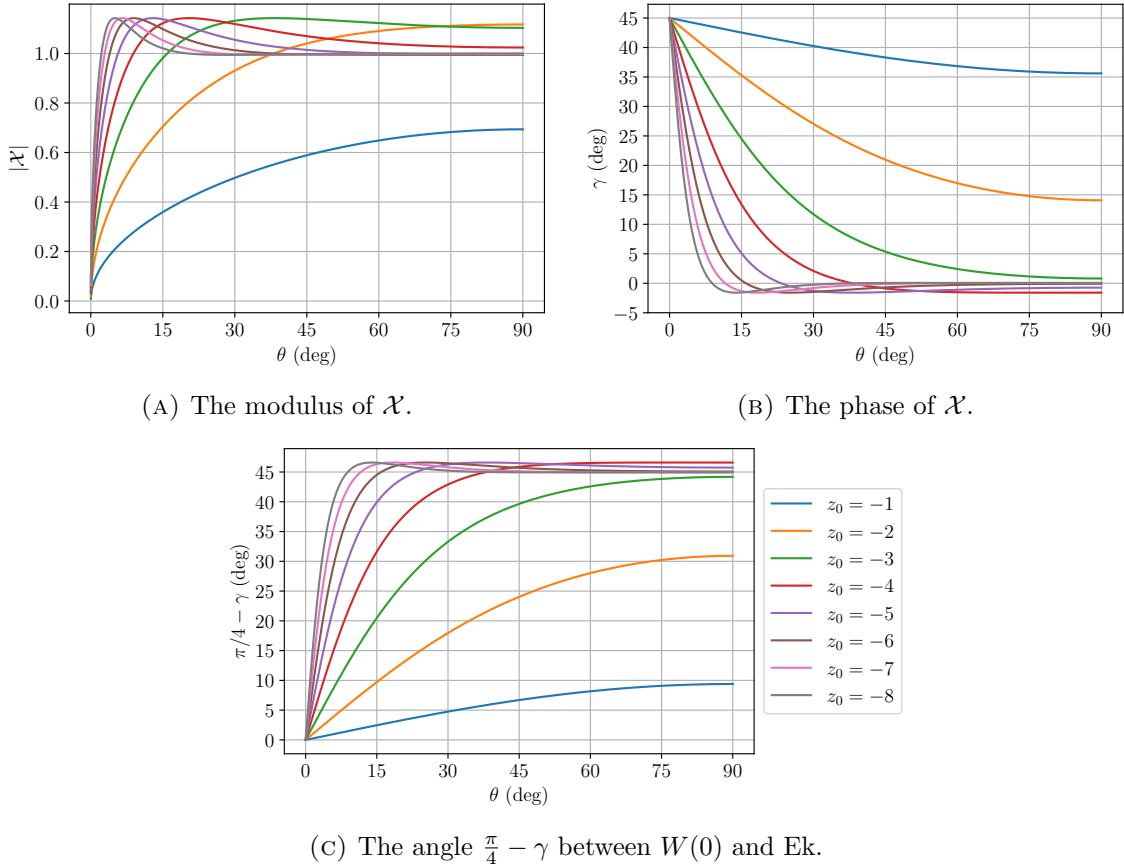


FIGURE 7. Numerical plots for the Ekman transport in the case of constant eddy viscosity.

However, we can numerically compute its modulus and phase—see figures 7a and 7b. Moreover, writing

$$\mathcal{X} = |\mathcal{X}| e^{i \operatorname{sign}(\theta) \gamma},$$

we can rewrite (5.7) as

$$\operatorname{Ek} = |\mathcal{X}| \frac{e^{-i \operatorname{sign}(\theta) (\frac{\pi}{4} - \gamma)}}{\sqrt{2 |\sin \theta|}} W(0).$$

figure 7c shows some numerical plots of the angle  $\frac{\pi}{4} - \gamma$  between the Ekman transport  $\operatorname{Ek}$  and the surface wind-wriff current  $W(0)$  for various values of  $\theta$  and  $z_0$ . It is interesting to note that, for larger values of  $|z_0|$ , this angle actually exceeds  $45^\circ$ . For fixed  $\theta \neq 0$ , increasing  $|z_0|$  leads to  $\mathcal{X}$  approaching 1 in the complex plane, because then

$$\coth((1 + i \operatorname{sign}(\theta)) \sqrt{|\sin \theta|} |z_0|) \approx 1 \quad \text{and} \quad \left| \sinh((1 + i \operatorname{sign}(\theta)) \sqrt{|\sin \theta|} |z_0|) \right|^{-1} \ll 1;$$

in other words, in the limit of infinite depth, the Ekman transport reduces to  $45^\circ$  to the right of the wind-drift surface current in the northern hemisphere (where  $\theta > 0$ ), and to  $45^\circ$  to the left in the southern hemisphere (where  $\theta < 0$ ), in agreement with the classical theory for the Ekman layer in the infinite-depth approximation (see, e.g., Pedlosky (1987) or Talley et al. (2011)).

**5.2. Linearly decaying eddy viscosity.** The second case we study is that of an eddy viscosity that decays linearly to a small value, denoted by  $\mathfrak{m}$ . Recalling that from (2.10) we have

$$A'_v(z) = m(z) \bar{A}'_v,$$

where  $\bar{A}'_v$  is the mean vertical eddy viscosity on the surface, we must have

$$m(0) = 1,$$

so the eddy viscosity profile is given by

$$m(z) = 1 + \frac{\mathfrak{m} - 1}{z_0} z, \quad z_0 \leq z \leq 0. \quad (5.8)$$

Since the concept of eddy viscosity is inherently associated with the presence of turbulence, which in the present case is generated by wind forcing, it is reasonable to assume that below the Ekman layer, where wind-induced effects are negligible, turbulence should be absent and the viscosity for  $z < z_0$  should reduce the molecular viscosity, which is typically approximately four orders of magnitude smaller than the eddy viscosity close to the surface; therefore, we can set  $\mathfrak{m} \approx 10^{-4}$ .

In order to solve the differential equations (5.1) for  $m$  given by (5.8), we use the monotonicity of  $m$  to introduce the change of variable

$$X(z) = \sqrt{m(z)} = \sqrt{1 + \frac{\mathfrak{m} - 1}{z_0} z} \quad (5.9)$$

(Constantin and Johnson, 2019b). Then, denoting

$$W(z) = G(X),$$

the differential equation (5.1) is transformed into the Bessel equation

$$X^2 \frac{d^2 G}{dX^2}(X) + X \frac{dG}{dX}(X) - \frac{8i z_0^2 \sin \theta}{(\mathfrak{m} - 1)^2} X^2 G(X) = 0, \quad X(z_0) = \sqrt{\mathfrak{m}} < X < 1. \quad (5.10)$$

The general solution of (5.10) is the so-called cylindrical function given by

$$G(X) = c_1 J_0 \left( \frac{z_0}{\mathfrak{m} - 1} \sqrt{8|\sin \theta|} X e^{-i \operatorname{sign}(\theta) \frac{\pi}{4}} \right) + c_2 Y_0 \left( \frac{z_0}{\mathfrak{m} - 1} \sqrt{8|\sin \theta|} X e^{-i \operatorname{sign}(\theta) \frac{\pi}{4}} \right)$$

(Polyanin and Zaitsev, 2003), where  $c_1, c_2 \in \mathbb{C}$  and  $J_0$  and  $Y_0$  are the complex-valued Bessel functions of the first and second kind, respectively;  $J_0$  and  $Y_0$  are also known as Neumann functions (Arfken and Weber, 2005). Of course, the coefficients  $c_1$  and  $c_2$  in fact depend parametrically on  $\varphi$  and  $\theta$ , although we will not explicitly denote this dependence. Setting  $\tilde{c}_2 = \frac{c_2}{c_1}$  and reverting from  $X$  to  $z$ , we can write the general solution of (5.1) as

$$W(z) = c_1 \left[ J_0 \left( \frac{z_0}{\mathfrak{m} - 1} \sqrt{8|\sin \theta|} \left( 1 + \frac{\mathfrak{m} - 1}{z_0} z \right) e^{-i \operatorname{sign}(\theta) \frac{\pi}{4}} \right) \right. \\ \left. + \tilde{c}_2 Y_0 \left( \frac{z_0}{\mathfrak{m} - 1} \sqrt{8|\sin \theta|} \left( 1 + \frac{\mathfrak{m} - 1}{z_0} z \right) e^{-i \operatorname{sign}(\theta) \frac{\pi}{4}} \right) \right]. \quad (5.11)$$

The explicit Ekman flow (depicted in figure 8, in addition the ratio between the intensity of the surface current  $W(0)$  and that of the wind  $W_w$  for  $|W_w| = 10$  and  $|W_w| = 100$  shown in figure 9) is determined by calculating the coefficients  $c_1$  and  $\tilde{c}_2$  as follows. The value of  $\tilde{c}_2$  is determined by the condition (5.3), according to which the velocity field must vanish at the bottom of the Ekman layer. Thus, setting  $z = z_0$  in (5.11), we obtain

$$\tilde{c}_2 = - \frac{J_0 \left( \frac{z_0}{\mathfrak{m} - 1} \sqrt{8\mathfrak{m}|\sin \theta|} e^{-i \operatorname{sign}(\theta) \frac{\pi}{4}} \right)}{Y_0 \left( \frac{z_0}{\mathfrak{m} - 1} \sqrt{8\mathfrak{m}|\sin \theta|} e^{-i \operatorname{sign}(\theta) \frac{\pi}{4}} \right)}. \quad (5.12)$$

It remains to determine the coefficient  $c_1$ . Recalling the formulae

$$\frac{dJ_0(s)}{ds} = -J_1(s) \quad \text{and} \quad \frac{dY_0(s)}{ds} = -Y_1(s) \quad (5.13)$$

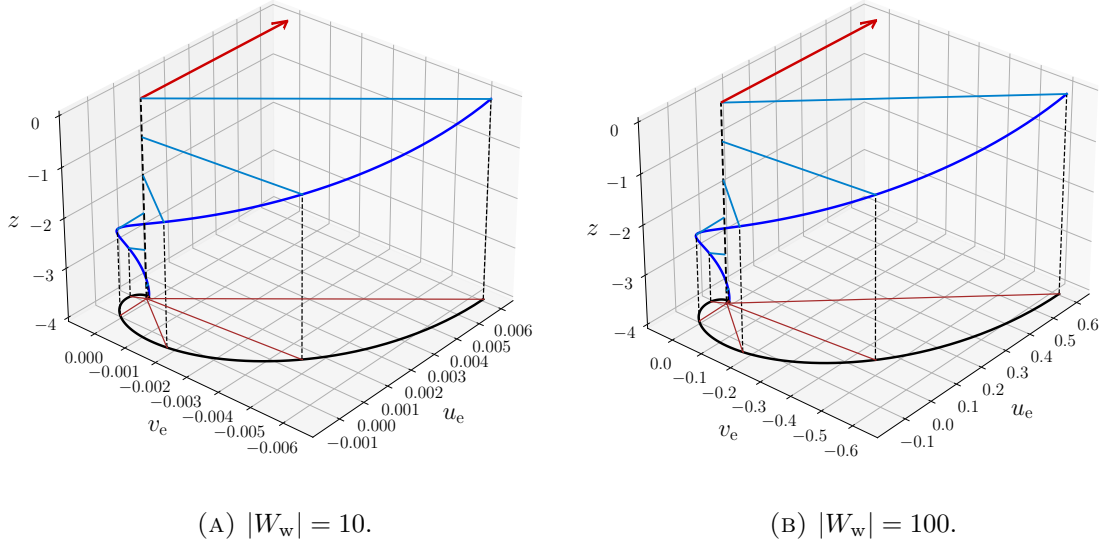


FIGURE 8. Depiction of the solution (5.11) (in blue) for  $\theta = 45^\circ$  and  $z_0 = -4$ , with the direction of the wind (in red) and the projection onto the bottom plane (in black).

for the derivatives of the Bessel functions (Arfken and Weber, 2005; Polyanin and Zaitsev, 2003), we can compute the  $z$ -derivative of (5.11), which reads

$$W'(z) = -c_1 \sqrt{\frac{2|\sin \theta|}{1 + \frac{m-1}{z_0} z}} e^{-i \operatorname{sign}(\theta) \frac{\pi}{4}} \left[ J_1 \left( \frac{z_0}{m-1} \sqrt{8|\sin \theta|} \left( 1 + \frac{m-1}{z_0} z \right) e^{-i \operatorname{sign}(\theta) \frac{\pi}{4}} \right) \right. \\ \left. + \tilde{c}_2 Y_1 \left( \frac{z_0}{m-1} \sqrt{8|\sin \theta|} \left( 1 + \frac{m-1}{z_0} z \right) e^{-i \operatorname{sign}(\theta) \frac{\pi}{4}} \right) \right]. \quad (5.14)$$

Evaluating the expressions (5.11) and (5.14) at  $z = 0$  and using the definition (4.13), we obtain

$$\lambda = -\sqrt{2|\sin \theta|} e^{-i \operatorname{sign}(\theta) \frac{\pi}{4}} \times \\ \times \frac{\left[ J_1 \left( \frac{z_0}{m-1} \sqrt{8|\sin \theta|} e^{-i \operatorname{sign}(\theta) \frac{\pi}{4}} \right) + \tilde{c}_2 Y_1 \left( \frac{z_0}{m-1} \sqrt{8|\sin \theta|} e^{-i \operatorname{sign}(\theta) \frac{\pi}{4}} \right) \right]}{\left[ J_0 \left( \frac{z_0}{m-1} \sqrt{8|\sin \theta|} e^{-i \operatorname{sign}(\theta) \frac{\pi}{4}} \right) + \tilde{c}_2 Y_0 \left( \frac{z_0}{m-1} \sqrt{8|\sin \theta|} e^{-i \operatorname{sign}(\theta) \frac{\pi}{4}} \right) \right]}.$$

Then, letting  $\varrho$  be the unique positive solution of the corresponding equation (4.8), we see from (4.11) that

$$c_1 = \frac{\mathcal{C}_{aw} \varrho}{\mathcal{C}_{aw} \varrho + \lambda} \cdot \frac{W_w}{J_0 \left( \frac{z_0}{m-1} \sqrt{8|\sin \theta|} e^{-i \operatorname{sign}(\theta) \frac{\pi}{4}} \right) + \tilde{c}_2 Y_0 \left( \frac{z_0}{m-1} \sqrt{8|\sin \theta|} e^{-i \operatorname{sign}(\theta) \frac{\pi}{4}} \right)}.$$

Moreover, according to (4.14), the surface deflection angle is then given by

$$\Gamma - \Theta = \tan^{-1} \left( \frac{\operatorname{Im}(\lambda)}{\mathcal{C}_{aw} \varrho + \operatorname{Re}(\lambda)} \right),$$

Some numerical plots for  $\Gamma - \Theta$  are provided in figure 10.

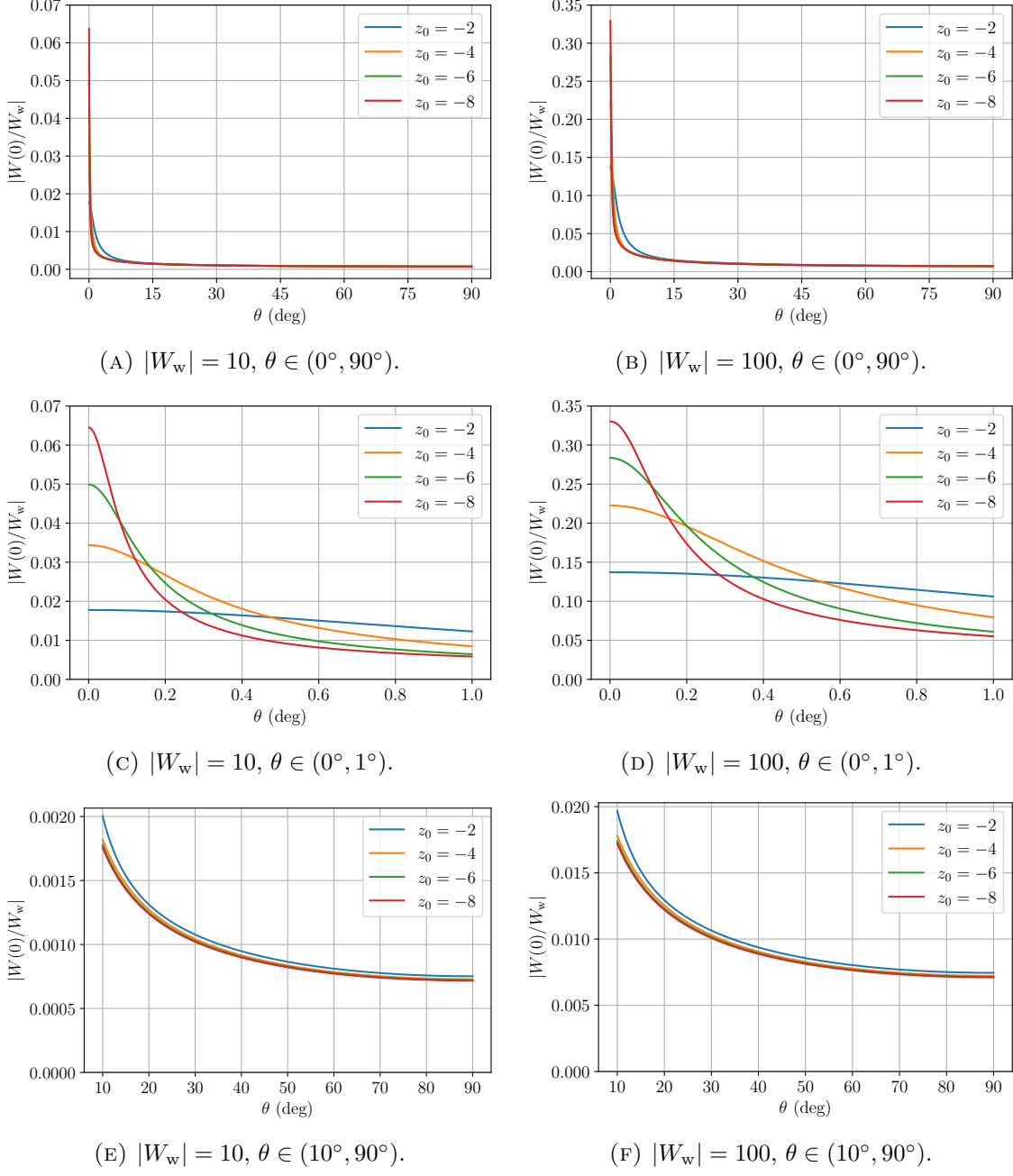


FIGURE 9. The ratio between  $|W(0)|$  and  $|W_w|$  for  $\theta \in (0^\circ, 90^\circ)$  and  $|W_w| = 10$  and  $|W_w| = 100$  (panels (a) and (b)), as well as close-ups for  $\theta \in (0^\circ, 1^\circ)$  (panels (c) and (d)) and  $\theta \in (10^\circ, 90^\circ)$  (panels (e) and (f)).

We now turn to computing the angle between the surface current and Ekman transport. On the one hand, the Ekman transport is

$$\begin{aligned} \text{Ek} = \int_{z_0}^0 W(z) dz &= c_1 \int_{z_0}^0 \left[ J_0 \left( \frac{z_0}{\mathfrak{m} - 1} \sqrt{8|\sin \theta| \left( 1 + \frac{\mathfrak{m} - 1}{z_0} z \right)} e^{-i \text{sign}(\theta) \frac{\pi}{4}} \right) \right. \\ &\quad \left. + \tilde{c}_2 Y_0 \left( \frac{z_0}{\mathfrak{m} - 1} \sqrt{8|\sin \theta| \left( 1 + \frac{\mathfrak{m} - 1}{z_0} z \right)} e^{-i \text{sign}(\theta) \frac{\pi}{4}} \right) \right] dz; \end{aligned}$$

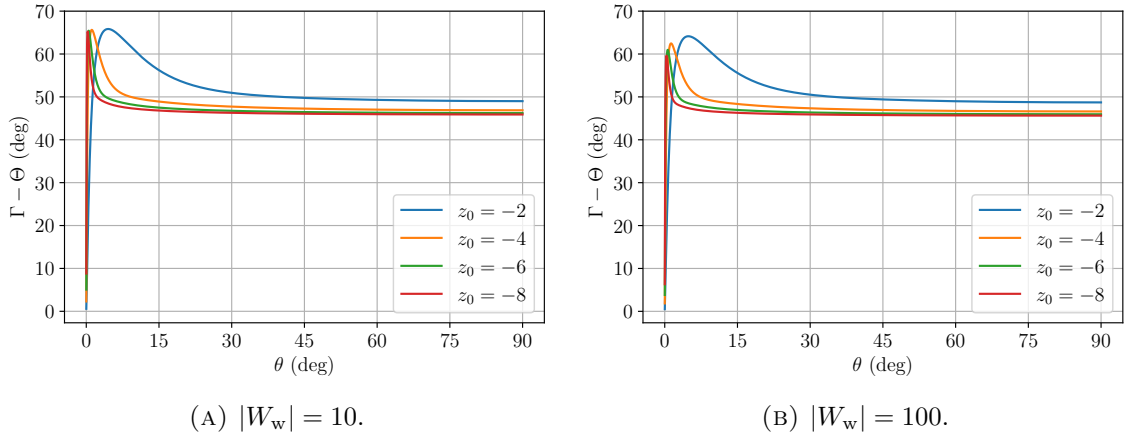


FIGURE 10. The surface deflection angle  $\Gamma - \Theta$  in the case of linearly decaying eddy viscosity.

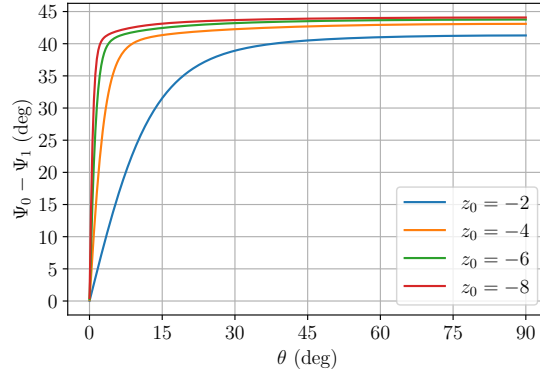


FIGURE 11. The angle  $\Psi_0 - \Psi_1$  between the surface Ekman current  $W(0)$  and the Ekman transport  $\text{Ek}$  in the case of linearly decaying eddy viscosity.

on the other hand, from (5.11) we see that the surface current is given by

$$W(0) = c_1 \left[ J_0 \left( \frac{z_0 \sqrt{8|\sin \theta|}}{m-1} e^{-i \text{sign}(\theta) \frac{\pi}{4}} \right) + \tilde{c}_2 Y_0 \left( \frac{z_0 \sqrt{8|\sin \theta|}}{m-1} e^{-i \text{sign}(\theta) \frac{\pi}{4}} \right) \right],$$

with  $\tilde{c}_2$  as in (5.12). Therefore, the angle between the surface Ekman current and the Ekman transport is

$$\arg \left( \frac{W(0)}{\text{Ek}} \right) = \Psi_0 - \Psi_1,$$

where

$$\Psi_0 = \arg \left( J_0 \left( \frac{z_0 \sqrt{8|\sin \theta|}}{m-1} e^{-i \text{sign}(\theta) \frac{\pi}{4}} \right) + \tilde{c}_2 Y_0 \left( \frac{z_0 \sqrt{8|\sin \theta|}}{m-1} e^{-i \text{sign}(\theta) \frac{\pi}{4}} \right) \right) \quad (5.15)$$

and

$$\begin{aligned} \Psi_1 = \arg & \left( \int_{z_0}^0 \left[ J_0 \left( \frac{z_0}{m-1} \sqrt{8|\sin \theta|} \left( 1 + \frac{m-1}{z_0} z \right) e^{-i \text{sign}(\theta) \frac{\pi}{4}} \right) \right. \right. \\ & \left. \left. + \tilde{c}_2 Y_0 \left( \frac{z_0}{m-1} \sqrt{8|\sin \theta|} \left( 1 + \frac{m-1}{z_0} z \right) e^{-i \text{sign}(\theta) \frac{\pi}{4}} \right) \right] dz \right). \end{aligned} \quad (5.16)$$

Some curves for the angle  $\Psi_0 - \Psi_1$  in dependence of  $\theta$  for several values of  $z_0$  are shown in figure 11.

**5.3. Linearly increasing eddy viscosity.** For the next example, we draw inspiration from Madsen (1977), who, under the assumption of infinite depth, proposed the following parametrisation of the eddy viscosity (in dimensional form):

$$A'_v(z) \approx 0.4 z' \sqrt{\frac{|\tau'_s|}{\rho'}},$$

where  $\tau'_s$  represents the surface shear stress. This idea is adapted in our context using the scaling (2.10) and assuming that the eddy viscosity attains its maximum at  $z = z_0$ . For  $z < z_0$  we assume, as before, that the eddy viscosity rapidly drops to the molecular one, denoted by  $\mathfrak{m}$ , although this is not relevant to our solution. Although this may not seem an entirely realistic model, we nevertheless elect to consider it, as our intention is to obtain and compare some explicit results that relate the profile of the eddy viscosity to that of the deflection angle. The models in the subsequent two examples (piecewise linear and exponentially decaying) are more physically reasonable, and more complicated and realistic eddy viscosity profiles could be an interesting subject for future work.

With our scaling, the profile for the eddy viscosity to be used is

$$m(z) = 1 + \frac{M-1}{z_0} z,$$

where

$$M = \frac{0.4 D'}{\bar{A}'_v} \sqrt{\frac{|\tau'_s|}{\rho'}},$$

which turns out to be  $M \approx 5$ , roughly corresponding to a surface wind stress of magnitude  $0.1 \text{ N m}^{-2}$  on the ocean surface (Paldor, 2024; Talley et al., 2011). For comparison with the piecewise linear profile in the next example, we will also look at  $M = 10$ .

Analogously to the linear case from § 5.2, the general solution is

$$W(z) = c_1 \left[ J_0 \left( \frac{z_0}{M-1} \sqrt{8|\sin \theta|} \left( 1 + \frac{M-1}{z_0} z \right) e^{-i \operatorname{sign}(\theta) \frac{\pi}{4}} \right) \right. \\ \left. + c_2 Y_0 \left( \frac{z_0}{M-1} \sqrt{8|\sin \theta|} \left( 1 + \frac{M-1}{z_0} z \right) e^{-i \operatorname{sign}(\theta) \frac{\pi}{4}} \right) \right], \quad (5.17)$$

where  $c_1$  and  $c_2$  are complex constants (depending parametrically on  $\varphi$  and  $\theta$ ). Determining them will yield the explicit solution, which is depicted in figure 12, in addition to the ratio between the intensity of the surface current and that of the wind given in figure 13. The calculations are identical to those in the previous case of a linearly decaying eddy viscosity: imposing  $W(z_0) = 0$  yields

$$c_2 = - \frac{J_0 \left( \frac{z_0 \sqrt{8|\sin \theta|} M}{M-1} e^{-i \operatorname{sign}(\theta) \frac{\pi}{4}} \right)}{Y_0 \left( \frac{z_0 \sqrt{8|\sin \theta|} M}{M-1} e^{-i \operatorname{sign}(\theta) \frac{\pi}{4}} \right)},$$

and (4.13) in this case reads

$$\lambda = -\sqrt{2|\sin \theta|} e^{-i \operatorname{sign}(\theta) \frac{\pi}{4}} \frac{J_1 \left( \frac{z_0 \sqrt{8|\sin \theta|}}{M-1} e^{-i \operatorname{sign}(\theta) \frac{\pi}{4}} \right) + c_2 Y_1 \left( \frac{z_0 \sqrt{8|\sin \theta|}}{M-1} e^{-i \operatorname{sign}(\theta) \frac{\pi}{4}} \right)}{J_0 \left( \frac{z_0 \sqrt{8|\sin \theta|}}{M-1} e^{-i \operatorname{sign}(\theta) \frac{\pi}{4}} \right) + c_2 Y_0 \left( \frac{z_0 \sqrt{8|\sin \theta|}}{M-1} e^{-i \operatorname{sign}(\theta) \frac{\pi}{4}} \right)}, \quad (5.18)$$

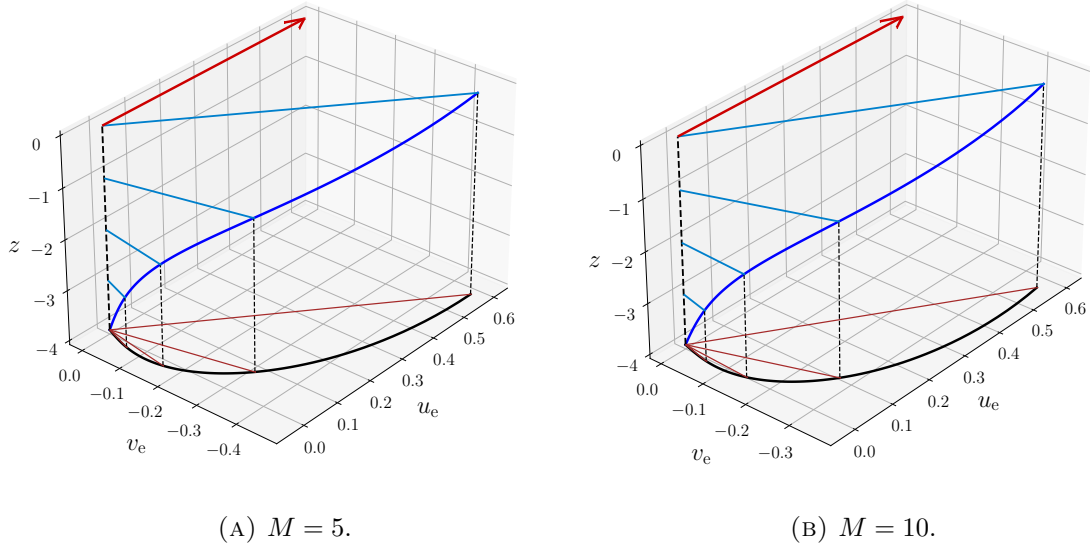


FIGURE 12. Depiction of the solution (5.17) (in blue) for  $\theta = 45^\circ$  and  $z_0 = -4$ , with the direction of the wind (in red) and the projection onto the bottom plane (in black). Observe how the surface deflection angle is visibly smaller than  $45^\circ$ .

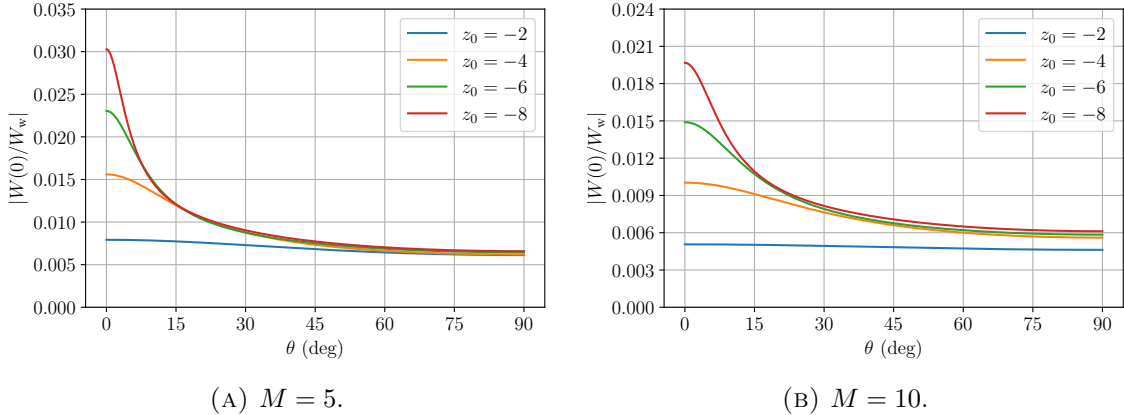


FIGURE 13. The ratio  $|W(0)/W_w|$  between the intensity of the surface current and that of the wind for the case of linearly increasing eddy viscosity.

from which  $c_1$  is determined as

$$c_1 = \frac{\mathcal{C}_{aw}\varrho}{\mathcal{C}_{aw}\varrho + \lambda} \cdot \frac{W_w}{J_0\left(\frac{z_0}{M-1}\sqrt{8|\sin\theta|} e^{-i\text{sign}(\theta)\frac{\pi}{4}}\right) + \tilde{c}_2 Y_0\left(\frac{z_0}{M-1}\sqrt{8|\sin\theta|} e^{-i\text{sign}(\theta)\frac{\pi}{4}}\right)},$$

where  $\varrho$  is the unique positive solution of (4.8) for  $\lambda$  as in (5.18).

From this, using (4.14), we can also calculate the values of the deflection angles, which are plotted in figure 14. In this case, we see that the deflection angles are smaller than the  $45^\circ$  of Ekman's classical theory. Observe how, in the argument of the Bessel functions entering the computation of  $\lambda$ , the relevant parameter is not  $M$  itself, but rather the ratio  $z_0\sqrt{8|\sin\theta|}/(M-1)$ . In the work of Madsen (1977), the author obtained a deflection angle of approximately  $10^\circ$ , a value that we recover for sufficiently small values of  $z_0$  and/or  $\theta$ . Moreover, from figure 14 it is evident that increasing  $M$  leads to a decrease in the deflection

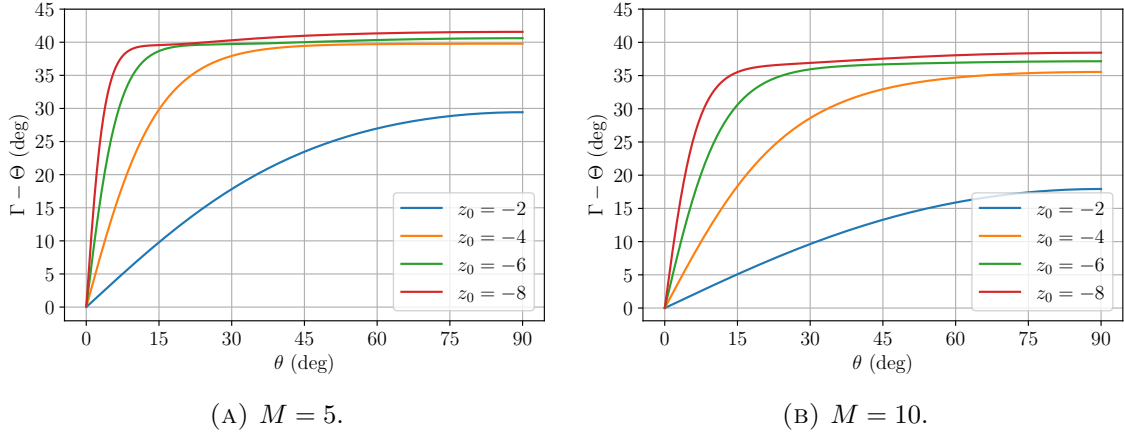


FIGURE 14. The surface deflection angle  $\Gamma - \Theta$  for  $|W_w| = 100$  in the case of linearly increasing eddy viscosity.

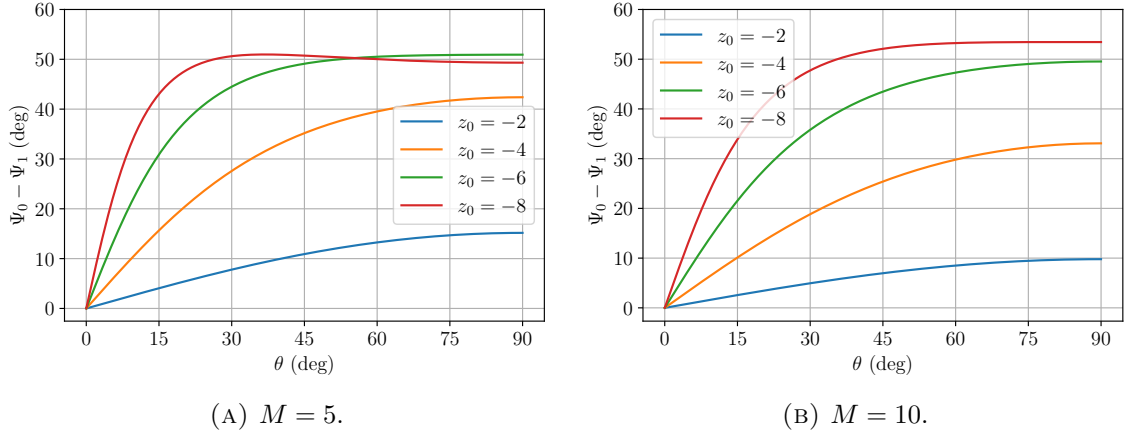


FIGURE 15. The angle  $\Psi_0 - \Psi_1$  between the surface Ekman current  $W(0)$  and the Ekman transport  $\text{Ek}$  for the case of linearly increasing eddy viscosity.

angle. Therefore, the results of Madsen (1977) can be regarded as a limiting case of our analysis, corresponding to the regime of a tiny ratio  $z_0 \sqrt{8|\sin \theta|}/(M - 1)$ , although it should be pointed out that Madsen's solution involved Kelvin functions of order zero, whereas ours is based on Bessel functions. Observe also that, for  $z_0 \sqrt{8|\sin \theta|}/(M - 1) = 0$ , we find that the deflection angle is zero.

Finally, denoting, as before,

$$\Psi_0 = \arg \left( \frac{W(0)}{c_1} \right) \quad \text{and} \quad \Psi_1 = \arg \left( \frac{\text{Ek}}{c_1} \right),$$

where the Ekman transport is given by

$$\text{Ek} = \int_{z_0}^0 W(z) \, dz,$$

we can compute the angle between the surface Ekman flow  $W(0)$  and the Ekman transport  $\text{Ek}$ , which is given by (5.15) and (5.16); in figure 15, we provide some numerical plots for different values of  $z_0$ .

**5.4. Piecewise linear eddy viscosity.** In this section, we consider the model proposed by Zikanov et al. (2003) of an eddy viscosity that increases linearly up to a depth of approximately  $z_0/4$  and then decreases linearly to the molecular viscosity  $\mathfrak{m}$  at the depth  $z_0$ . This model is a simplified version of the models used by Weber (1981) or McWilliams and Huckle (2006), and is related to the fact that the eddy viscosity may reach a maximum as the turbulence length scale becomes smaller at a certain depth below the surface. Within our setting, we take

$$m(z) = \begin{cases} 1 + \frac{4}{z_0}(M-1)z =: a_1 + b_1 z & \text{for } \frac{z_0}{4} < z \leq 0, \\ \frac{1}{3}(4M-\mathfrak{m}) - \frac{4}{3} \frac{M-\mathfrak{m}}{z_0} z =: a_2 + b_2 z & \text{for } z_0 \leq z \leq \frac{z_0}{4}, \end{cases} \quad (5.19)$$

where  $M$  is the maximum value achieved by the non-dimensional eddy viscosity at  $z = \frac{z_0}{4}$  and  $\mathfrak{m} \approx 10^{-4}$  is, as in the previous section, the small value of the molecular eddy viscosity below  $z = z_0$ . The constant  $M$  can be estimated as  $M \approx 10$  (Zikanov et al., 2003).

Analogously to (5.9), in each of the intervals  $I_1 = [\frac{z_0}{4}, 0]$  and  $I_2 = [z_0, \frac{z_0}{4}]$  we perform the change of variable

$$X_k(z) = \sqrt{a_k + b_k z}, \quad k \in \{1, 2\},$$

so in each of  $I_1$  and  $I_2$  the differential equation (5.1) is transformed into the Bessel equation

$$X_k^2 \frac{d^2 G_k}{dX_k^2}(X_k) + X_k \frac{dG}{dX_k}(X_k) - \frac{8ia_k}{b_k^2} \sin \theta X_k^2 G(X_k) = 0, \quad k \in \{1, 2\}, \quad (5.20)$$

for  $\sqrt{M} < X_1 < 1$  and  $\sqrt{\mathfrak{m}} < X_2 < \sqrt{M}$ . The solution of the Bessel equation (5.20) is

$$G_k(X_k) = C_{1,k} J_0 \left( \frac{\sqrt{8a_k |\sin \theta|}}{b_k} X_k e^{-i \operatorname{sign}(\theta) \frac{\pi}{4}} \right) + C_{2,k} Y_0 \left( \frac{\sqrt{8a_k |\sin \theta|}}{b_k} X_k e^{-i \operatorname{sign}(\theta) \frac{\pi}{4}} \right), \quad k \in \{1, 2\},$$

where  $C_{1,k}$  and  $C_{2,k}$  are complex constants (depending parametrically on  $\varphi$  and  $\theta$ ). Thus, reverting to the variable  $z$  by inverting (5.9) in each interval, in view of (5.19) we have

$$W(z) = c_1 J_0 \left( \frac{\sqrt{1 + \frac{4}{z_0}(M-1)z}}{4(M-1)} \sqrt{8|\sin \theta|} z_0 e^{-i \operatorname{sign}(\theta) \frac{\pi}{4}} \right) + c_2 Y_0 \left( \frac{\sqrt{1 + \frac{4}{z_0}(M-1)z}}{4(M-1)} \sqrt{8|\sin \theta|} z_0 e^{-i \operatorname{sign}(\theta) \frac{\pi}{4}} \right), \quad z \in I_1 \quad (5.21)$$

and

$$W(z) = c_3 J_0 \left( \frac{\sqrt{\frac{1}{3}(4M-\mathfrak{m}) - \frac{4}{3} \frac{M-\mathfrak{m}}{z_0} z}}{\frac{4}{3}(\mathfrak{m}-M)} \sqrt{8|\sin \theta|} z_0 e^{-i \operatorname{sign}(\theta) \frac{\pi}{4}} \right) + c_4 Y_0 \left( \frac{\sqrt{\frac{1}{3}(4M-\mathfrak{m}) - \frac{4}{3} \frac{M-\mathfrak{m}}{z_0} z}}{\frac{4}{3}(\mathfrak{m}-M)} \sqrt{8|\sin \theta|} z_0 e^{-i \operatorname{sign}(\theta) \frac{\pi}{4}} \right), \quad z \in I_2, \quad (5.22)$$

where, for simplicity, we denoted  $(C_{1,1}, C_{1,2}, C_{2,1}, C_{2,2}) = (c_1, c_2, c_3, c_4)$ . These constants must be chosen so that  $W$  and  $W'$  are continuous in  $z = \frac{z_0}{4}$  and satisfy the boundary conditions (5.2) and (5.3). Determining them, as we will do presently, will give the explicit solution sketched in figure 16, as well as the ratio between the intensity of the surface current  $W(0)$  and that of the wind  $W_w$  determined from (4.12) and depicted in figure 17.

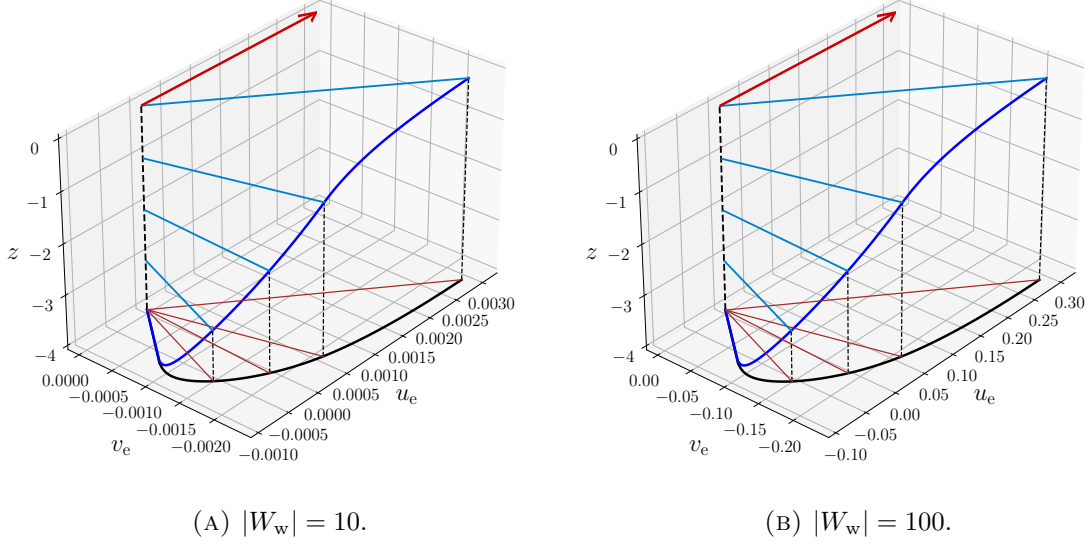


FIGURE 16. Depiction of the solution (5.21)–(5.22) (in blue) for  $\theta = 45^\circ$  and  $z_0 = -4$ , with the direction of the wind (in red) and the projection onto the bottom plane (in black).

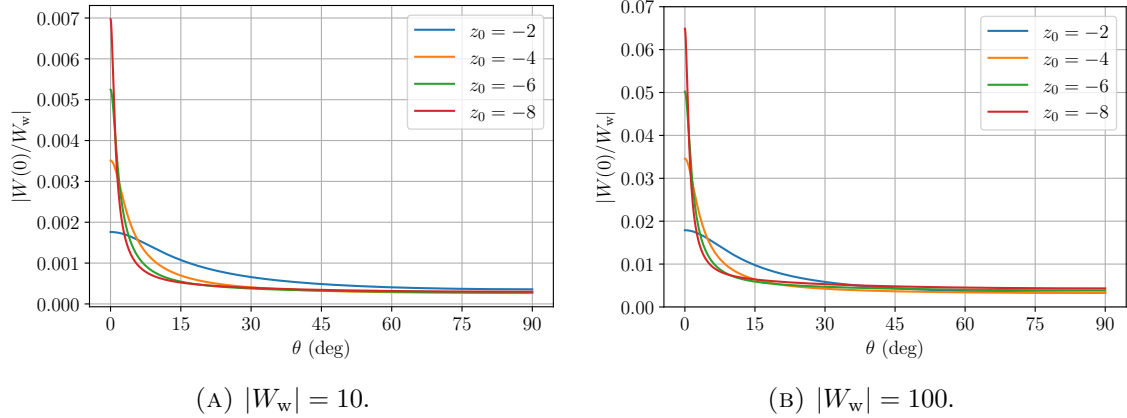


FIGURE 17. The ratio  $|W(0)/W_w|$  between the intensity of the surface current and that of the wind for the case of piecewise linear eddy viscosity.

Let us work our way from the bottom up. Plugging  $z = z_0$  into (5.22), we see that (5.3) is satisfied if and only if

$$c_4 = \mathcal{K} c_3, \quad \text{with} \quad \mathcal{K} = -\frac{J_0 \left( \frac{\sqrt{8m|\sin \theta|} z_0}{\frac{4}{3}(m-M)} e^{-i \operatorname{sign}(\theta) \frac{\pi}{4}} \right)}{Y_0 \left( \frac{\sqrt{8m|\sin \theta|} z_0}{\frac{4}{3}(m-M)} e^{-i \operatorname{sign}(\theta) \frac{\pi}{4}} \right)}.$$

Recalling the formula (5.13) for the derivative of the Bessel functions and denoting  $\tilde{c}_2 = \frac{c_2}{c_1}$ , we have

$$\begin{aligned} W'(z) = & -c_1 \frac{\sqrt{2|\sin \theta|}}{\sqrt{(1 + \frac{4}{z_0}(M-1)z)}} e^{-i \operatorname{sign}(\theta) \frac{\pi}{4}} \times \\ & \times \left[ J_1 \left( \frac{\sqrt{8|\sin \theta|(1 + \frac{4}{z_0}(M-1)z)}}{4(M-1)} z_0 e^{-i \operatorname{sign}(\theta) \frac{\pi}{4}} \right) \right. \\ & \left. + \tilde{c}_2 Y_1 \left( \frac{\sqrt{8|\sin \theta|(1 + \frac{4}{z_0}(M-1)z)}}{4(M-1)} z_0 e^{-i \operatorname{sign}(\theta) \frac{\pi}{4}} \right) \right], \quad z \in I_1, \end{aligned} \quad (5.23)$$

and

$$\begin{aligned} W'(z) = & -c_3 \frac{\sqrt{2|\sin \theta|}}{\sqrt{\frac{1}{3}(4M-\mathfrak{m}) - \frac{4}{3}\frac{M-\mathfrak{m}}{z_0}z}} e^{-i \operatorname{sign}(\theta) \frac{\pi}{4}} \times \\ & \times \left[ J_1 \left( \frac{\sqrt{\frac{1}{3}(4M-\mathfrak{m}) - \frac{4}{3}\frac{M-\mathfrak{m}}{z_0}z}}{\frac{4}{3}(\mathfrak{m}-M)} \sqrt{8|\sin \theta|} z_0 e^{-i \operatorname{sign}(\theta) \frac{\pi}{4}} \right) \right. \\ & \left. + \mathcal{K} Y_1 \left( \frac{\sqrt{\frac{1}{3}(4M-\mathfrak{m}) - \frac{4}{3}\frac{M-\mathfrak{m}}{z_0}z}}{\frac{4}{3}(\mathfrak{m}-M)} \sqrt{8|\sin \theta|} z_0 e^{-i \operatorname{sign}(\theta) \frac{\pi}{4}} \right) \right], \quad z \in I_2. \end{aligned}$$

Thus, denoting  $\tilde{c}_3 = \frac{c_3}{c_1}$ , the requirement of continuity of  $W$  and  $W'$  in  $\frac{z_0}{4}$  results in the linear system of equations

$$\begin{aligned} & J_0 \left( \frac{\sqrt{8M|\sin \theta|} z_0}{4(M-1)} e^{-i \operatorname{sign}(\theta) \frac{\pi}{4}} \right) + \tilde{c}_2 Y_0 \left( \frac{\sqrt{8M|\sin \theta|} z_0}{4(M-1)} e^{-i \operatorname{sign}(\theta) \frac{\pi}{4}} \right) \\ & = \tilde{c}_3 \left[ J_0 \left( \frac{\sqrt{8M|\sin \theta|} z_0}{\frac{4}{3}(\mathfrak{m}-M)} e^{-i \operatorname{sign}(\theta) \frac{\pi}{4}} \right) + \mathcal{K} Y_0 \left( \frac{\sqrt{8M|\sin \theta|} z_0}{\frac{4}{3}(\mathfrak{m}-M)} e^{-i \operatorname{sign}(\theta) \frac{\pi}{4}} \right) \right] \end{aligned}$$

and

$$\begin{aligned} & J_1 \left( \frac{\sqrt{8M|\sin \theta|} z_0}{4(M-1)} e^{-i \operatorname{sign}(\theta) \frac{\pi}{4}} \right) + \tilde{c}_2 Y_1 \left( \frac{\sqrt{8M|\sin \theta|} z_0}{4(M-1)} e^{-i \operatorname{sign}(\theta) \frac{\pi}{4}} \right) \\ & = \tilde{c}_3 \left[ J_1 \left( \frac{\sqrt{8M|\sin \theta|} z_0}{\frac{4}{3}(\mathfrak{m}-M)} e^{-i \operatorname{sign}(\theta) \frac{\pi}{4}} \right) + \mathcal{K} Y_1 \left( \frac{\sqrt{8M|\sin \theta|} z_0}{\frac{4}{3}(\mathfrak{m}-M)} e^{-i \operatorname{sign}(\theta) \frac{\pi}{4}} \right) \right] \end{aligned}$$

for  $\tilde{c}_2$  and  $\tilde{c}_3$ , which can be easily solved, yielding

$$\tilde{c}_2 = \frac{A_1(C_0 + D_0) - A_0(C_1 + D_1)}{B_0(C_1 + D_1) - B_1(C_0 + D_0)}$$

and

$$\tilde{c}_3 = \frac{A_1 B_0 - A_0 B_1}{B_0(C_1 + D_1) - B_1(C_0 + D_0)},$$

where, for simplicity, we abbreviated

$$\begin{aligned} A_0 & = J_0 \left( \frac{\sqrt{8M|\sin \theta|} z_0}{4(M-1)} e^{-i \operatorname{sign}(\theta) \frac{\pi}{4}} \right), \quad B_0 = Y_0 \left( \frac{\sqrt{8M|\sin \theta|} z_0}{4(M-1)} e^{-i \operatorname{sign}(\theta) \frac{\pi}{4}} \right), \\ C_0 & = J_0 \left( \frac{\sqrt{8M|\sin \theta|} z_0}{\frac{4}{3}(\mathfrak{m}-M)} e^{-i \operatorname{sign}(\theta) \frac{\pi}{4}} \right), \quad D_0 = \mathcal{K} Y_0 \left( \frac{\sqrt{8M|\sin \theta|} z_0}{\frac{4}{3}(\mathfrak{m}-M)} e^{-i \operatorname{sign}(\theta) \frac{\pi}{4}} \right), \end{aligned}$$

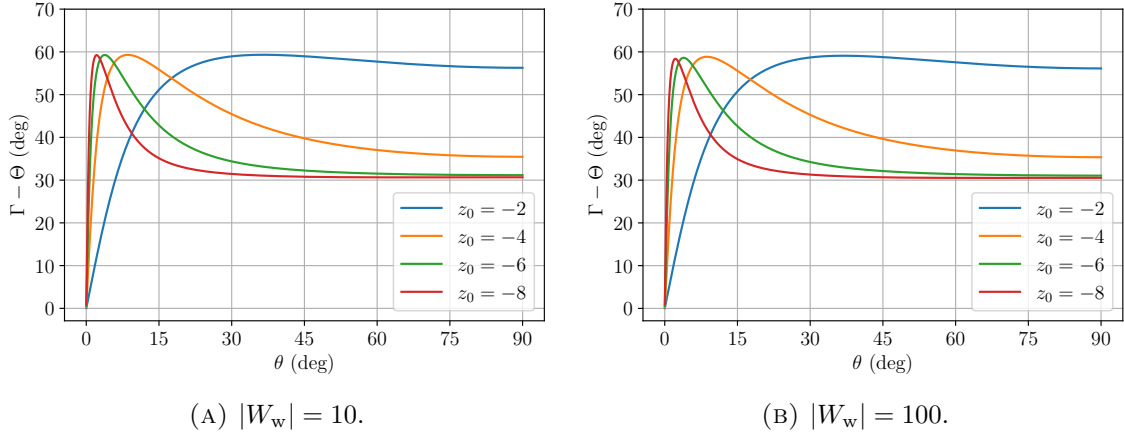


FIGURE 18. The surface deflection angle  $\Gamma - \Theta$  in the case of piecewise linear eddy viscosity.

and

$$\begin{aligned} A_1 &= J_1 \left( \frac{\sqrt{8M|\sin \theta|} z_0}{4(M-1)} e^{-i \operatorname{sign}(\theta) \frac{\pi}{4}} \right), \quad B_1 = Y_1 \left( \frac{\sqrt{8M|\sin \theta|} z_0}{4(M-1)} e^{-i \operatorname{sign}(\theta) \frac{\pi}{4}} \right), \\ C_1 &= J_1 \left( \frac{\sqrt{8M|\sin \theta|} z_0}{\frac{4}{3}(\mathfrak{m} - M)} e^{-i \operatorname{sign}(\theta) \frac{\pi}{4}} \right), \quad D_1 = \mathcal{K} Y_1 \left( \frac{\sqrt{8M|\sin \theta|} z_0}{\frac{4}{3}(\mathfrak{m} - M)} e^{-i \operatorname{sign}(\theta) \frac{\pi}{4}} \right). \end{aligned}$$

It remains to determine the coefficient  $c_1$ . Computing (5.21) and (5.23) for  $z = 0$  yields

$$W(0) = c_1 \left[ J_0 \left( \frac{\sqrt{8|\sin \theta|}}{4(M-1)} z_0 e^{-i \operatorname{sign}(\theta) \frac{\pi}{4}} \right) + \tilde{c}_2 Y_0 \left( \frac{\sqrt{8|\sin \theta|}}{4(M-1)} z_0 e^{-i \operatorname{sign}(\theta) \frac{\pi}{4}} \right) \right]$$

and

$$\begin{aligned} W'(0) &= -c_1 \sqrt{2|\sin \theta|} e^{-i \operatorname{sign}(\theta) \frac{\pi}{4}} \times \\ &\quad \times \left[ J_1 \left( \frac{\sqrt{8|\sin \theta|}}{4(M-1)} z_0 e^{-i \operatorname{sign}(\theta) \frac{\pi}{4}} \right) + \tilde{c}_2 Y_1 \left( \frac{\sqrt{8|\sin \theta|}}{4(M-1)} z_0 e^{-i \operatorname{sign}(\theta) \frac{\pi}{4}} \right) \right]. \end{aligned}$$

Thus, for the number  $\lambda$  from (4.13) we find

$$\begin{aligned} \lambda &= -\sqrt{2|\sin \theta|} e^{-i \operatorname{sign}(\theta) \frac{\pi}{4}} \times \\ &\quad \times \frac{J_1 \left( \frac{\sqrt{8|\sin \theta|}}{4(M-1)} z_0 e^{-i \operatorname{sign}(\theta) \frac{\pi}{4}} \right) + \tilde{c}_2 Y_1 \left( \frac{\sqrt{8|\sin \theta|}}{4(M-1)} z_0 e^{-i \operatorname{sign}(\theta) \frac{\pi}{4}} \right)}{J_0 \left( \frac{\sqrt{8|\sin \theta|}}{4(M-1)} z_0 e^{-i \operatorname{sign}(\theta) \frac{\pi}{4}} \right) + \tilde{c}_2 Y_0 \left( \frac{\sqrt{8|\sin \theta|}}{4(M-1)} z_0 e^{-i \operatorname{sign}(\theta) \frac{\pi}{4}} \right)}. \end{aligned}$$

Then, once more letting  $\varrho$  be the unique positive solution of (4.8), the formula (4.11) yields

$$c_1 = \frac{\mathcal{C}_{aw} \varrho}{\mathcal{C}_{aw} \varrho + \lambda} \cdot \frac{W_w}{J_0 \left( \frac{\sqrt{8|\sin \theta|}}{4(M-1)} z_0 e^{-i \operatorname{sign}(\theta) \frac{\pi}{4}} \right) + \tilde{c}_2 Y_0 \left( \frac{\sqrt{8|\sin \theta|}}{4(M-1)} z_0 e^{-i \operatorname{sign}(\theta) \frac{\pi}{4}} \right)}.$$

Using this, the surface deflection angle can be calculated from the formula (4.14), as before; some numerical plots are shown in figure 18.

Finally, we examine the Ekman transport, which is given by

$$\text{Ek} = \int_{z_0}^0 W(z) dz = \int_{\frac{z_0}{4}}^0 W(z) dz + \int_{z_0}^{\frac{z_0}{4}} W(z) dz,$$

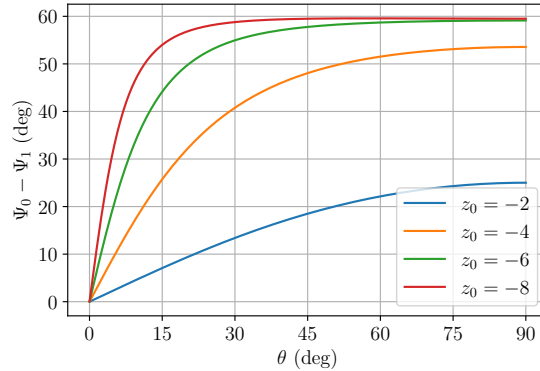


FIGURE 19. The angle  $\Psi_0 - \Psi_1$  between the surface Ekman current  $W(0)$  and the Ekman transport  $\text{Ek}$  for the case of piecewise linear eddy viscosity.

where each of the expressions (5.21) and (5.22) must be used in the corresponding integration interval. As in the previous sections, it is interesting to compute the angle between the surface Ekman flow  $W(0)$  and the Ekman transport  $\text{Ek}$ . Thus, using the same notation as in (5.15) and (5.16), we set

$$\Psi_0 = \arg \left( \frac{W(0)}{c_1} \right) \quad \text{and} \quad \Psi_1 = \arg \left( \frac{\text{Ek}}{c_1} \right);$$

then, the angle that we are looking for is  $\Psi_0 - \Psi_1$ . In figure 19, we provide some numerical plots for different values of  $z_0$ .

**5.5. Exponentially decaying eddy viscosity.** The final case we consider is that, proposed as a model dictated by some turbulence measurements in non-equatorial regions (Cronin and Kessler, 2009; Wenegrat and McPhaden, 2016; Sentchev et al., 2023), of an exponentially decreasing eddy viscosity of the form

$$m(z) = e^{qz}, \quad z_0 < z < 0,$$

where

$$q = \frac{\ln(m)}{z_0}, \quad (5.24)$$

which ensures that  $m(z_0) = m$ . Note that, for  $m = 10^{-4}$  and  $z_0 = -4$ , it follows that  $q \approx 2.3$ , a value that, with respect to our scaling, is very close to that determined by Wenegrat and McPhaden (2016). With this choice for  $m$ , (5.1) becomes

$$W''(z) + qW'(z) - 2i e^{-qz} \sin \theta W(z) = 0, \quad z_0 < z < 0. \quad (5.25)$$

Let us define the function  $H$  through

$$W(z) = H(z) e^{-\frac{qz}{2}}.$$

Then

$$W'(z) = e^{-\frac{qz}{2}} \left( H'(z) - \frac{q}{2} H(z) \right) \quad \text{and} \quad W''(z) = e^{-\frac{qz}{2}} \left( H''(z) - qW'(z) + \frac{q^2}{4} H(z) \right),$$

and (5.25) becomes

$$H''(z) - \left( 2i e^{-qz} \sin \theta + \frac{q^2}{4} \right) H(z) = 0, \quad z_0 < z < 0. \quad (5.26)$$

Introducing the change of variables

$$X = \frac{2}{q} \sqrt{2i \sin \theta} e^{-\frac{qz}{2}},$$

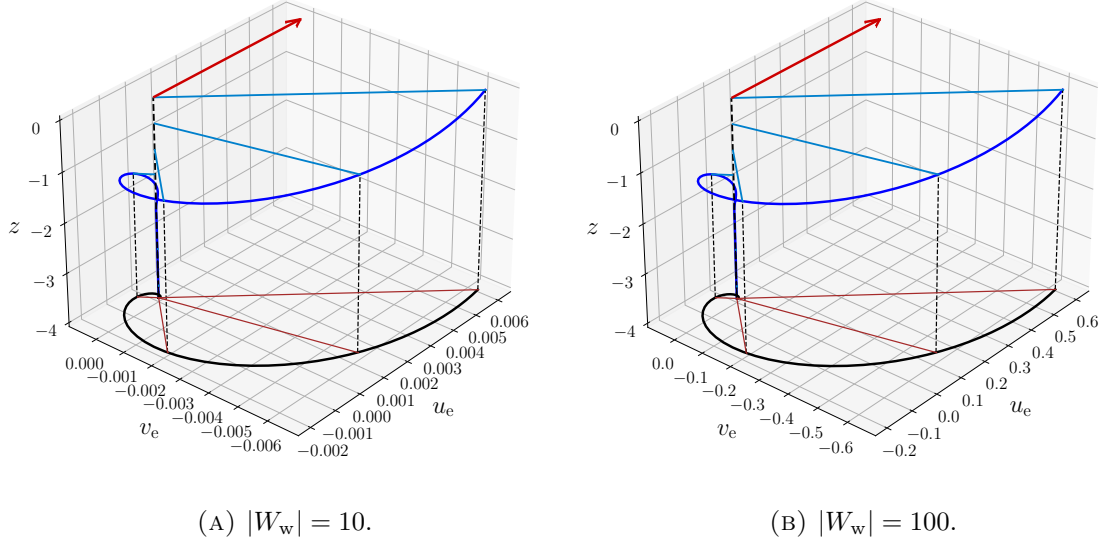


FIGURE 20. Depiction of the solution (5.27) (in blue) for  $\theta = 45^\circ$  and  $z_0 = -4$ , with the direction of the wind (in red) and the projection onto the bottom plane (in black).

for which we have

$$\frac{d}{dz} = -\frac{q}{2}X \frac{d}{dX} \quad \text{and} \quad \frac{d^2}{dz^2} = \frac{q^2}{4} \left( X^2 \frac{d^2}{dX^2} + X \frac{d}{dX} \right),$$

and, denoting

$$H(z) = G(X),$$

(5.26) transforms into the equation

$$X^2 \frac{d^2 G}{dX^2}(X) + X \frac{dG}{dX}(X) - (X^2 + 1)G(X) = 0, \quad \frac{2}{q} \sqrt{2i \sin \theta} < X < \frac{2}{q} \sqrt{\frac{2i \sin \theta}{m}},$$

whose general solution is

$$G(X) = c_1 I_1(X) + c_2 K_1(X), \quad \frac{2}{q} \sqrt{2i \sin \theta} < X < \frac{2}{q} \sqrt{\frac{2i \sin \theta}{m}},$$

where  $c_1, c_2 \in \mathbb{C}$  and  $I_1$  and  $K_1$  are the modified Bessel functions of the first and second kind, respectively, both of order 1. Thus, we obtain

$$\begin{aligned} W(z) &= e^{-\frac{qz}{2}} \left[ c_1 I_1 \left( \frac{2}{q} \sqrt{2i \sin \theta} e^{-\frac{qz}{2}} \right) + c_2 K_1 \left( \frac{2}{q} \sqrt{2i \sin \theta} e^{-\frac{qz}{2}} \right) \right], \\ &= c_1 e^{-\frac{qz}{2}} \left[ I_1 \left( \frac{2}{q} \sqrt{2i \sin \theta} e^{-\frac{qz}{2}} \right) + \tilde{c}_2 K_1 \left( \frac{2}{q} \sqrt{2i \sin \theta} e^{-\frac{qz}{2}} \right) \right], \quad z_0 < z < 0, \end{aligned} \tag{5.27}$$

as the general solution of (5.25), where  $\tilde{c}_2 = c_2/c_1$ . We now determine  $c_1$  and  $c_2$  through the boundary conditions; the corresponding plots for the solution and the ratio  $|W(0)/W_w|$  is given in figure 20.

Setting  $W(z_0) = 0$  to satisfy the boundary condition (5.3), we find

$$\tilde{c}_2 = -\frac{I_1 \left( \frac{2z_0(1+i \sin \theta)}{\ln(m)} \sqrt{\frac{|\sin \theta|}{m}} \right)}{K_1 \left( \frac{2z_0(1+i \sin \theta)}{\ln(m)} \sqrt{\frac{|\sin \theta|}{m}} \right)}.$$

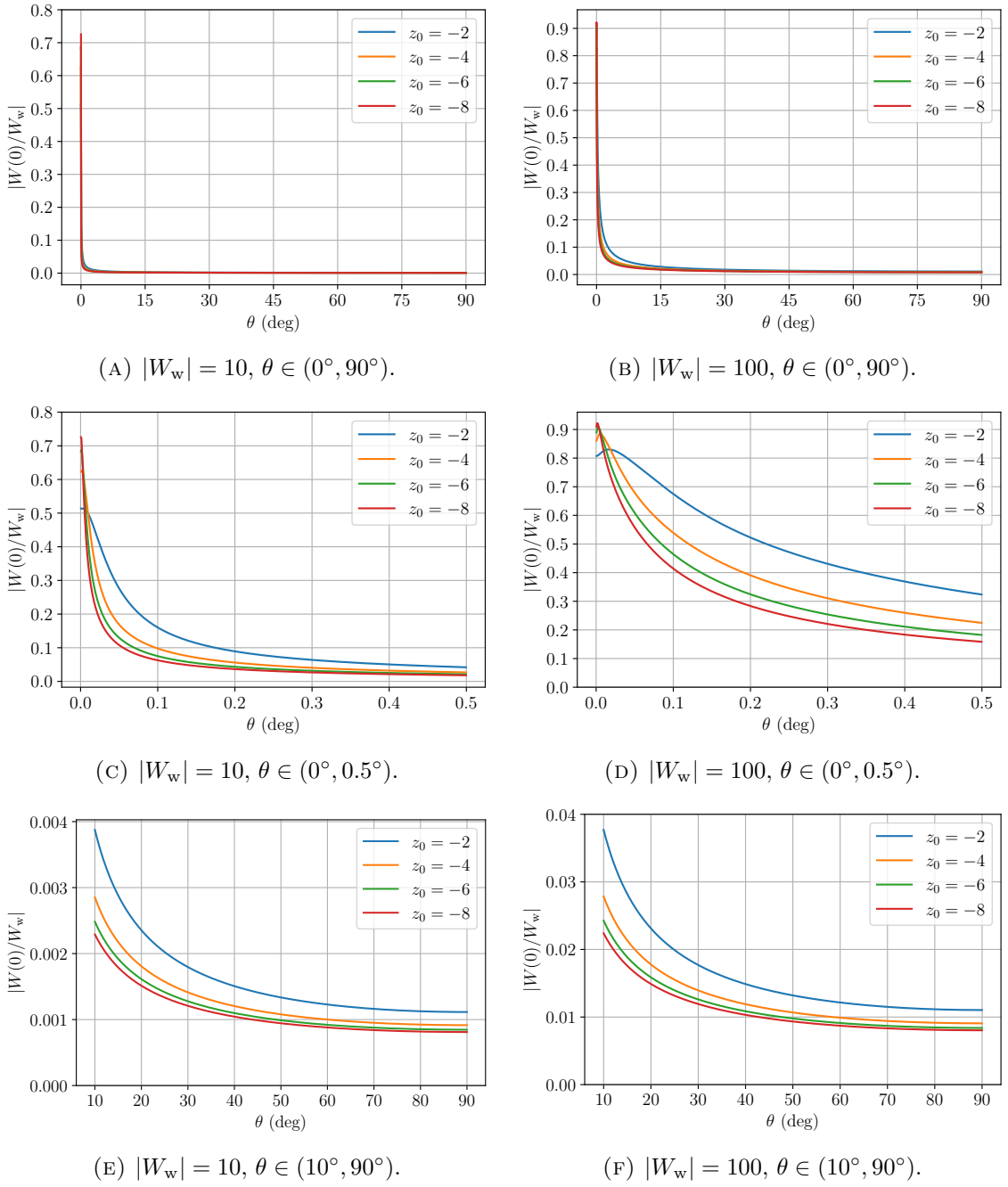


FIGURE 21. The ratio between  $|W(0)|$  and  $|W_w|$  for  $\theta \in (0^\circ, 90^\circ)$  and  $|W_w| = 10$  and  $|W_w| = 100$  (panels (a) and (b)), as well as close-ups for  $\theta \in (0^\circ, 0.5^\circ)$  (panels (c) and (d)) and  $\theta \in (10^\circ, 90^\circ)$  (panels (e) and (f)), in the case of exponentially decaying eddy viscosity.

Moreover, recalling that

$$\frac{dI_1(t)}{dt} = \frac{1}{2}(I_0(t) + I_2(t)) \quad \text{and} \quad \frac{dK_1(t)}{dt} = -\frac{1}{2}(K_0(t) + K_2(t))$$

and denoting

$$f(z) = \frac{2(1 + i \operatorname{sign} \theta)}{q} \sqrt{|\sin \theta|} e^{-\frac{qz}{2}}, \quad \text{with} \quad f'(z) = -(1 + i \operatorname{sign} \theta) \sqrt{|\sin \theta|} e^{-\frac{qz}{2}},$$

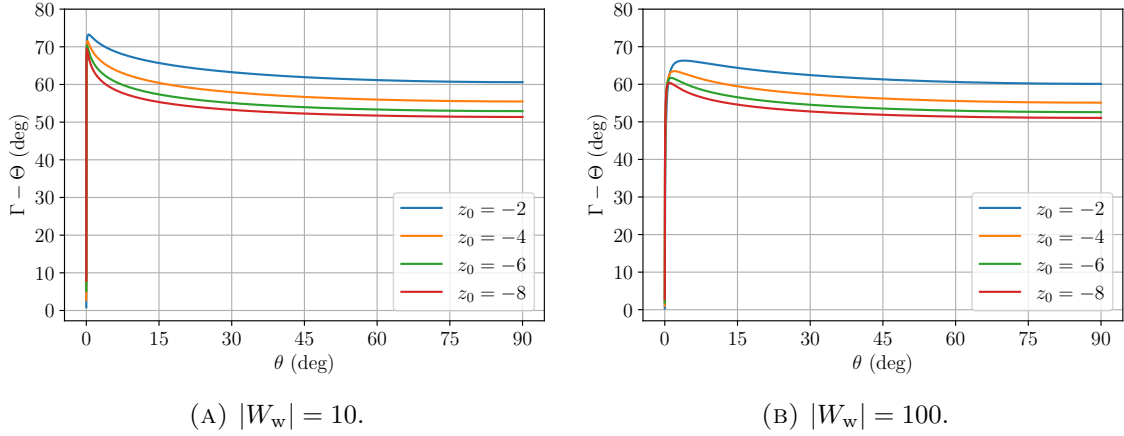


FIGURE 22. The surface deflection angle  $\Gamma - \Theta$  in the case of exponentially decaying eddy viscosity.

we obtain

$$W'(z) = -\frac{q}{2}W(z) + \frac{A e^{-\frac{qz}{2}} f'(z)}{2} [I_0(f(z)) + I_2(f(z)) - \tilde{c}_2 K_0(f(z)) - \tilde{c}_2 K_2(f(z))].$$

Note that, using the expression for  $q$  in (5.24), we have

$$f(0) = \frac{2z_0(1 + i \operatorname{sign} \theta)}{\ln(m)} \sqrt{|\sin \theta|}, \quad \text{with} \quad f'(0) = -(1 + i \operatorname{sign} \theta) \sqrt{|\sin \theta|},$$

so that for (4.13) we obtain

$$\lambda = -\frac{\ln(m)}{2z_0} + \frac{f'(0)}{2} \left[ \frac{I_0(f(0)) + I_2(f(0)) - \tilde{c}_2 K_0(f(0)) - \tilde{c}_2 K_2(f(0))}{I_1(f(0)) + \tilde{c}_2 K_1(f(0))} \right];$$

and thus, in view of (4.11),

$$c_1 = \frac{\mathcal{C}_{aw} \varrho}{\mathcal{C}_{aw} \varrho + \lambda} \cdot \frac{W_w}{I_1(f(0)) + \tilde{c}_2 K_1(f(0))},$$

where, as usual,  $\varrho$  is the unique positive solution of (4.8).

The ratio  $|W(0)|/W_w$  between the intensity of the surface current and that of the wind, computed according to (4.12), is shown in figure 21. Furthermore, the surface deflection angle can be calculated from the formula (4.14), as before. Some curves for the deflection angle depending on the latitude  $\theta$  are sketched in figure 22.

We conclude this section by numerically computing the angle between the surface current  $W(0)$  and the Ekman transport  $\text{Ek}$ . The former is

$$W(0) = c_1 [I_1(f(0)) + \tilde{c}_2 K_1(f(0))],$$

and the latter can be computed as

$$\text{Ek} = \int_{z_0}^0 W(z) dz = c_1 \int_{z_0}^0 e^{-\frac{qz}{2}} (I_1(f(z)) + \tilde{c}_2 K_1(f(z))) dz.$$

Denoting

$$\Psi_0 = \arg(I_1(f(0)) + \tilde{c}_2 K_1(f(0)))$$

and

$$\Psi_1 = \arg \left( \int_{z_0}^0 e^{-\frac{qz}{2}} (I_1(f(z)) + \tilde{c}_2 K_1(f(z))) dz \right),$$

as in the previous section, the angle between  $W(0)$  and  $\text{Ek}$  is given by  $\Psi_0 - \Psi_1$ . Some numerical values are reported in figure 23.

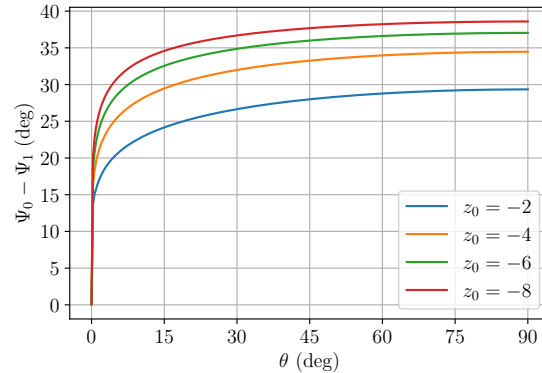


FIGURE 23. The angle  $\Psi_0 - \Psi_1$  between the surface Ekman current  $W(0)$  and the Ekman transport  $\mathbf{E}_k$  in the case of exponentially decaying eddy viscosity.

## 6. DISCUSSION

We conclude with a summary of what this work has achieved and an overview of the possible directions for future research that it opens up.

Starting from the governing equations for a viscous fluid in spherical coordinates, we derived an asymptotic model for the analysis of large-scale wind-drift currents. The derivation was based on asymptotic expansions with respect to the two small parameters  $\varepsilon$  and  $\mathcal{R}$  that characterise the problem and whose smallness reflects the underlying physical regime. Specifically,  $\varepsilon$ , defined as the ratio between the characteristic depth scale and the Earth's radius, encodes the weakness of vertical variations, while the small Rossby number  $\mathcal{R}$  corresponds to flows dominated by rotation rather than by advection. In particular, in the study of wind-driven drift currents, it is standard to assume that the vertical velocity is of order  $\varepsilon$  lower than the horizontal velocity components, implying a weak coupling between vertical and horizontal motions (see, for instance, the discussions by Constantin and Johnson (2019a,b) and Puntini (2025, 2026)); in fact, we showed that this is not an assumption, but is actually dictated by the scaling. Unlike the traditional  $f$ -plane or  $\beta$ -plane approximations, our approach retains the full spherical geometry, in the spirit of recent works by Constantin and Johnson (2018, 2019a,b) and provides a consistent framework for investigating wind-driven flows on large spatial scales, with direct relevance to oceanic circulation (Wunsch and Ferrari, 2004). Only two assumptions were made *a priori*: the water density is taken to be constant above the thermocline, and the eddy viscosity is assumed to depend only on the depth.

Later on, we made a further simplifying assumption, namely that the free surface should be flat. Although, as we pointed out earlier, this assumption can be justified in view of the weak coupling between vertical and horizontal velocities, it is nonetheless an obvious shortcoming, since it neglects physical processes that are known to play a central role in the dynamics of the upper ocean. In particular, the drift in the upper layer is not driven solely by mean ocean currents, but is also influenced by surface waves (see, for example, Raschle and Arduin (2009) and Röhrs et al. (2012)), and, in the upper few metres of the ocean, the wave-induced Stokes drift contributes significantly to the overall transport and structure of the flow (Stokes, 1847; Monismith and Fong, 2004; Röhrs et al., 2014). This influence is further enhanced by the dissipation of wave momentum (Carniel et al., 2009; Christensen and Terrile, 2009), which couples with Earth's rotation through the Coriolis–Stokes force. The resulting wave–current interactions can substantially modify both the magnitude and direction of near-surface currents (Ursell, 1950; Hasselmann, 1970; Lewis and Belcher, 2004; Polton et al., 2005). However, in principle, our model can also account

for wave motion: the kinematic boundary (3.5) provides an equation for the free surface, which also enters the equations directly through the dynamic boundary conditions (2.16). In particular, this would affect the geostrophic flow, which would then be given by

$$\left. \begin{aligned} 2\tilde{v}_g \sin \theta &= \frac{1}{\cos \theta} \left( \frac{\partial P_s}{\partial \varphi} + \wp \frac{\partial h_0}{\partial \varphi} \right) \\ 2\tilde{u}_g \sin \theta &= -\frac{\partial P_s}{\partial \theta} - \wp \frac{\partial h_0}{\partial \varphi} \end{aligned} \right\} \quad \text{in } \{d_0(\varphi, \theta, t) < z < h_0(\varphi, \theta, t)\}.$$

Clearly, this significantly complicates the analysis; this is a problem that we hope to tackle in future work.

Nevertheless, even with the assumption of a flat surface, the results we obtain are strikingly in agreement with the experimental observations. First, we were able to prove analytically that the leading-order problem possesses a unique solution that behaves qualitatively like an Ekman spiral, and we were able to characterise the surface deflection angle and the intensity of the surface current. Then, to obtain some explicit values to compare with the experimental data available in the literature, we adopted five different explicit parametrisations for the eddy viscosity: constant, linearly decreasing, linearly increasing, piecewise linear, and exponentially decaying; in all cases, we assumed that the eddy viscosity below the Ekman layer, where wind effects are negligible, the eddy viscosity is constant and equal to the molecular one (although this does not really affect our solution). We point out that even in the absence of waves in our model, the piecewise linear viscosity adopted in the third case is a simplified version of that by Kitaigorodsky (1961) and Weber (1981), who proposed an eddy viscosity proportional to the shear of the wave orbital velocity in a turbulent wave times the square of the mixing length.

We chose reasonable values both for the depth  $z_0$  and the wind intensity  $|W_w|$ : the former lies in the range  $-3$  to  $-8$ , corresponding to approximately  $-35$  to  $-100$  metres, while for the latter we mostly considered the values  $|W_w| = 10$  or  $|W_w| = 100$ , which correspond, with our scaling, to a wind speed of the order of  $1 \text{ m s}^{-1}$  or  $10 \text{ m s}^{-1}$ , respectively. With these choices, we found values for the deflection angle that match the observations excellently. In practice, the deflection angle can be observed to be both greater (Chereskin, 1995; Arduin et al., 2009; Yoshikawa and Masuda, 2009; Kim et al., 2010; Röhres and Christensen, 2015; Lodise et al., 2019) and lower (Poulain et al., 2009; Senchev et al., 2017; Berta et al., 2018; Lodise et al., 2019) than  $45^\circ$ ; we recover both regimes, obtaining highly realistic values. Our results from § 5 seem to point toward the conclusion that an eddy viscosity that decays with depth leads to deflection angles exceeding  $45^\circ$ , while increasing eddy viscosity profiles result in deflection angles below this threshold. As shown in the figures, the largest deflection angles are obtained for exponentially decaying eddy viscosity, followed by the linearly decaying case. For constant eddy viscosity, the deflection angle remains close to  $45^\circ$ . The piecewise linear profile, which combines the increasing and decreasing cases, yields deflection angles smaller than  $45^\circ$ , suggesting that the increasing part dominates the decreasing one. A similar reduction in the deflection angle is observed for the linearly increasing eddy viscosity. Moreover, in the case of  $|W_w| = 100$  (the more realistic one to compare with measurements), the intensity of the surface current is invariably found to be about 1% of the wind's intensity at mid to high latitudes, consistent with observations (see the data by Lodise et al. (2019)). Additionally, measurements show that the speed of the Ekman current decays with depth more rapidly than its directional rotation, in contrast to the theoretical predictions from Ekman's classical theory (Wijffels et al., 1994). This effect is known as Ekman spiral flattening or compression (Schudlich and Price, 1998) and, with the exception of the simplest case of constant eddy viscosity, is very evident in our explicit solutions.

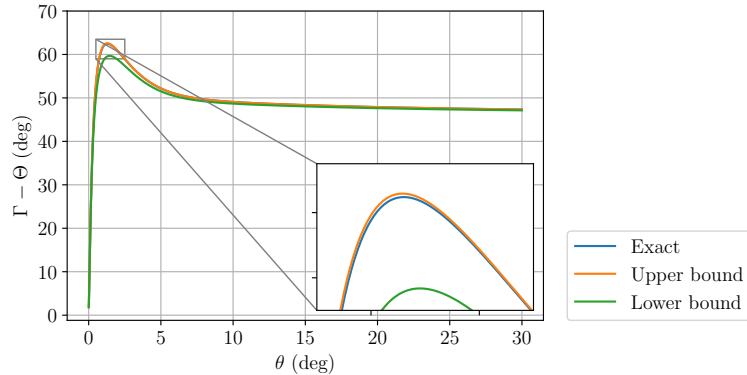


FIGURE 24. Comparison between the surface deflection angle  $\Gamma - \Theta$  for linearly decaying eddy viscosity and the bounds (4.15), with  $z_0 = -4$ ,  $|W_w| = 100$ , and  $\theta \in (0^\circ, 30^\circ)$ .

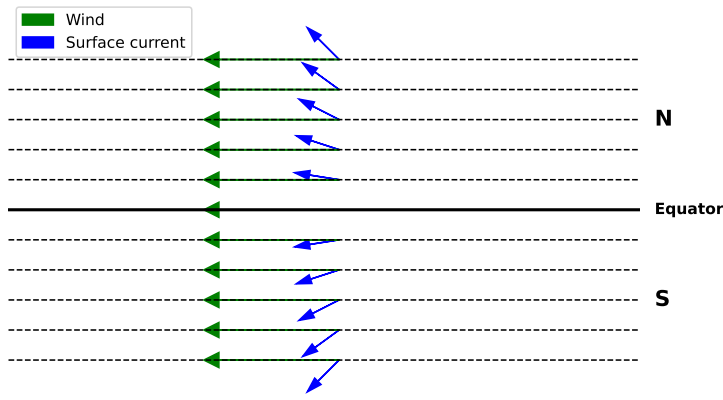


FIGURE 25. Conceptual diagram showing the progressive decrease in the wind-current deflection angle toward the equator as the Coriolis force approaches zero. Not to scale.

It may be interesting to observe that although explicitly calculating the deflection angle entails determining the unique positive solution of the fourth-order polynomial equation (4.8), the upper and lower bounds provided in (4.15), which can be computed without the need to solve (4.8), are excellent approximations. figure 24 shows the deflection angle with the corresponding bounds (4.15) in the case of the linearly decaying eddy viscosity of § 5.2, for  $z_0 = -4$  and  $|W_w| = 100$ ; especially the upper bound is exceptionally close to the exact curve. The bounds in the other cases are even more accurate, and the upper bound in particular is almost indistinguishable from the actual deflection angle.

Note that the analysis in the present article was carried out for  $\theta \notin \{\pm\frac{\pi}{2}\}$ —that is, avoiding the poles, where the classical spherical coordinates have a singularity (as mentioned in the Introduction)—and, crucially, for  $\theta \neq 0$ , that is, away from the Equator. The latter restriction arises because the definition of the geostrophic component of the velocity field, which entails dividing by  $\sin \theta$ , breaks down for  $\theta = 0$ . Therefore, a radically different approach, as in Stommel's theory of wind-driven drift currents (Stommel, 1960; Webb, 2018), is required to extend our methods to equatorial flows, extending the results by Constantin and Johnson (2019a). This is left for future work. Nevertheless, in Theorem 4.5 we recovered the classical result that in regions close to the equator—where the Coriolis effect from Earth's rotation is negligible—the wind-driven surface current

flows essentially in the same direction as the wind (Boyd, 2018). This behaviour, which is illustrated schematically in figure 25, is apparent in all graphs we provided for the surface deflection angle for the explicit solutions we discussed.

Another crucial point is that, as we pointed out when deriving the leading-order problem in § 3.1, our model is essentially steady, due to the inertial scale that we chose for the time variable. Incorporating time dependence within the model by choosing a smaller time scale may be an interesting direction for further research that we plan to pursue in subsequent work. This would allow us to include (near-)inertial oscillations within the picture, along the lines of the works by Lewis and Belcher (2004), Shrira and Almela (2020), Roberti (2022), and Puntini (2025, 2026).

Of course, having variable density would also be a possible generalisation, although one should expect that this would have relatively little impact on the solutions, since the water density in the upper ocean is only subject to tiny variations, mostly due to changes in salinity (Vallis, 2017). Thus, non-constant density would introduce considerable technical difficulties for seemingly little gain. Nevertheless, this is an avenue that we might explore in the future, although other matters (such as including a non-flat free surface or the time dependence) appear to be more pressing.

**Funding.** C.P. is supported by the Austrian Science Fund (FWF) [grant number Z 387-N, grant doi: [10.55776/Z387](https://doi.org/10.55776/Z387)].

**Declaration of interests.** The authors report no conflict of interest.

**Data availability statement.** All data used in this work are properly cited throughout the manuscript.

**Author contributions.** C.P. proposed the topic, developed the governing equations in § 2 and § 3, carried out the theory and numerics of § 5, and contributed to writing, alongside minor contributions to the theory of § 4. L.R. developed the governing equations in § 2 and § 3 and the theory of § 4 and contributed to the theory and numerics of § 5 and to writing. E.S. contributed to the development of the theory of § 4.

#### Author ORCIDs.

Christian Puntini <https://orcid.org/0009-0008-5454-0922>;  
 Luigi Roberti <https://orcid.org/0000-0001-7678-7389>;  
 Eduard Stefanescu <https://orcid.org/0009-0001-6507-9691>.

#### REFERENCES

Ardhuin, F., Marié, L., Rasclle, N., Forget, P. and Roland, A. (2009). Observation and estimation of Lagrangian, Stokes, and Eulerian currents induced by wind and waves at the sea surface, *J. Phys. Oceanogr.* **39**: 2820–2838.

Arfken, G. B. and Weber, H. J. (2005). *Mathematical Methods for Physicists*, 6th edn, Elsevier Academic Press, Amsterdam.

Balmforth, N. J. and Liu, J. J. (2004). Roll waves in mud, *J. Fluid Mech.* **519**: 33–54.

Berta, M., Bellomo, L., Griffa, A., Magaldi, M. G., Molcard, A., Mantovani, C., Gasparini, G. P., Marmain, J., Vetrano, A., Béguery, L., Borghini, M., Barbin, Y., Gaggelli, J. and Quentin, C. (2018). Wind-induced variability in the Northern Current (northwestern Mediterranean Sea) as depicted by a multi-platform observing system, *Ocean Sci.* **14**: 689–710.

Boyd, J. P. (2018). *Dynamics of the Equatorial Ocean*, Springer Berlin, Heidelberg.

Carniel, S., C., J., Warner, Chiggiato, J. and Sclavo, M. (2009). Investigating the impact of surface wave breaking on modeling the trajectories of drifters in the northern Adriatic Sea during a wind-storm event, *Ocean Modell.* **30**(2-3): 225–239.

Chambon, G., Freydier, P., Naaim, M. and Vila, J.-P. (2020). Asymptotic expansion of the velocity field within the front of viscoplastic surges: Comparison with experiments, *J. Fluid Mech.* **884**: A43.

Chereskin, T. K. (1995). Direct evidence for an Ekman balance in the California Current, *J. Geophys. Res.* **100**(C9): 18,261–18,269.

Christensen, K. H. and Terrile, E. (2009). Drift and deformation of oil slicks due to surface waves, *J. Fluid Mech.* **620**: 313–332.

Constantin, A. (2021). Frictional effects in wind-driven ocean currents, *Geophys. Astrophys. Fluid Dyn.* **115**: 1–14.

Constantin, A. (2022). Nonlinear wind-drift ocean currents in arctic regions, *Geophys. Astrophys. Fluid Dyn.* **116**(2): 101–115.

Constantin, A., Dritschel, D. G. and Paldor, N. (2020). The deflection angle between a wind-forced surface current and the overlying wind in an ocean with vertically varying eddy viscosity, *Phys. Fluids* **32**: 116604.

Constantin, A. and Johnson, R. S. (2008). On the non-dimensionalisation, scaling and resulting interpretation of the classical governing equations for water waves, *J. Nonlinear Math. Phys.* **15**(Suppl. 2): 58–73.

Constantin, A. and Johnson, R. S. (2017). Large gyres as a shallow-water asymptotic solution of Euler's equation in spherical coordinates, *Proc. A.* **473**: 20170063.

Constantin, A. and Johnson, R. S. (2018). Steady large-scale ocean flows in spherical coordinates, *Oceanography* **31**(3): 42–50.

Constantin, A. and Johnson, R. S. (2019a). Ekman-type solutions for shallow-water flows on a rotating sphere: A new perspective on a classical problem, *Phys. Fluids* **31**(2): 021401.

Constantin, A. and Johnson, R. S. (2019b). Large scale oceanic currents as shallow-water asymptotic solutions of the Navier–Stokes equation in rotating spherical coordinates, *Deep Sea Res. II* **160**: 32–40.

Constantin, A. and Johnson, R. S. (2021). On the modelling of large-scale atmospheric flows, *J. Differ. Equ.* **285**: 751–798.

Constantin, A. and Johnson, R. S. (2023). On the dynamics of the near-surface currents in the Arctic Ocean, *Nonlinear Anal. Real World Appl.* **73**: 103894.

Constantin, A. and Johnson, R. S. (2024a). The dynamics of the Transpolar Drift Current, *Geophys. Astrophys. Fluid Dyn.* **118**(3): 165–182.

Constantin, A. and Johnson, R. S. (2024b). Spherical coordinates for Arctic Ocean flows, in D. Henry (ed.), *Nonlinear Dispersive Waves: Based on the 2023 Workshop at University College Cork, Ireland*, Springer Nature Switzerland, Cham, pp. 239–282.

Cromwell, T. (1953). Circulation in a meridional plane in the central equatorial Pacific, *J. Mar. Res.* **12**: 196–213.

Cronin, M. F. and Kessler, W. S. (2009). Near-surface shear flow in the tropical Pacific cold tongue front, *J. Phys. Oceanogr.* **39**: 1200–1215.

Cronin, M. F. and Tozuka, T. (2016). Steady state ocean response to wind forcing in extratropical frontal regions, *Sci. Rep.* **6**: 28842.

Ekman, V. W. (1905). On the influence of the Earth's rotation on ocean-currents, *Ark. Mat. Astron. Fys.* **2**: 1–52.

Fernández-Nieto, E. D., Noble, P. and Vila, J.-P. (2010). Shallow water equations for Non-Newtonian fluids, *J. Non-Newton. Fluid Mech.* **165**: 712–732.

Gill, A. E. (1982). *Atmosphere–Ocean Dynamics*, Vol. 30 of *International Geophysics Series*, Academic Press, New York, NY.

Grisogono, B. (1995). A generalized Ekman layer profile with gradually varying eddy diffusivities, *Quart. J. Roy. Meteorol. Soc.* **121**: 445–453.

Hardy, G. H. (1949). *Divergent Series*, Clarendon, Oxford, UK.

Hasselmann, K. (1970). Wave-driven inertial oscillations, *Geophys. Fluid Dyn.* **1**(3-4): 463–502.

Henry, D. and Villari, G. (2022). Flow underlying coupled surface and internal waves, *J. Differ. Equ.* **310**: 404–442.

Holmes, M. H. (2015). *Introduction to Perturbation Methods*, Vol. 20 of *Texts in Applied Mathematics*, 2 edn, Springer-Verlag, New York, NY.

Johnson, R. S. (1980). Water waves and Korteweg-de Vries equations, *J. Fluid Mech.* **97**: 701–719.

Johnson, R. S. (2005). *Singular Perturbation Theory: Mathematical and Analytical Techniques with Applications to Engineering*, Springer Science + Business Media, Inc., Boston, MA.

Johnson, R. S. (2018). The value of asymptotic theories in physical oceanography, *Oceanography* **31**(3): 14–21.

Johnson, R. S. (2022). The ocean and the atmosphere: An applied mathematician’s view, *Commun. Pure Appl. Anal.* **21**(7): 2357–2381.

Kamenkovich, V. M. (1977). *Fundamentals of Ocean Dynamics*, Vol. 16 of *Elsevier Oceanography Series*, Elsevier Scientific Publishing Company, Amsterdam.

Kantha, L. H. and Clayson, C. A. (2000). *Numerical Models of Oceans and Oceanic Processes*, Vol. 66 of *International Geophysics Series*, Academic Press, San Diego, CA.

Kim, S. Y., Cornuelle, B. D. and Terrill, E. J. (2010). Decomposing observations of high-frequency radar-derived surface currents by their forcing mechanisms: Locally wind-driven surface currents, *J. Geophys. Res.-Oceans* **115**: C12046.

Kitaigorodsky, S. A. (1961). On the possibility of theoretical calculation of vertical temperature profile in the upper layer of the sea, *Bull. Acad. Sci. USSR Geophys. Ser.* **3**: 313–318.

Lewis, D. M. and Belcher, S. E. (2004). Time-dependent, coupled, Ekman boundary layer solutions incorporating Stokes drift, *Dyn. Atmos. Oceans* **37**(4): 313–351.

Lodise, J., Özgökmen, T., Griffa, A. and Berta, M. (2019). Vertical structure of ocean surface currents under high winds from massive arrays of drifters, *Ocean Sci.* **15**(6): 1627–1651.

Madsen, O. S. (1977). A realistic model of the wind-induced Ekman boundary layer, *J. Phys. Oceanogr.* **7**: 248–255.

Marynets, K. (2022). Stability analysis of the boundary value problem modeling a two-layer ocean, *Comm. Pure Appl. Anal.* **21**(7): 2433–2445.

McWilliams, J. C. and Huckle, E. (2006). Ekman layer rectification, *J. Phys. Oceanogr.* **36**: 1646–1659.

Monismith, S. G. and Fong, D. A. (2004). A note on the potential transport of scalars and organisms by surface waves, *Limnol. Oceanogr.* **49**(4): 1214–1217.

Nansen, F. (1897). *Farthest North. Volumes I and II*, Archibald Constable & Co., London.

Paldor, N. (2024). A Lagrangian theory of equatorial upwelling, *Phys. Fluids* **36**: 046605.

Pedlosky, J. (1987). *Geophysical Fluid Dynamics*, 2nd edn, Springer-Verlag, New York, NY.

Peregrine, D. H. (1967). Long waves on a beach, *J. Fluid Mech.* **27**: 815–827.

Phillips, N. A. (1987). Principles of large-scale numerical weather prediction, in P. Morel (ed.), *Dynamic Meteorology*, D. Reidel Publishing Company, Dordrecht, pp. 1–96.

Polton, J. A., Lenn, Y.-D., Eliot, S., K. Chereskin, T. and Sprintall, J. (2013). Can Drake Passage observations match Ekman’s classic theory?, *J. Phys. Oceanogr.* **43**(8): 1733–1740.

Polton, J. A., Lewis, D. M. and Belcher, S. E. (2005). The role of wave-induced Coriolis–Stokes forcing on the wind-driven mixed layer, *J. Phys. Oceanogr.* **35**(4): 444–457.

Polyanin, A. D. and Zaitsev, V. F. (2003). *Handbook of Exact Solutions for Ordinary Differential Equations*, Chapman & Hall / CRC, Boca Raton, FL.

Pope, S. B. (2000). *Turbulent Flows*, Cambridge University Press, Cambridge, UK.

Poulain, R.-M., Gerin, R., Mauri, E. and Pennel, R. (2009). Wind effects on drogued and undrogued drifters in the eastern Mediterranean, *J. Atmos. Oceanic Technol.* **26**(6): 1144–1156.

Puntini, C. (2025). On the modeling of nonlinear wind-induced ice-drift ocean currents at the North Pole, *J. Math. Fluid Mech.* **27**: No. 71.

Puntini, C. (2026). Nonlinear dynamics of wind-drift currents at mid-latitudes, *Nonlinear Anal. Real World Appl.* **90**: 104557.

Raschle, N. and Arduhin, F. (2009). Drift and mixing under the ocean surface revisited: Stratified conditions and model-data comparisons, *J. Geophys. Res. Oceans* **114**(C2): C02016.

Renteln, P. (2013). *Manifolds, Tensors, and Forms: An Introduction for Mathematicians and Physicists*, Cambridge University Press, Cambridge, UK.

Robert, L. (2021). Perturbation analysis for the surface deflection angle of Ekman-type flows with variable eddy viscosity, *J. Math. Fluid Mech.* **23**: No. 57.

Robert, L. (2022). The surface current of Ekman flows with time-dependent eddy viscosity, *Comm. Pure Appl. Anal.* **21**(7): 2463–2477.

Röhrs, J. and Christensen, K. H. (2015). Drift in the uppermost part of the ocean, *Geophys. Res. Lett.* **42**: 10349–10356.

Röhrs, J., Christensen, K. H., Hole, L. R., Broström, G., Drivdal, M. and Sundby, S. (2012). Observation-based evaluation of surface wave effects on currents and trajectory forecasts, *Ocean Dyn.* **62**(10): 1519–1533.

Röhrs, J., Christensen, K. H., Vikebø, F., Sundby, S., Saetra, Ø. and Broström, G. (2014). Wave-induced transport and vertical mixing of pelagic eggs and larvae, *Limnol. Oceanogr.* **59**(4): 1213–1227.

Schudlich, R. R. and Price, J. F. (1998). Observations of seasonal variation in the Ekman layer, *J. Phys. Oceanogr.* **28**(6): 1187–1204.

Sentchev, A., Forget, P. and Fraunié, P. (2017). Surface current dynamics under sea breeze conditions observed by simultaneous HF radar, ADCP and drifter measurements, *Ocean Dynam.* **67**: 499–512.

Sentchev, A., Yaremchuk, M., Bourras, D., Pairaud, I. and Fraunié, P. (2023). Estimation of the eddy viscosity profile in the sea surface boundary layer from underway ADCP observations, *J. Atmos. Oceanic Technol.* **40**: 1291–1305.

Shrira, V. I. and Almelah, R. B. (2020). Upper-ocean Ekman current dynamics: A new perspective, *J. Fluid Mech.* **887**: A24.

Smith, S. D. (1988). Coefficients for sea surface wind stress, heat flux, and wind profiles as a function of wind speed and temperature, *J. Geophys. Res.* **93**: 15467–15472.

Söderlind, G. (2024). *Logarithmic Norms*, Vol. 63 of *Springer Series in Computational Mathematics*, Springer-Verlag, New York, NY.

Soloviev, A. and Lucas, R. (2014). *The Near-Surface Layer of the Ocean. Structure, Dynamics and Applications*, Vol. 31 of *Atmospheric and Oceanographic Sciences Library*, Springer, Dordrecht.

Stefanescu, E. (2024). The atmospheric Ekman spiral for piecewise-uniform eddy viscosity, *Phys. Scr.* **99**: 095018.

Stokes, G. G. (1847). On the theory of oscillatory waves, *Trans. Cambridge Philos. Soc.* **8**: 441–455.

Stommel, H. (1960). Wind-drift near the Equator, *Deep Sea Res.* **6**: 298–302.

Talley, L. D., Pickard, G. L., Emery, W. J. and Swift, J. H. (2011). *Descriptive Physical Oceanography: An Introduction*, 6 edn, Elsevier Academic Press, Amsterdam.

Teschl, G. (2012). *Ordinary Differential Equations and Dynamical Systems*, Vol. 140 of *Graduate Studies in Mathematics*, American Mathematical Society, Providence, RI.

Trenberth, K. E., Large, W. G. and Olson, J. G. (1990). The mean annual cycle in global ocean wind stress, *J. Phys. Oceanogr.* **20**: 1742–1760.

Ursell, F. (1950). On the theoretical form of ocean swell on a rotating Earth, *Mon. Not. R. Astron. Soc. Geophys. Suppl.* **6**(1): 1–8.

Vallis, G. K. (2017). *Atmospheric and Oceanic Fluid Dynamics. Fundamentals and Large-Scale Circulation*, 2 edn, Cambridge University Press, Cambridge, UK.

Van Dyke, M. (1975). *Perturbation Methods in Fluid Mechanics*, annotated edn, Parabolic Press, Stanford, CA.

Webb, D. J. (2018). *A Note on Stommel's Theory of the Tropical Cell, Research and Consultancy Report No. 63*, National Oceanography Centre, Southampton, UK.

Weber, J. E. (1981). Ekman currents and mixing due to surface gravity waves, *J. Phys. Oceanogr.* **11**: 1431–1435.

Wenegrat, J. O. and McPhaden, M. J. (2016). Wind, waves, and fronts: frictional effects in a generalized Ekman model, *J. Phys. Oceanogr.* **46**: 371–394.

Wenegrat, J. O., McPhaden, M. J. and Lien, R. C. (2014). Wind stress and near-surface shear in the equatorial Atlantic ocean, *Geophys. Res. Lett.* **41**: 1226–1231.

White, A. A. (2002). A view of the equations of meteorological dynamics and various approximations, in J. Norbury and I. Roulstone (eds), *Large-Scale Atmosphere-Ocean Dynamics*, Cambridge University Press, Cambridge, UK, pp. 1–100.

Wijffels, S., Firing, E. and Bryden, H. (1994). Direct observations of the Ekman balance at 10°N in the Pacific, *J. Phys. Oceanogr.* **24**(7): 1666–1679.

Wunsch, C. and Ferrari, R. (2004). Vertical mixing, energy, and the general circulation of the oceans, *Annu. Rev. Fluid Mech.* **36**: 281–314.

Yelland, M. and Taylor, P. K. (1996). Wind stress measurements from the open ocean, *J. Phys. Oceanogr.* **26**: 541–558.

Yoshikawa, Y. and Masuda, A. (2009). Seasonal variations in the speed factor and deflection angle of the wind driven surface flow in the Tsushima Strait, *J. Geophys. Res.* **114**: C12022.

Yuan, C., Zhang, S., Wang, Z., Chen, Z. and Johnson, E. R. (2025). A novel Kadomtsev-Petviashvili type model for nonlinear internal waves with horizontally two-dimensional shear currents and Earth's rotation, *J. Fluid Mech.* **1015**: A3.

Zhang, W. and Zhang, H. (2025). Exact solutions of the Beaufort Gyre in the presence of ice, *Phys. Fluids* **37**: 086628.

Zikanov, O., Slinn, D. N. and Dhanak, M. R. (2003). Large-eddy simulations of the wind-induced turbulent Ekman layer, *J. Fluid Mech.* **495**: 343–368.